Εθνικό Μετσόβιο Πολυτεχνείο
Σχολή Πολιτικών Μηχανικών
Τομέας Γεωτεχνικής

National Technical University
School of Civil Engineering
Geotechnical Division

Μεταπτυχιακή Εργασία

Νόνικα Αντωνάκη

Επιβλέποντες:
Καθηγητής Γ. Γκαζέτας
Δρ. Ι. Αναστασόπουλος

ΠΕΙΡΑΜΑΤΙΚΗ ΜΕΛΕΤΗ ΜΟΝΩΣΗΣ ΜΕΣΩ ΛΙΚΝΙΣΜΟΥ : ΕΦΑΡΜΟΓΗ ΣΤΗΝ ΕΝΙΣΧΥΣΗ ΥΦΙΣΤΑΜΕΝΟΥ ΚΤΙΡΙΟΥ

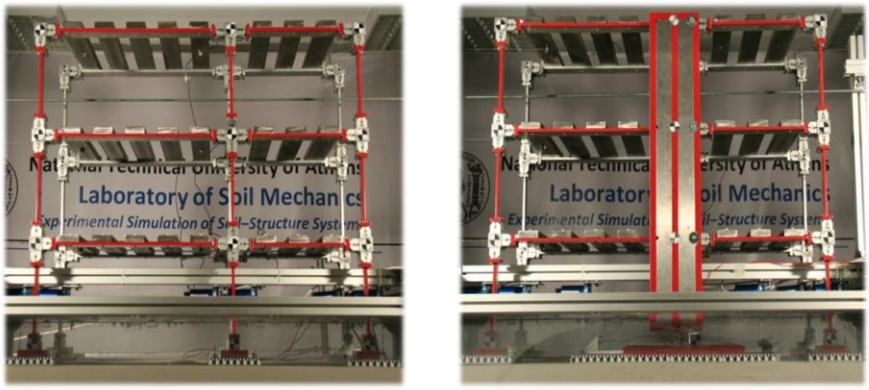

EXPERIMENTAL STUDY OF ROCKING ISOLATION : APPLICATION TO THE RETROFIT OF AN EXISTING BUILDING

MSc Thesis

Nonika Antonaki

Supervized by
Professor G. Gazetas
Dr. I. Anastasopoulos

Ιούνιος 2012 **June 2012**

Ευχαριστίες

Ολοκληρώνοντας τη μεταπτυχιακή μου εργασία, επιθυμώ να ευχαριστήσω όλους όσους συνεισέφεραν σε αυτή κατά τη διάρκεια της εκπόνησής της.

Αρχικά ευχαριστώ θερμά τον καθηγητή μου, κ. Γιώργο Γκαζέτα, για την ευκαιρία που μου χάρισε απλόχερα, καθώς και την έμπνευση που μου προσέφερε καθ' όλη τη διάρκεια των σπουδών μου.

Θερμές ευχαριστίες οφείλω στο Δρ. Ιωάννη Αναστασόπουλο, χωρίς τη συνεχή καθοδήγηση του οποίου δε θα τα είχα καταφέρει. Επιπλέον ευχαριστώ το Δρ. Βασίλη Δρόσο για την προθυμία και τη σημαντική συμβολή του.

Θα ήθελα επίσης να ευχαριστήσω όλο το προσωπικό του εργαστηρίου Εδαφομηχανικής για κάθε βοήθεια που μου παρείχε.

Τέλος, ευχαριστώ την οικογένειά μου που με στηρίζει σταθερά στην εκπλήρωση των στόχων μου.

TABLE OF CONTENTS

Appendix A

I. Model Components

II. Calibration of Artificial Plastic Hinges

Appendix B

Accelerations and Inter – storey Drifts for the full Sequence of Seismic Motions

1

Introduction

1. INTRODUCTION

Earthquake Design of Structures

It has been more than 30 years since the realization that structural damage is inevitable under unexpectedly strong seismic motions, and that the increase of strength does not always result in enhanced safety. This recognition led to the development of modern seismic design principles, which aim at controlling seismic damage rather than to avoid it. Ductility design aims at ensuring that critical structural members may sustain loads that exceed their capacity without collapsing, while capacity design focuses on guiding failure to less important structural members (beams instead of columns) and to non-brittle mechanisms (bending instead of shearing) [Park & Paulay, 1976]. Moreover, understanding that structural damage is more directly related to deformation lead to the development of displacement-based and performance-based design [Bertero, 1996; Calvi, 1999; Priestley, 2000], and to a rather substantial improvement of seismic codes.

Unfortunately, however, most existing structures do not comply with current seismic design provisions. In Greece, for example, about 85% of the building stock dates before 1985, built in accordance with obsolete seismic codes. Their vulnerability has been manifested rather dramatically during devastating earthquakes. Most importantly, even relatively small magnitude earthquakes may cause substantial damage or failure of existing structures. For example, a M_s 5.9 earthquake near Athens (Greece, 1999) lead to 145 fatalities due to collapse of 100 buildings, and damage beyond repair to 13000 buildings [Papadopoulos et al., 2000]. Moreover, the lack of adequate ductility and capacity design is bound to lead to brittle types of failure. Therefore the need of methods to improve and reinforce them, in terms of strength, stiffness or ductility is imperative.

In regards to the foundation, design remains strictly elastic, thus to avoid notable residual rotation or displacement after a strong earthquake. Soil is a heterogeneous material and accurate measurement of its properties entails a lot of uncertainties. Therefore, “failure” mechanisms such as mobilisation of soil bearing-capacity, foundation uplifting, sliding, or

any combination of the above are averted in order to avoid the laborious task of inspecting and repairing the soil – foundation system. However, *over – designing* the foundation can increase the strength or ductility required from the members of the superstructure.

Rocking Isolation

A "new design philosophy", based on which the foundation is intentionally under-designed, has been introduced by Anastasopoulos et al. (2010). The concept has been investigated numerically and experimentally and recent studies have shown that such exploitation of strongly nonlinear foundation response may be beneficial, limiting the inertia transmitted onto the superstructure [Paolucci, 1997; Pecker, 1998; 2003; Gazetas et al., 2003; Gajan et al., 2005; Apostolou et al., 2007; Pender, 2007; Paolucci et al., 2008; Gajan & Kutter, 2008; 2009; Shirato et al. 2008; Vassiliou & Makris, 2011; Panagiotidou et al., 2012; Gelagoti et al., 2011].

Reduction of foundation size allows the exploitation of the soil's strength and ductility and can serve as a fuse for the superstructure. Therefore, failure is guided to the soil-foundation system instead of the structural elements (Figure 1.1). The increased ductility of the soil – foundation system in comparison to that of structural members, especially in cases of structures that were designed based on seismic codes that did not place emphasis on ductility design, is but one of the advantages of this new approach. An additional advantage is the reversibility of the soil – foundation system's "failure" mechanisms, due to the cyclic and kinematic nature of seismic motions. However, increased settlement or rotation is the price to pay for the energy dissipation gained via rocking.

Scope of this Thesis

This thesis investigates experimentally the seismic performance of an existing building, with emphasis on the effects of nonlinear soil–foundation–structure interaction (SFSI). For this purpose, an idealized 3-storey structure is considered, inspired from the large-scale tests of the SPEAR project [Fardis, 2002; Fardis & Negro, 2006; Di Ludovico, 2007]. A reduced-scale model of the soil-structure system is tested in the shaking table of the Laboratory of Soil

Mechanics of NTUA. The seismic performance of the original structure is simulated in a first step, confirming its vulnerability. Then, the building is retrofitted with the equivalent of a RC shear wall, following the provisions of modern seismic codes. In both cases, a variety of real seismic records is used as base excitation (Figure 1.2).

Three alternatives are considered with respect to the foundation of the shear wall: (a) conventional design, following the provisions of current seismic codes (KAN.EPE. 2009); (b) rocking isolation; and (c) addition of tie beams between the existing footings of columns and the footing of the shear wall. In the second case, the foundation is intentionally *under-designed* to promote uplifting and fully mobilize its moment capacity, thus acting as "rocking isolation" [Mergos & Kawashima, 2005]. As previously mentioned, allowing such "plastic hinging" at the foundation level may act as an energy dissipation mechanism that bounds the seismic demand, thus providing adequately large safety margins, even for seismic motions that substantially exceed the design limits [Anastasopoulos et al., 2010a; Gelagoti et al., 2012; Kourkoulis et al., 2012]. In the latter alternative, the effect of connecting the footings with hinged or fully fixed tie beams is studied (Figure 1.3).

Figures of Chapter 1

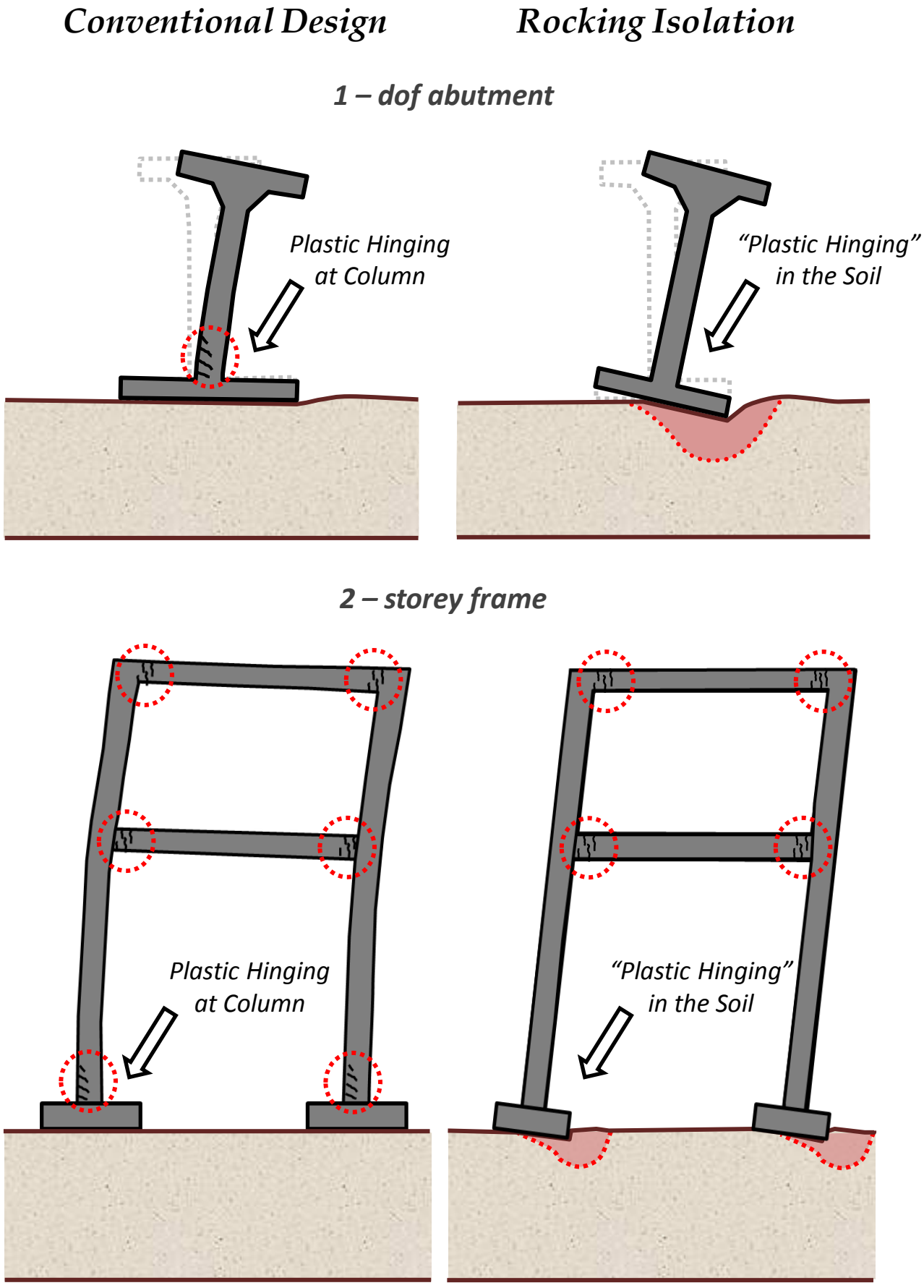

Figure 1.1 Schematic illustration of new design philosophy.

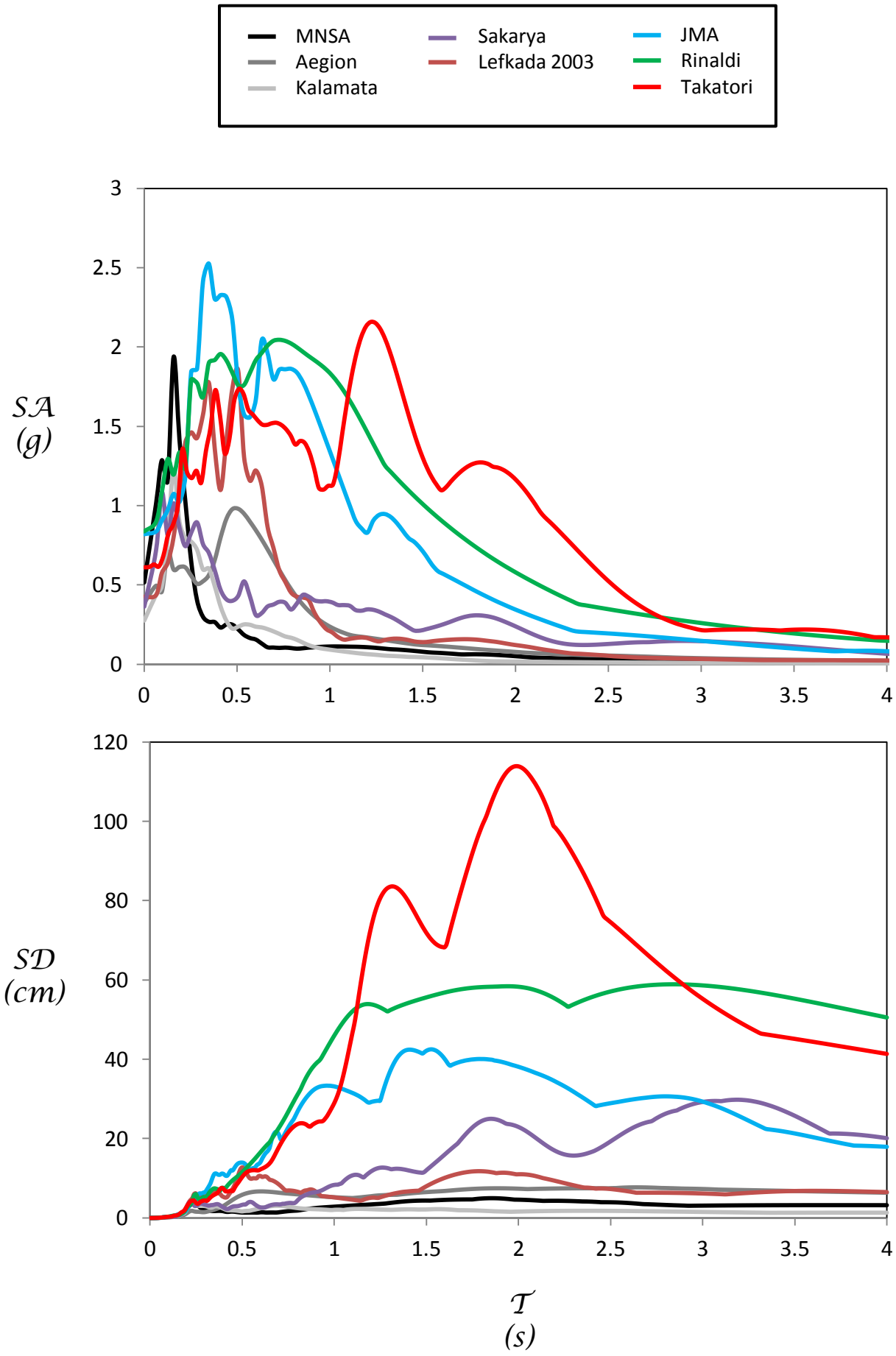

Figure 1.2 Acceleration and displacement spectra for real seismic records used as base excitation.

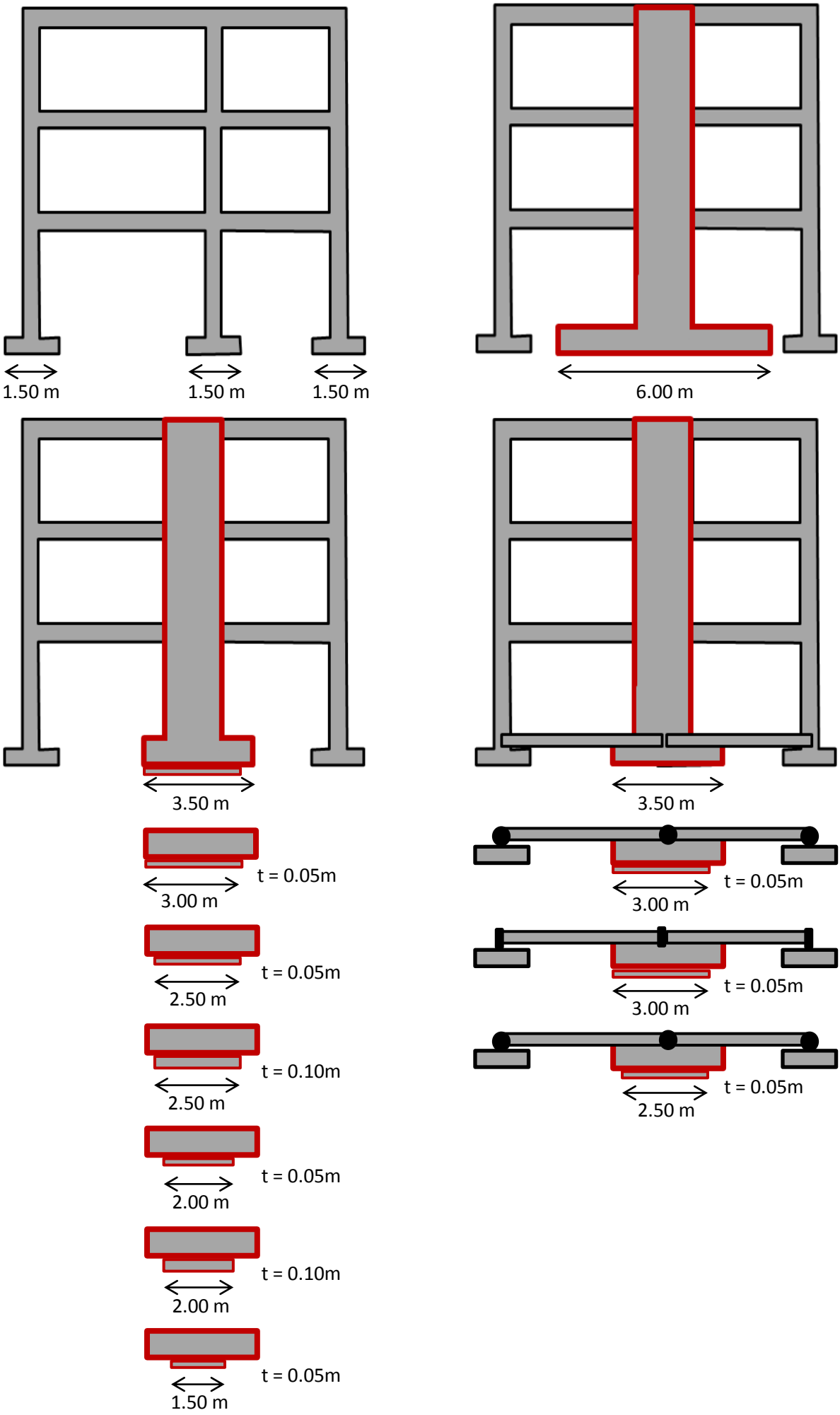

Figure 1.3 Schematic illustration of systems examined.

2

Problem Definition and Methodology

2. PROBLEM DEFINITION AND METHODOLOGY

2.1 Experimental Setup

Model

The under study structure is a typical 3 – storey building of Southern Europe, designed and constructed during the 70's (Figure 2.1). The structure does not comply with capacity design principles and is prone to soft - storey collapse. A representative "slice" of the building is modelled, corresponding to 1/3 of the whole structure. The square columns of the prototype are 25 cm in width, while the beams have a 25 cm x 50 cm (width x height) cross section.
The foundation consists of square surface foundations of width B = 1.5 m, considered realistic for competent soil. The construction materials of the building were reinforced concrete of 25 MPa nominal strength and smooth reinforcing steel bars of 320 MPa nominal strength. The bending strength of the members was calculated using these values and corresponding safety factors [Ageliki Rodogianni, 2011].

Taking account of the capacity of the shaking table, a scale factor N = 10 was selected. The physical model (Figure 2.2) consists of two identical frames, connected together through evenly distributed steel plates. They also represent the mass of each story, which is calculated through a combination of dead and live loads and is equal to 22 tn per story [Ageliki Rodogianni, 2011]. Therefore, the total mass imposed on each frame is equal to 66 kg (in model scale). The structural members (columns and beams) are made of commercially available aluminium plates of appropriate thickness and width, so as to maintain similarity in terms of stiffness [Gibson, 1997]. All members and parts used are depicted in detail in Appendix A.

At reduced-scale, it is practically impossible to model stiffness correctly (maintaining similarity) *and* achieve the desired (*scaled*) bending moment capacity of the structural members at the same time. For this purpose, each beam-column connection is modelled with custom-built artificial plastic hinges (Figure 2.2). The ultimate bending moment M_{ult} of each plastic hinge is calibrated through adjustment of the applied torque. The calibration of

each assembly was performed through static and slow-cyclic pushover testing, utilizing a screw-jack pushover apparatus.

After testing the original structure, the equivalent of a RC shear wall was added to the model to simulate the performance of the retrofitted structure (Figure 2.3). The shear wall was designed according to Greek regulations with a 1.5 m x 0.3 m cross section. The wall was connected to the middle column with an eccentricity towards the larger span of the frame. It was modeled by a stiff aluminum plate, rigidly connected on each floor, and equipped with an artificial plastic hinge at its base. The original footing of the central column was increased in width by rigidly connecting additional aluminum plates at both of its edges. With respect to the width of the shear wall footing different alternatives were tested, ranging (in prototype scale) from B = 6 m, corresponding to conventional design, to B = 1.5 m, for the rocking-isolated alternative.

Sandbox

The sandbox where the experiments were performed is of internal dimensions 1.48 m x 0.78 m x 0.645 m (Figure 2.4). Transparent barriers have been placed at the two opposite larger sides of the box, allowing the observation of the experiment. These barriers are a combination of Plexiglas at the external side and glass at the internal side, so that rigidity and durability are achieved on the outside, while minimizing friction and simultaneously protecting the Plexiglas on the inside.

Sand Raining System

The physical models of the building were installed inside a transparent soil container. The soil consists of dry “Longstone” sand, a very fine industrially-produced uniform quartz sand having a mean grain size d_{50} = 0.15 mm [Anastasopoulos et al., 2010b]. In order to ensure a specific value of sand density and its repeatability in every experiment, the Laboratory ’s sand raining system is used. Through this system, it is possible to choose and audit the mechanical characteristics of the soil. This procedure is called sand pluviation. The density depends on the height measured from the bottom of the sandbox, the aperture of the device and the velocity of the soil hopper. The selection of the suitable values of these three parameters is made according to Figure 2.5, which summarizes the results of an

experimental series performed to calibrate this particular device. Three different densities were used in this experimental series: Dr = 93 % (dense), Dr = 65 % (medium dense) and Dr = 45 % (loose).

Push-over Apparatus

Horizontal displacements are applied through a pushover apparatus, which consists of a servomotor joined to a screw-jack actuator (Figure 2.6). The servomotor is controlled by a computer, where the desired diplacement, acceleration and velocity can be selected. A device capable of measuring the applied load (load cell) is connected at the edge of the actuator. A load cell of 10 kg loading capacity is used for the calibration of beams and columns and one of 200 kg loading capacity for the walls.

Shaking Table

The Shaking Table of the Laboratory of Soil Mechanics in NTUA is of dimensions 1.3 m x 1.3 m and is capable of applying any type of excitation, including actual records (Figure 2.7). It is able to shake up to 2000 kg with a maximum acceleration of 1.6 g. It is connected to a data acquisition system and is controlled by an external digital system. The results of each experiment are collected and saved in the computer that controls the shaking table.

2.2 Experiment Preparation

2.2.1 *Calibration of artificial plastic hinges*

Every beam – column and column – footing connection was calibrated using the push – over apparatus. Each member was connected to its joint and then fixed on a base (using screws in the central hole of the junction). Afterwards, the push – over apparatus imposed controlled displacement and deformed the member until the artificial plastic hinge started to turn. The member was placed perpendicularly to the load cell that had been attached on the push – over apparatus, so that it was able to measure the reaction force of the member as the apparatus applied the displacement. The displacement was measured by a laser displacement transducer. Therefore, a force – displacement diagram was created for each member and consisted of an elastic and a plastic branch. The first represented the elastic

bending of the member utilizing its stiffness and the second represented the rotation of the joint without further increase of the reaction force. The joint was tightened or loosened until the required bending strength was achieved. Figure 2.8 shows the bending moment – displacement diagrams of the members that were connected in one joint, while the diagrams for all members and connections can be found in Appendix A. The same was repeated for the retrofitting walls.

2.2.2 *Model Preparation and Data Acquisition*

After the calibration of the junctions was completed the model is put together and the members were aligned, so that columns were vertical and beams horizontal. The calibration of the shaking table for a 1:10 scale followed. Before conducting every experiment the sand was layered utilizing the system that was described. Significant deformations of the building, during its placement from the floor into the sandbox with a crane bridge, were prevented using aluminum bars of small thickness as crosswise connectors of opposite joints.

The physical model of the building was installed on the soil by means of four mechanical jacks. Special care was taken during installation so as to achieve accurate positioning without disturbing the soil surface. Electronic spirit-levels were used to ensure that the building was placed horizontally on the soil surface without initial inclination. With the exception of accelerometers placed inside the soil mass, the instrumentation was installed on the first frame afterwards (Figure 2.10). After completion of the first two experiments, the walls were added to the frames externally and the additional parts were connected to the footings of the central columns. The central column of the ground floor was removed, so as not to provide unrealistic compressive or tensile strength, as the wall deformed. The footing of the wall was reduced in the experiments that followed, as previously mentioned (Table 1).

A number of instruments were used to measure accelerations and displacements. The horizontal in – plane acceleration was measured by accelerometers on every storey, as well as in a small depth from the soil surface. The exact set - up of the instruments is shown in Figure 2.9. The horizontal in – plane displacement of each storey was measured by wired displacement transducers and was processed in order to calculate the inter – storey drift. A fourth displacement transducer measured the sliding of the central footing, which was then

deducted from the displacement of each storey. Additionally, two wired displacement transducers were used for each footing of the first frame to measure the vertical displacement of each side of the footing. These measurements were necessary for the calculation of the in – plane rotation and the settlement of each footing. The data from all the instruments were gathered through proper cables and saved in the record system of the Laboratory. In addition, visual data were obtained using high definition cameras, when necessary.

The investigated soil–foundation–structure systems were subjected to a variety of seismic motions, including real records and artificial (sinusoidal motions) motions. Moderate intensity seismic records from Greece were utilized for the original (un-retrofitted) structure. The original building was found incapable of surviving stronger seismic motions. The retrofitted structure was also subjected to these records, but also to strong (Sakarya, Kocaeli 1999) and very strong seismic motions (Northridge 1994–Rinaldi; Kobe 1995–JMA and Takatori), as shown in Table 2. The latter records exceed substantially the design limits of the retrofit, and were investigated to explore the margins of safety of different foundation design alternatives. Each system was subjected to various sequences of seismic motions. Harmonic motions that were imposed are not presented for brevity.

2.2.3 *Documentation of Footing Behavior*

This series of tests places emphasis on the effect of the shear wall foundation properties on the seismic response of the superstructure (Table 1). Therefore the need to investigate the behavior of the footings that were tested was imperative and horizontal (monotonic and slow cyclic) pushover tests were conducted (Table 3).

The wall is assumed to bear approximately half of the total mass of the structure, which is 33 tn in real scale. The value of the vertical factor of safety for each footing tested was calculated using Meyerhof's formula for the bearing capacity of rectangular footings.

$$N_q = e^{\pi \times \tan \varphi} \times \frac{1 + \sin \varphi}{1 - \ sin \ \varphi}$$

$$N_c = \frac{N_q - 1}{\tan \varphi}$$

$$N_g = (N_q - 1) \times \tan 1.4\varphi$$

$$s_c = 1 + 0.3 \times {}^{B}/_{L}$$

$$s_q = 1$$

$$s_g = 1 - 0.2 \times {}^{B}/_{L}$$

$$\sigma_{uv} = c \times N_c \times s_c + \gamma \times D_{emb} \times N_q \times s_q + 0.5 \times \gamma \times N_g \times B \times s_g$$

where c equals zero for sand and ϕ is approximately equal to 44^{o} in this case [Anastasopoulos, Kokkali, Tsatsis, 2011].

The width of the footings tested varies between the width of the conventionally designed footing for the retrofitting wall (B = 6m) and the existing footing of the column (B = 1.5m), while the value of the FSv ranges from 55 to 14 respectively. The transverse dimension of the footing remained constant and equal to 1.5 m.

Whereas the footings of 6m and 3.5m width were formed by attachment of separate, additional parts laterally to the existing column footing (Index A), a different methodology was applied for further reduction of the footing width. Due to the significantly improved seismic behavior of the structure in the second case (B = 3.5m), the reduced footing remained and plates of different width (b) and height (t) were attached on its bottom, symmetrically to the center of the shear wall. That way, the footing is allowed to rock during the shaking, thanks to its reduced width, but additional settlement and rotation are restrained by the wider footing when the latter touches the soil. Once the rotation angle of the system exceeds a critical value, the upper part of this “hybrid” contacts the soil and starts mobilizing its strength and ductility. That value of rotation angle, θ_{con}, depends on the width and thickness of the added plate.

The system that was tested consisted of both retrofitting walls for balancing purposes. The mass - inducing steel plates were evenly distributed between the three storeys. The walls were rigidly connected with the steel plates and the artificial plastic hinges at the base of the walls were prevented from rotating, thus creating a rigid block. The model was placed on

dense sand as previously described. The horizontal displacement was applied by the pushover apparatus close to the center of mass of the model, below the second storey. Six wired displacement transducers were used to measure the displacement that was imposed, the settlements of both footings and the sliding of the system (Figure 2.11). A load cell was attached to the pushover apparatus and measured the reaction force throughout the test (Figure 2.12).

Figure 2.13 illustrates the three types of footings that were tested during this series. Figures 2.14 – 2.18 depict the monotonic curves derived from the pushover tests. All results ere presented in prototype scale. At first, the conventionally designed system was tested monotonically. Due to the large bending capacity of the soil – foundation system, it developed a failure mechanism through sliding long before reaching soil failure. Afterwards, sliding was prevented in order to measure the bending capacity of the system (Figure 2.14). The behavior of this system under slow cyclic loading was not tested due to its type of failure. Afterwards, all systems with reduced foundation were tested under both monotonic and slow cyclic loading. Figure 2.14 also includes the $M - \vartheta$ curve for the rocking isolated alternative. In this case, the failure occurs in the soil as expected.

Figures 2.15 – 2.18 depict the calculated bending moment at the base of the footing with regard to the rotation angle of the footing for all hybrid systems under monotonic loading. The same figures include the curves for the upper and the lower part of the footing separately. As expected, the $M - \vartheta$ curve of the hybrid footing is enveloped by the curves of the footings that constitute it. At small values of the rotation angle the upper part has no contact with the soil and only the lower part responds to loading. As the test progresses and the rotation angle increases, the upper part touches the soil, the bending moment increases and the curve tends to coincide with the curve of the upper footing. The form of the curves differs depending on the width and height of the added plate. When the rotation angle θ_{con} required for the upper part to contact the soil increases, the bending moment decreases significantly before rising again. In the cases that the additional plate is 10 cm high, the hybrid system benefits mostly in terms of plasticity rather than bending strength, since the rotation angle required for the bending moment to rise significantly is quite large. All hybrid

systems would overturn at practically the same rotation angle θ_{ult} as their upper part, but not all reach the same bending strength as it depends on the magnitude of θ_{con}.

Figures 2.19 – 2.25 depict the bending moment at the base of the footing and the settlement of the system with regard to its rotation angle, for all systems subjected to slow cyclic loading. The Figures also include the monotonic $M - \vartheta$ curve of the footing. The monotonic curve of the reduced footing (B = 3.5m) fully contains the cyclic curve (Figure 2.19), whereas the monotonic curves of the hybrid footings do not contain the cyclic curves for a small amplitude of the rotation angle (Figures 2.20 – 2.25). This can be easily explained, as the upper part of the footing contacts the soil, and therefore is loaded, for lower values of the rotation angle under cyclic loading, due to the accumulated settlement. That causes an increase in bending strength before the same happens for monotonic loading. The $w - \vartheta$ curves are not symmetric because the upper part of the footings is eccentric. It can be noticed that the accumulated settlement is of small significance for all systems, as it is lower than 3 cm after 14 cycles of gradually increasing displacement. On the contrary, the footings have the tendency to uplift, which was expected due to the large values of vertical factor of safety that they possess. The accumulated settlement slightly increases, while the maximum uplift decreases for footings of smaller width.

Figures of Chapter 2

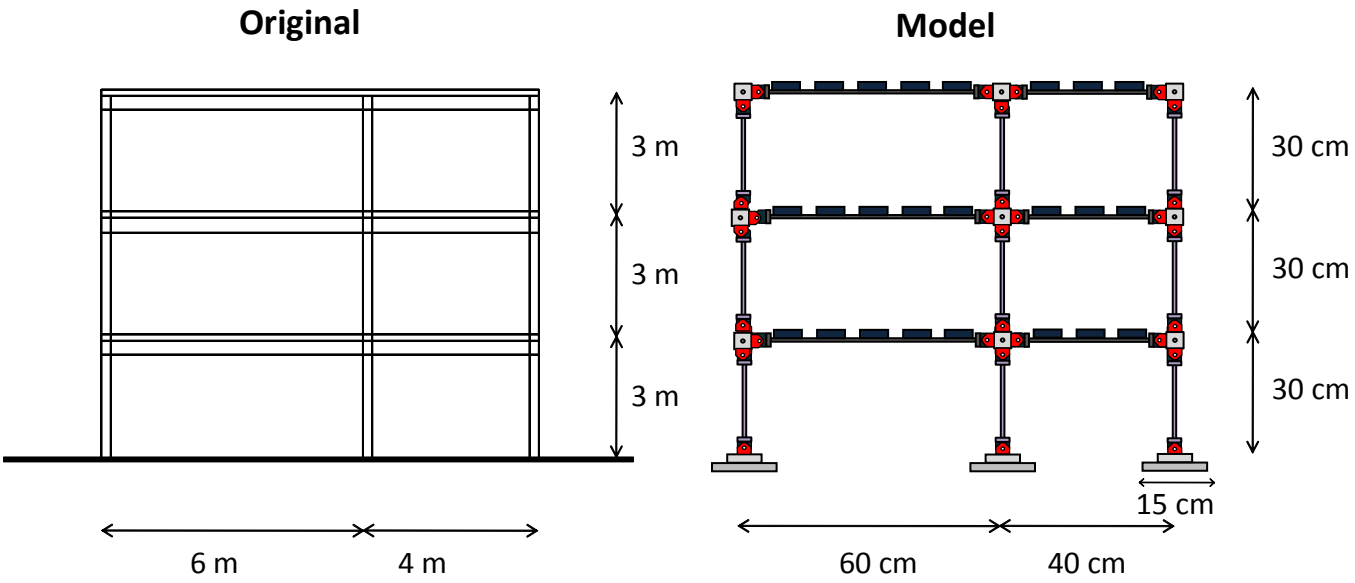

Figure 2.1 Schematic illustration of real scale frame and 2 – dimensional model.

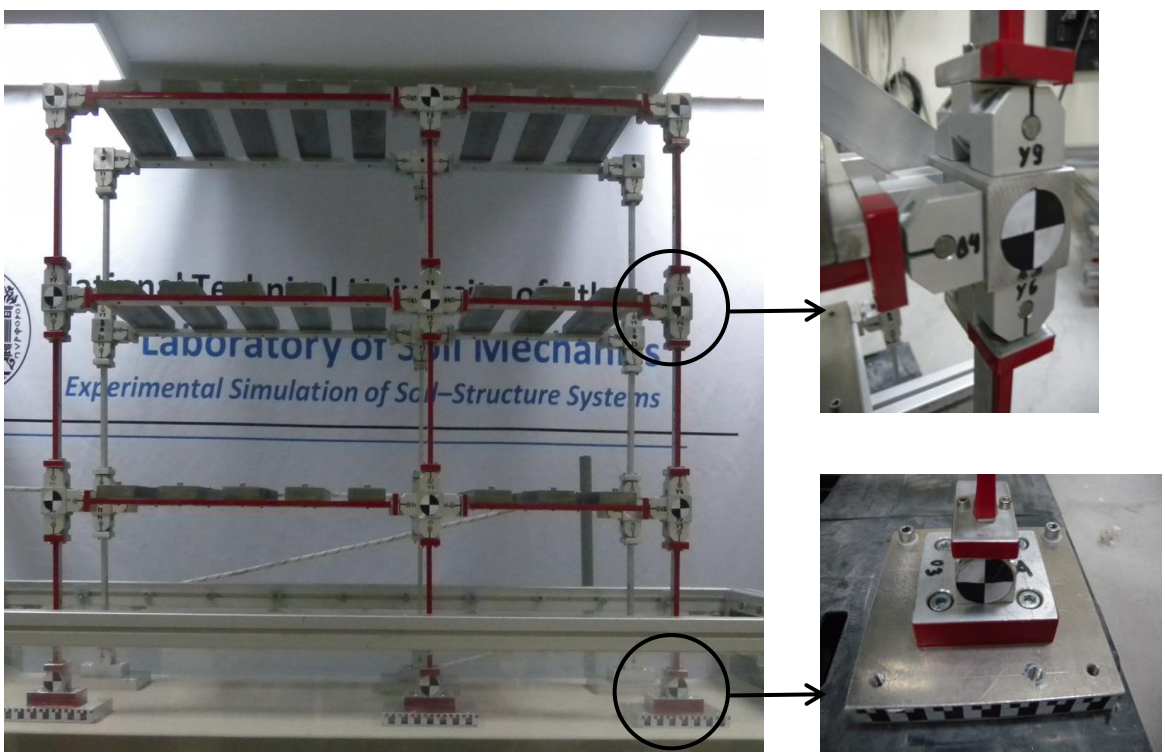

Figure 2.2 Photograph of physical model in the Laboratory of Soil Mechanics and detail of artificial plastic hinges.

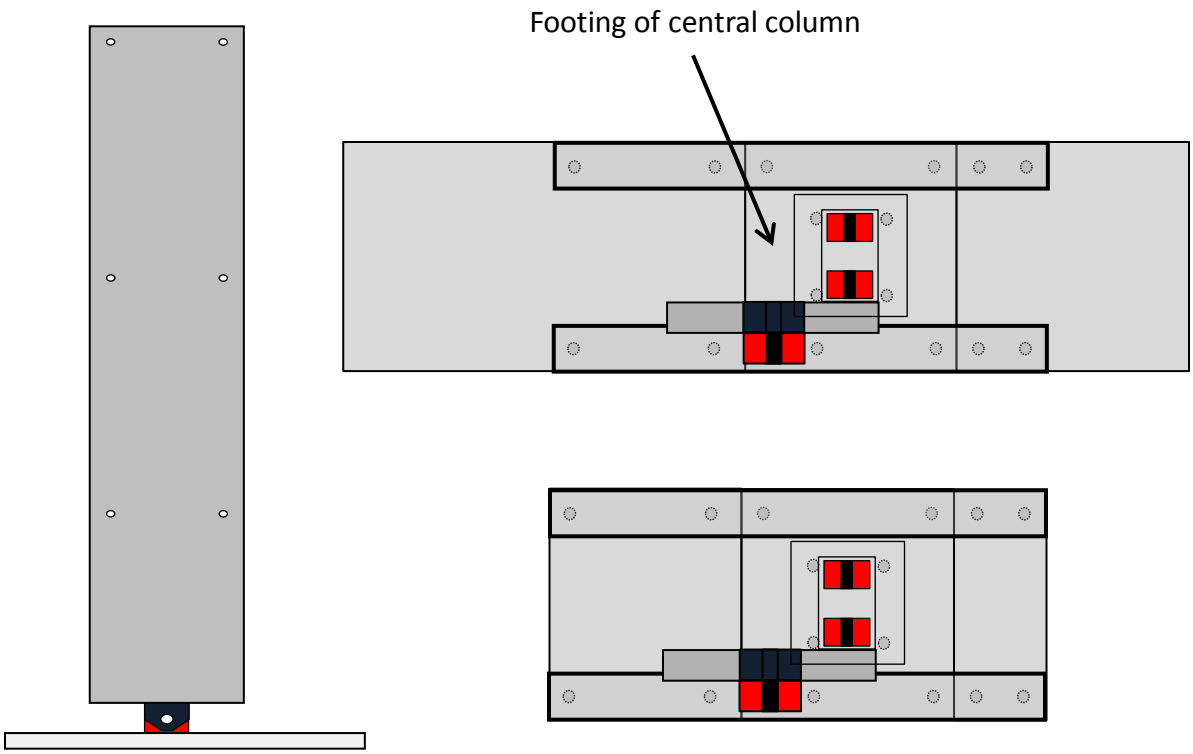

Figure 2.3 Schematic illustration of reinforcing wall and its foundation.

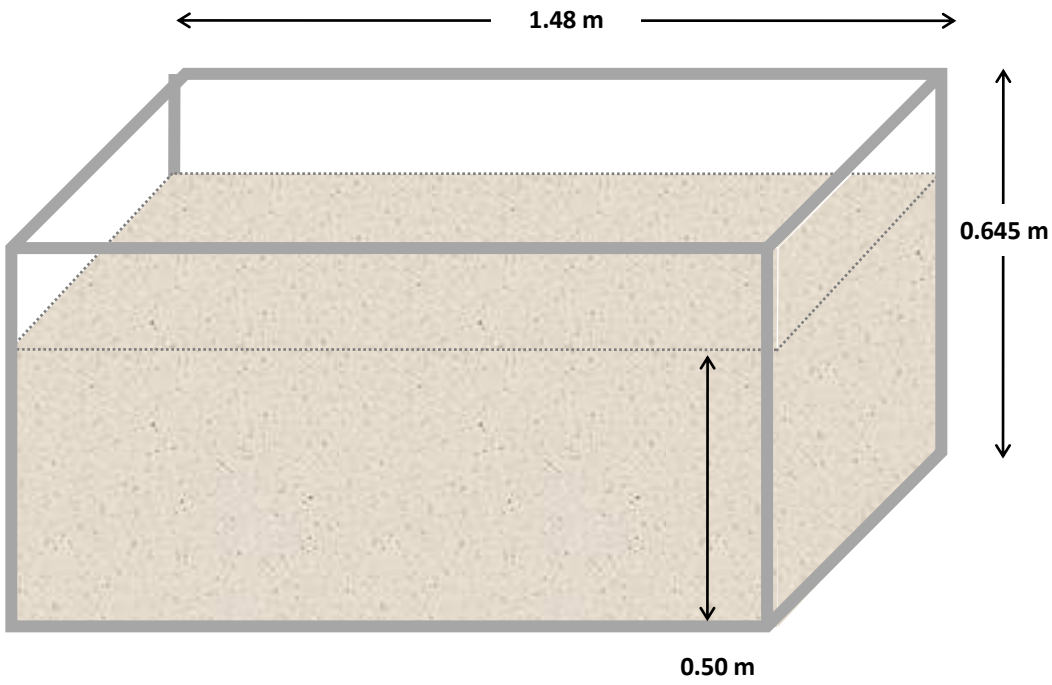

Figure 2.4 Schematic illustration of sandbox used in the experimental series.

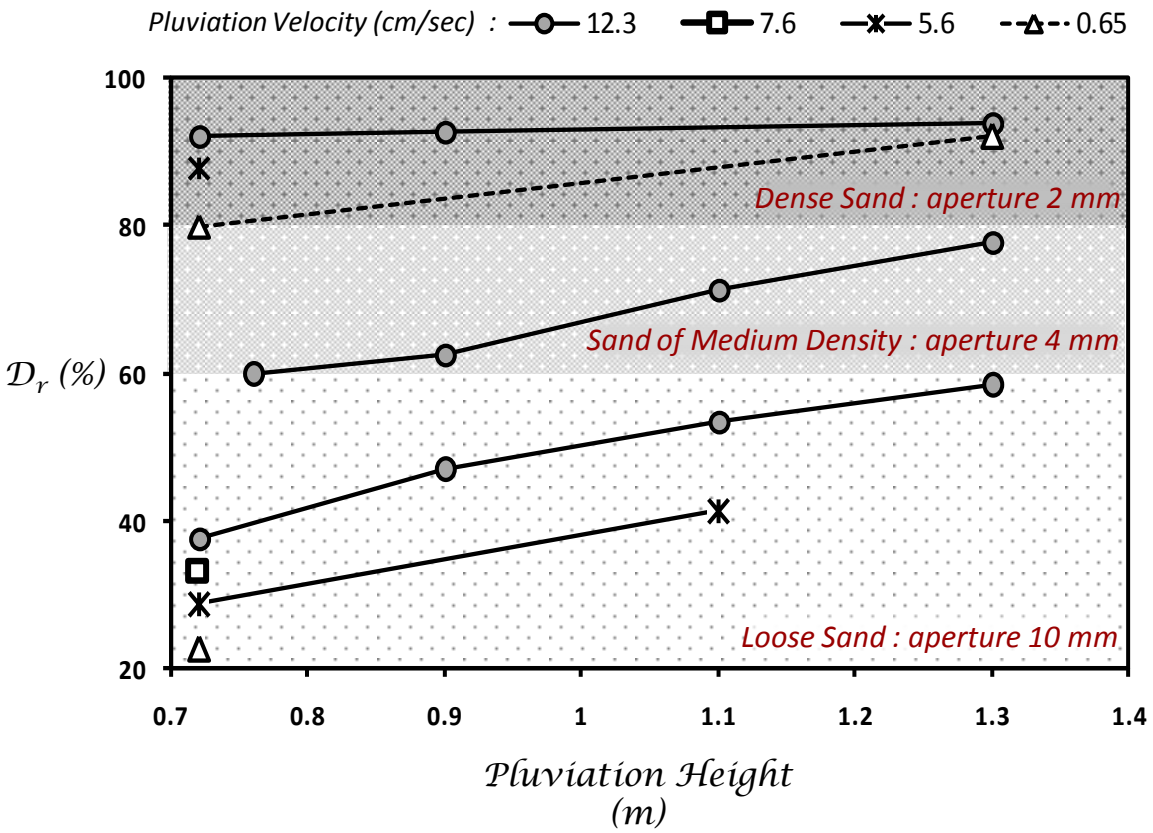

Figure 2.5 Photograph of electronically controlled sand raining system. Summary of pluviation results : relative density Dr versus pluviation height, raining speed and opening aperture size.

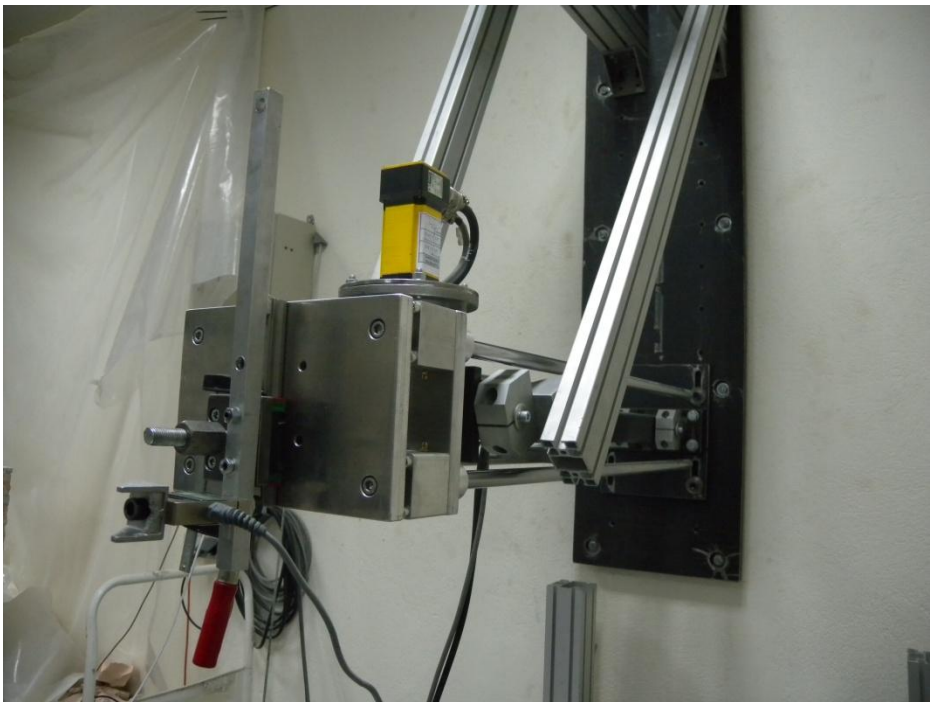

Figure 2.6 Photograph of the pushover apparatus.

Figure 2.7 Photograph of shaking table.

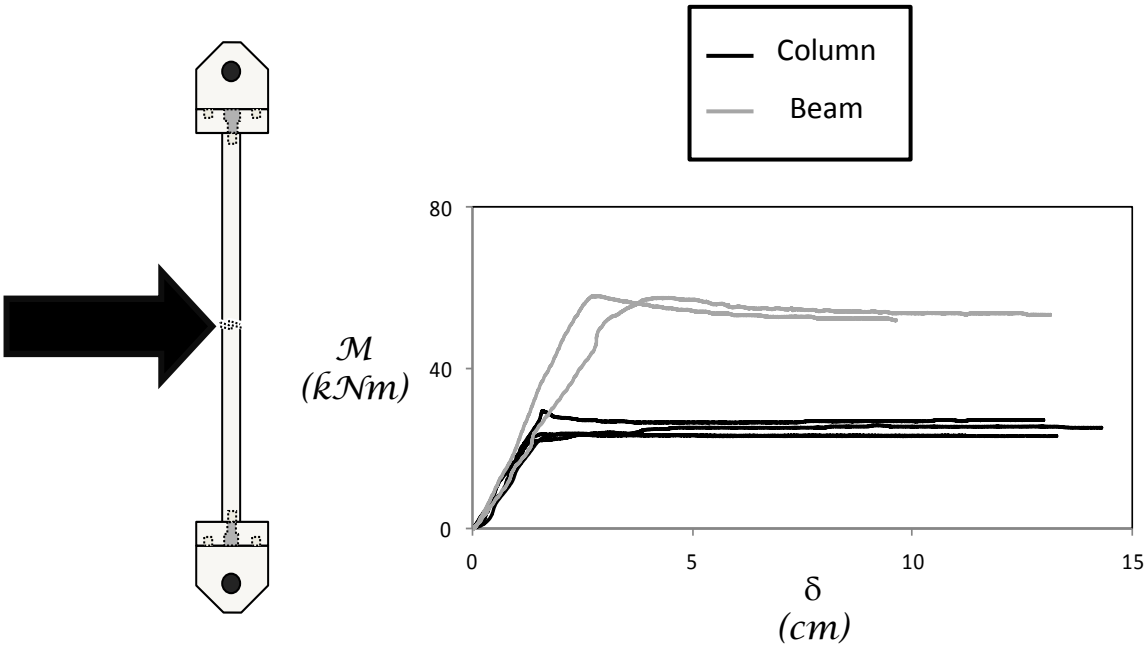

Figure 2.8 Indicative diagram of calibration of an artificial plastic hinge.

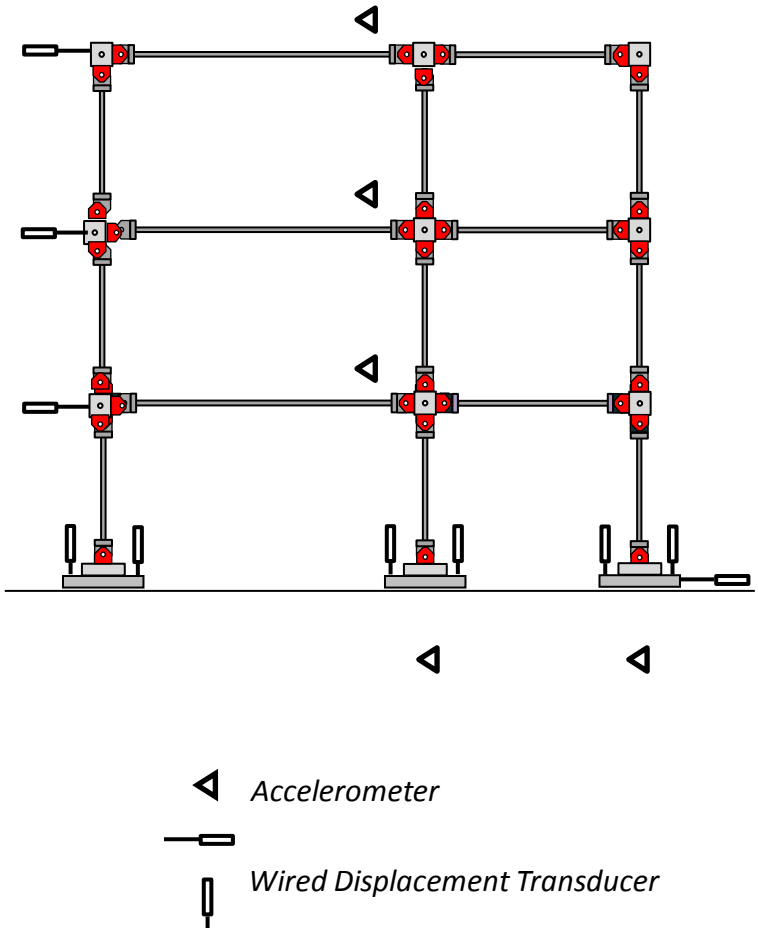

Figure 2.9 Schematic illustration of instrumentation of model.

Figure 2.10 Photograph of accelerometers and wired displacement transducers.

Table 1. List of Experiments.

Model	*Description of Experiment*					
	Experiment	**Shear wall foundation**			**Soil**	**Excitation**
		B (m)	**b (m)**	**t (m)**		
Original	1				Dense Sand	Seismic
	2					Sinusoidal
						Seismic
	35					Seismic
Retrofitted - Conventional	4	6.0	-	-	Dense Sand	Sinusoidal
						Seismic
	5	6.0	-	-		Seismic
	33	6.0	-	-		Strong Seismic
Retroffitted - Rocking Isolated	6	3.5	-	-	Dense Sand	Sinusoidal
						Seismic
	7	3.5	-	-		Seismic
	12	3.5	1.5	0.05		Seismic
	13	3.5	2.0	0.05		Seismic
	14	3.5	2.5	0.10		Seismic
	15	3.5	2.0	0.10		Seismic
	16	3.5	2.0	0.10		Seismic
	17	3.5	2.0	0.10		Strong Seismic
	18	3.5	2.5	0.10		Strong Seismic
	19	3.5	2.5	0.05		Seismic
	20	3.5	2.5	0.05		Strong Seismic
	21	3.5	3.0	0.05		Seismic
	22	3.5	3.0	0.05		Strong Seismic
	27	3.5	2.0	0.05		Strong Seismic
Retroffitted - Rocking Isolated with fixed tie beams	25	3.5	3.0	0.05	Dense Sand	Strong Seismic
Retroffitted - Rocking Isolated with hinged tie beams	23	3.5	3.0	0.05	Dense Sand	Strong Seismic
	24	3.5	3.0	0.05		Seismic
	26	3.5	2.5	0.05		Strong Seismic

Table 2. List of applied seismic records.

Seismic Records
Moderate Intensity Seismic Records
MNSA (Athens 1999)
Lefkada (2003)
Aegion (1995)
Kalamata (1986)
Sakarya (Kocaeli 1999)
Strong Seismic Records
JMA (Kobe 1995)
Rinaldi (Northridge 1994)
Takatori (Kobe 1995)

Table 3. List of Horizontal Pushover tests.

PUSHOVER TESTS					
Foundation Properties				**Description of Experiment**	
B (m)	**b (m)**	**t (m)**	**FSv**	**Soil**	**Type of Loading**
6.0	-	-	55	Dense Sand	Monotonic
6.0	2.5	0.15	32	Dense Sand	Monotonic
3.5	-	-	50	Dense Sand	Monotonic
					Slow Cyclic
3.5	3.0	0.05	42	Dense Sand	Monotonic
					Slow Cyclic
3.5	2.5	0.05	32	Dense Sand	Monotonic
					Slow Cyclic
3.5	2.5	0.10	32	Dense Sand	Monotonic
					Slow Cyclic
3.5	2.0	0.05	23	Dense Sand	Monotonic
					Slow Cyclic
3.5	2.0	0.10	23	Dense Sand	Monotonic
					Slow Cyclic
3.5	1.5	0.05	14	Dense Sand	Monotonic
					Slow Cyclic

Horizontal Pushover for Shear Wall Footings

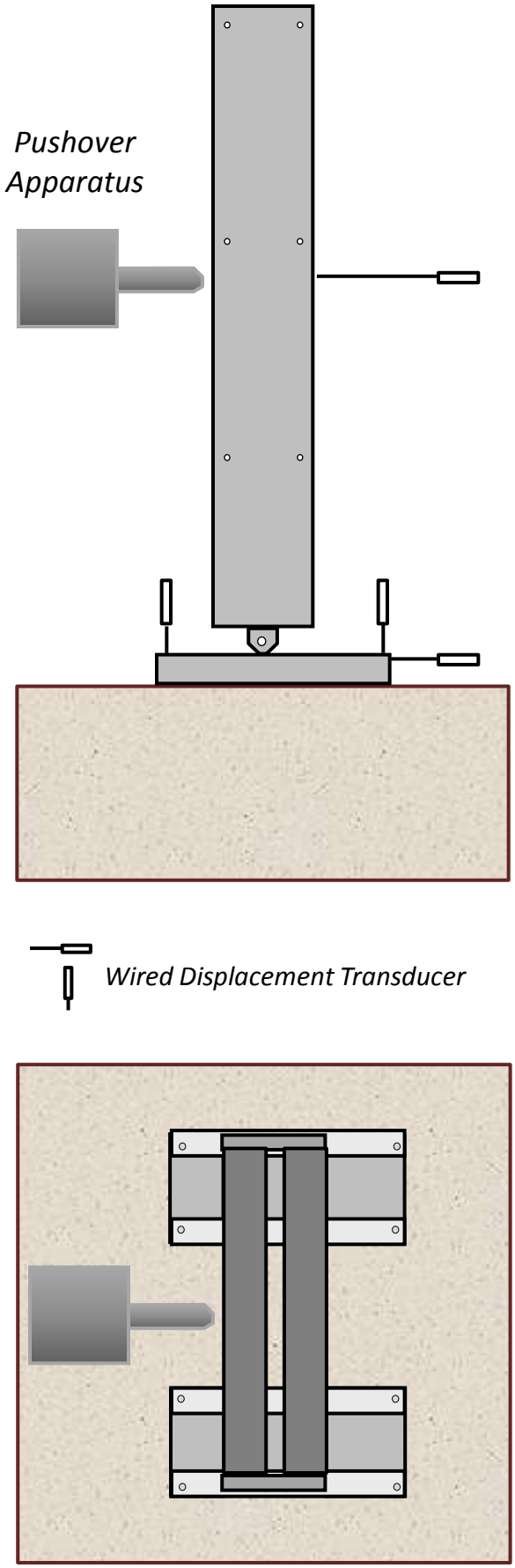

Figure 2.11 Schematic illustration of pushover tests and instrumentation.

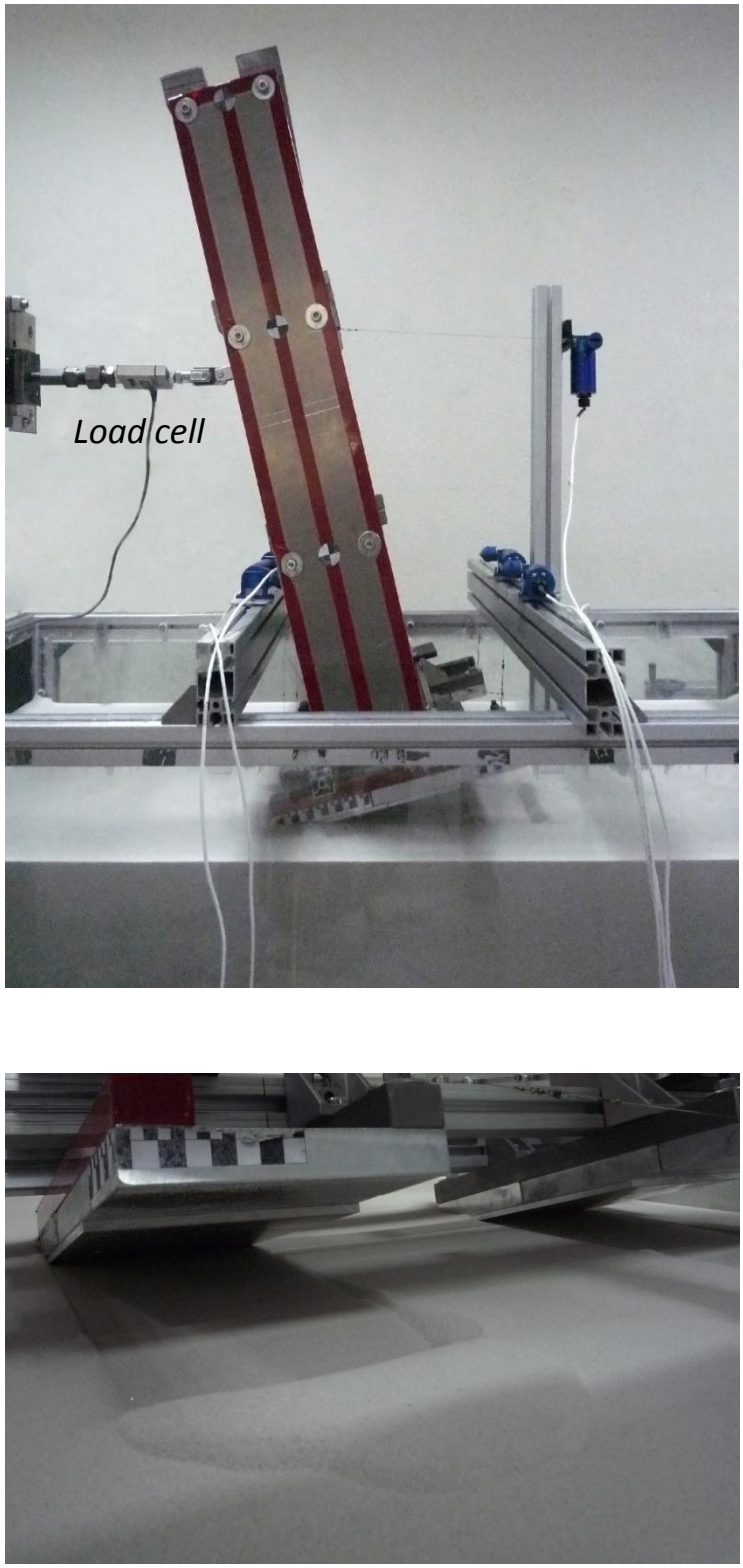

Figure 2.12 Photographs of model during a pushover test.

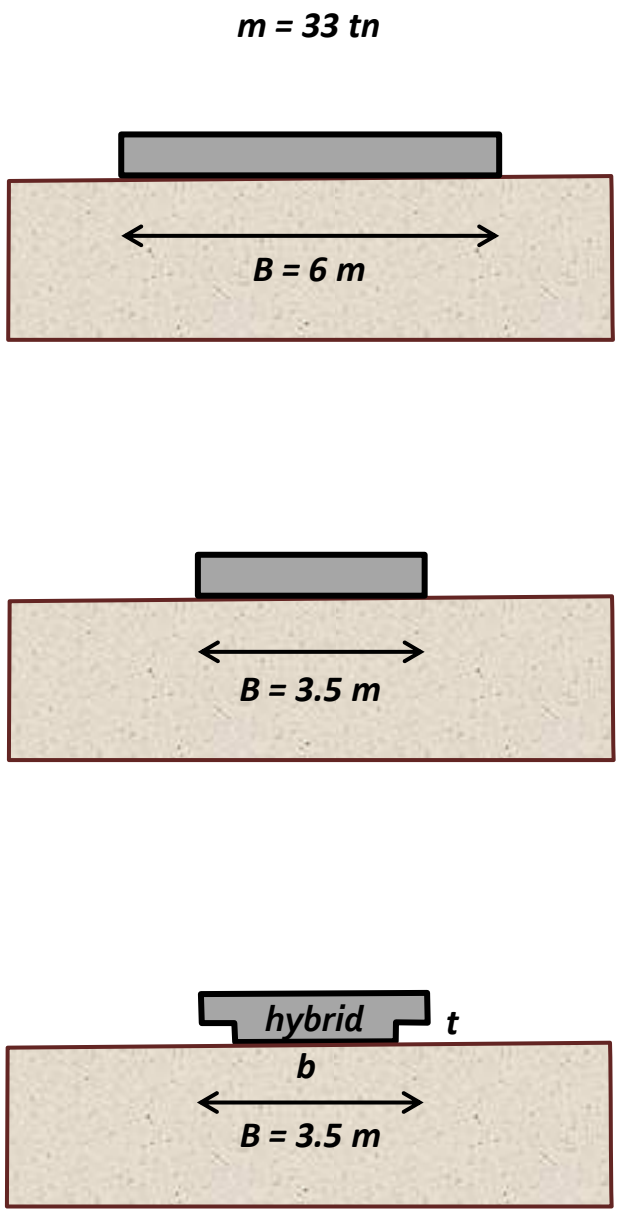

Figure 2.13 Schematic illustration of systems tested.

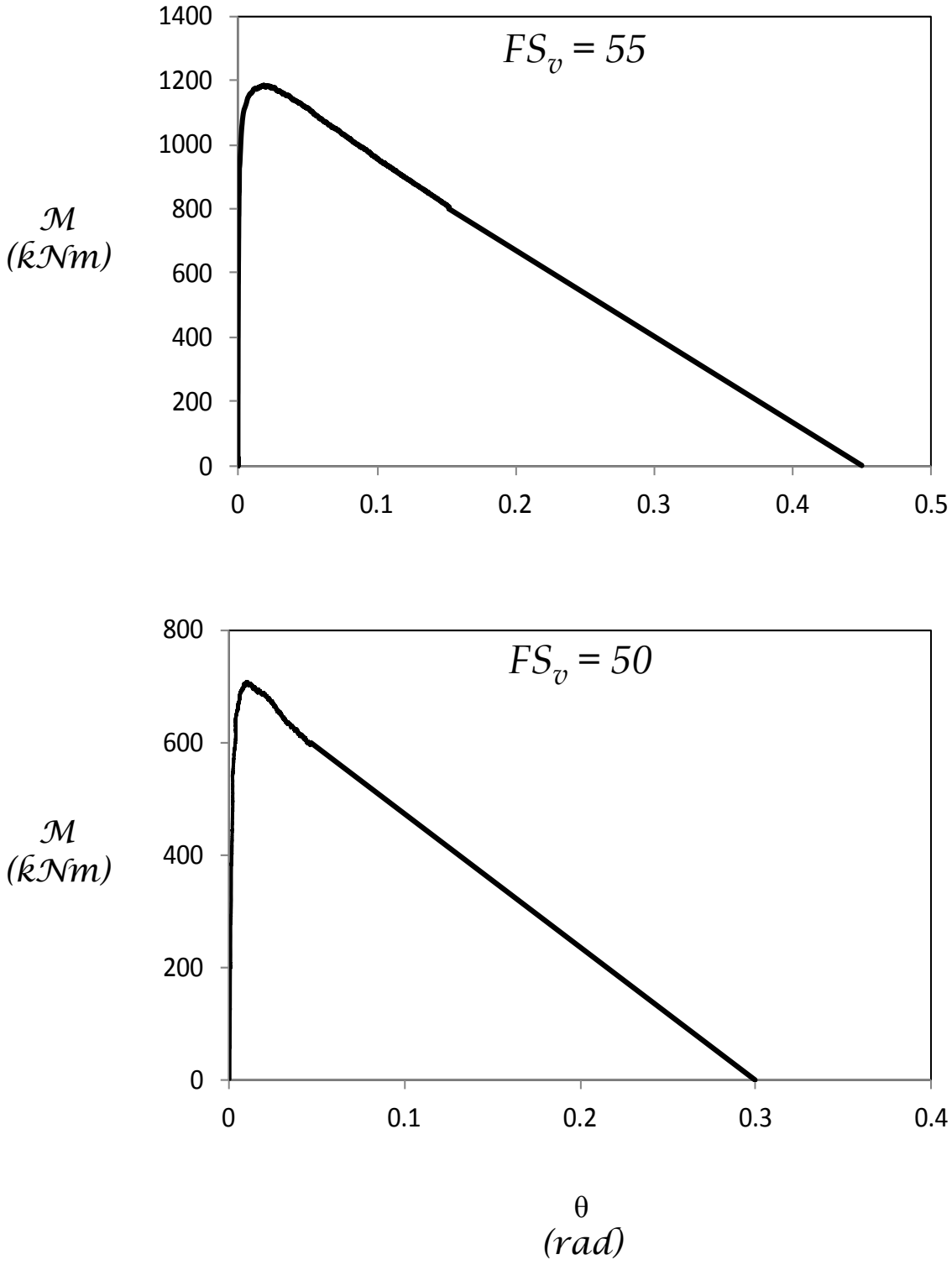

Figure 2.14 Diagrams of bending moment with respect to rotation angle derived from monotonic pushover testing for footings with B = 6m and B = 3.5m.

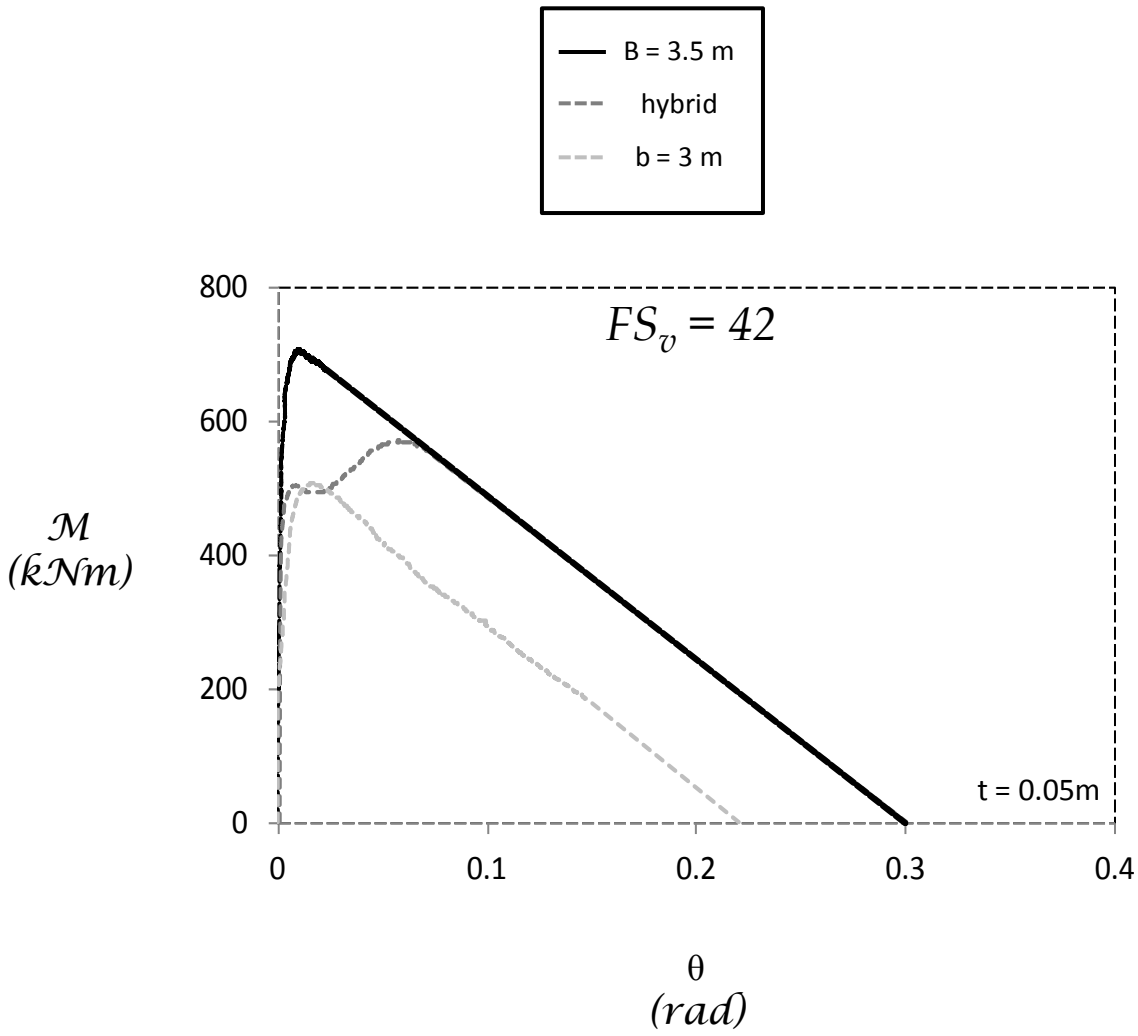

Figure 2.15 Diagram of bending moment with respect to rotation angle derived from monotonic pushover testing for the hybrid footing with b = 3m and t = 0.05m.

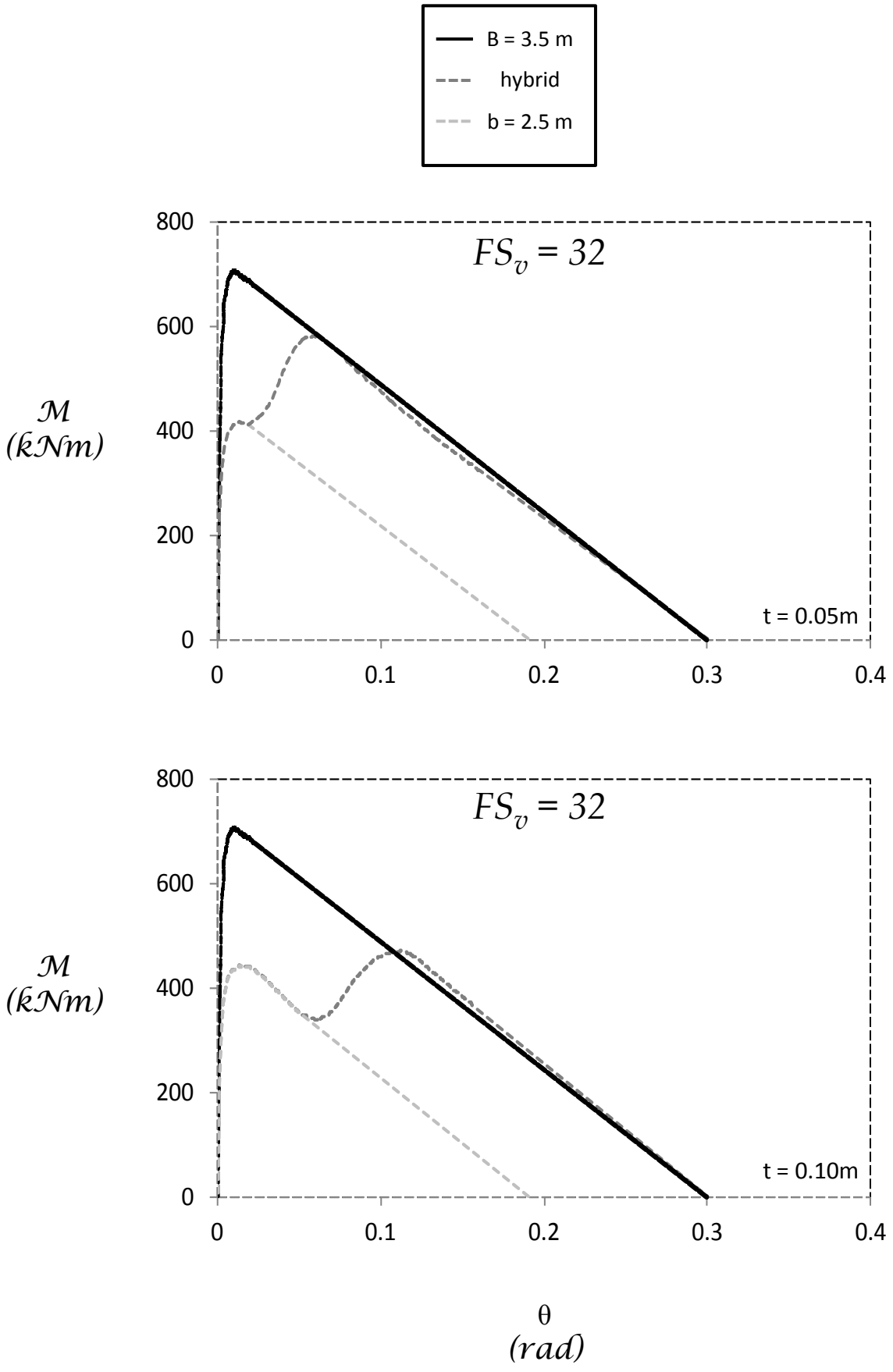

Figure 2.16 Diagrams of bending moment with respect to rotation angle derived from monotonic pushover testing for the hybrid footings with b = 2.5m, with t = 0.05m and t = 0.10m respectively.

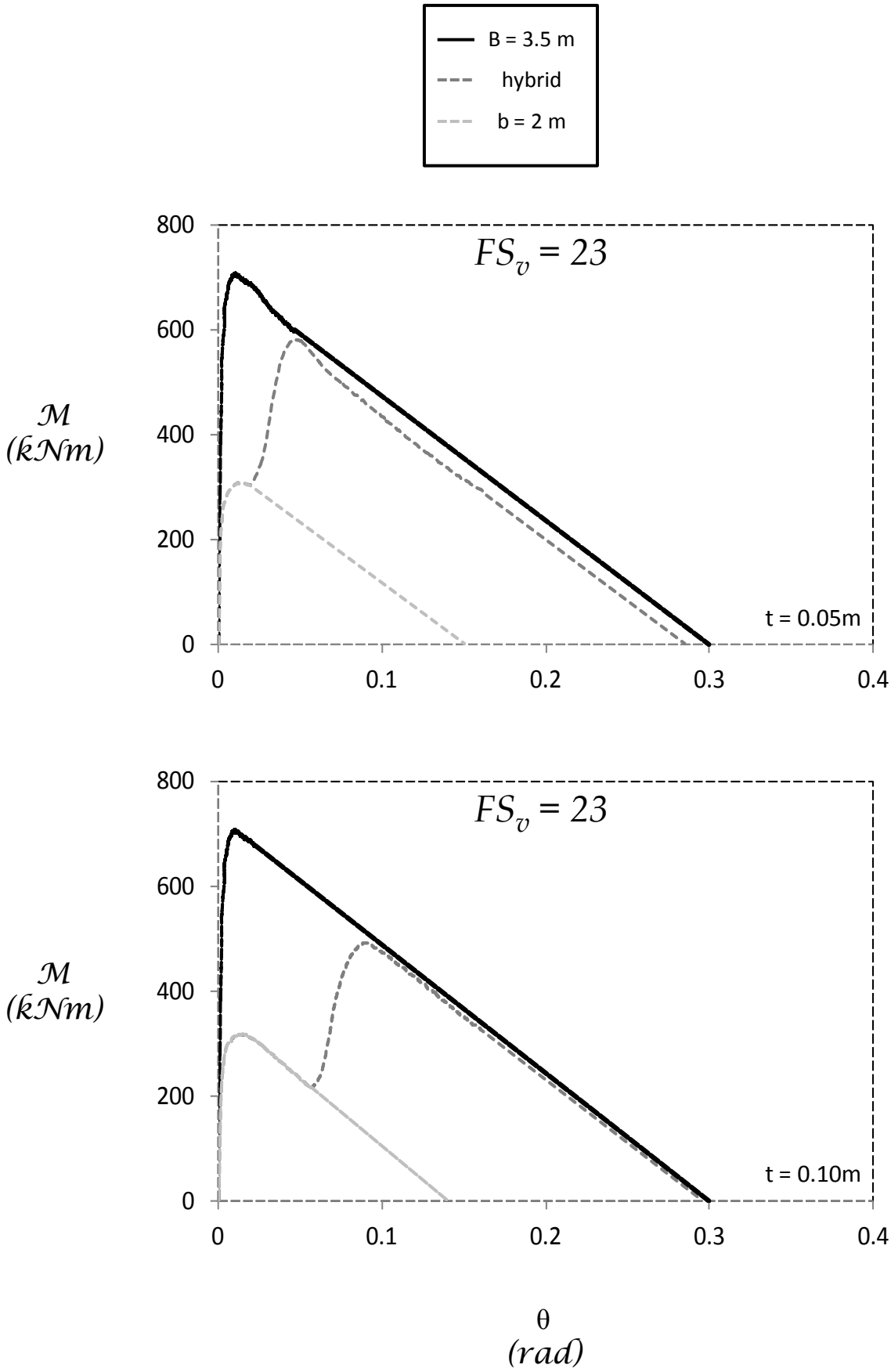

Figure 2.17 Diagrams of bending moment with respect to rotation angle derived from monotonic pushover testing for the hybrid footings with b = 2m, with t = 0.05m and t = 0.10m respectively.

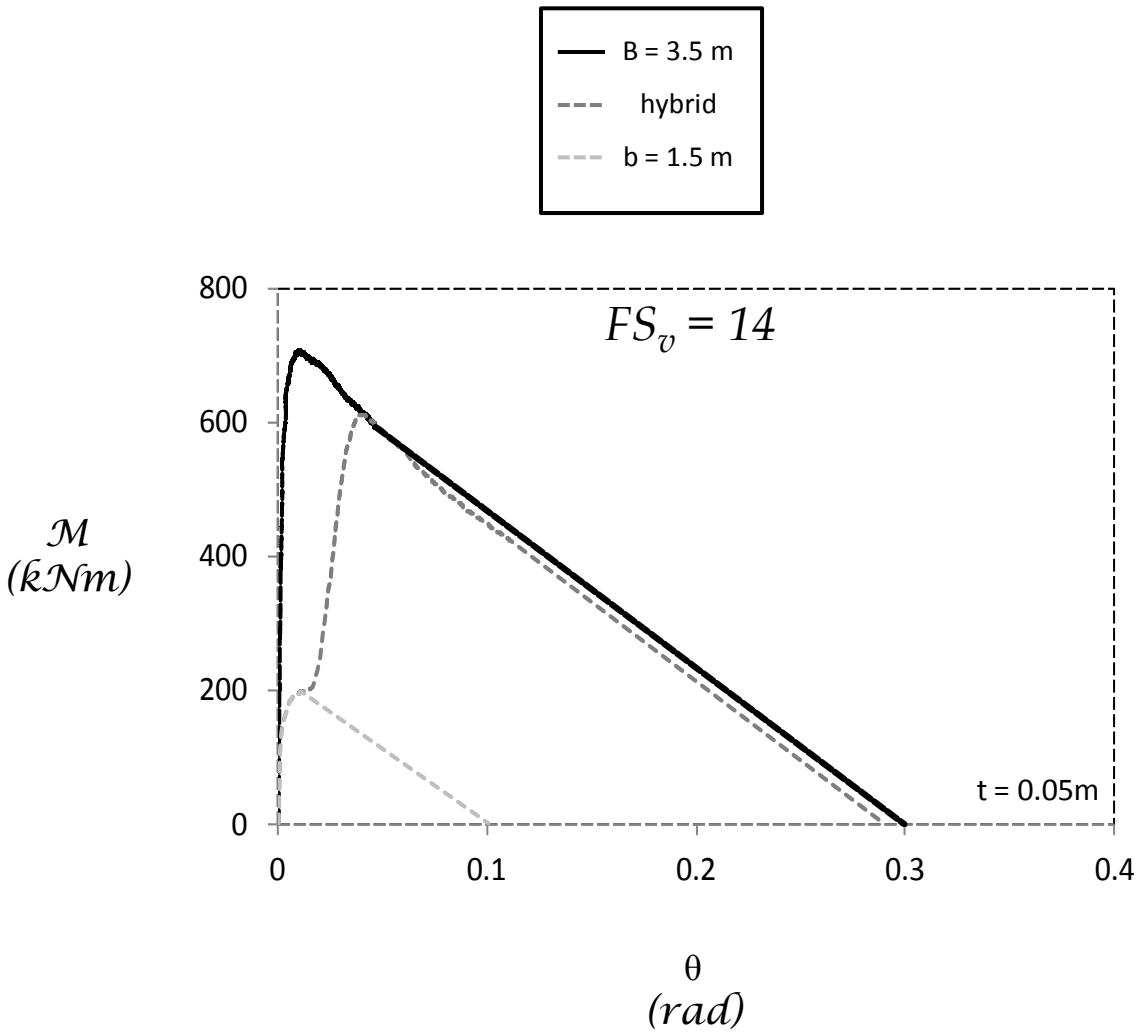

Figure 2.18 Diagram of bending moment with respect to rotation angle derived from monotonic pushover testing for the hybrid footing with b = 1.5m and t = 0.05m.

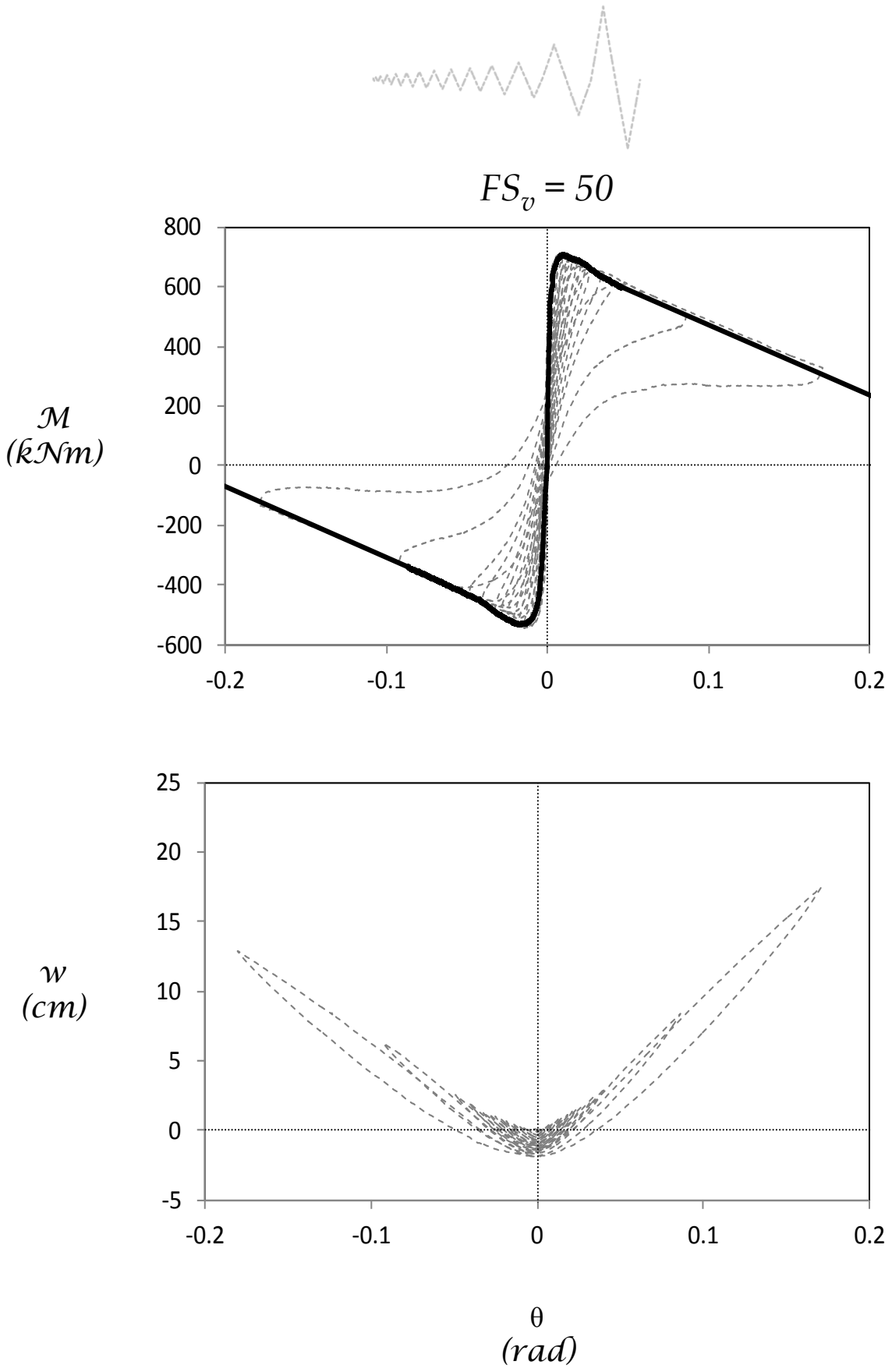

Figure 2.19 Diagrams of bending moment and settlement with respect to rotation angle derived from slow cyclic pushover testing for the footing with B = 3.5m.

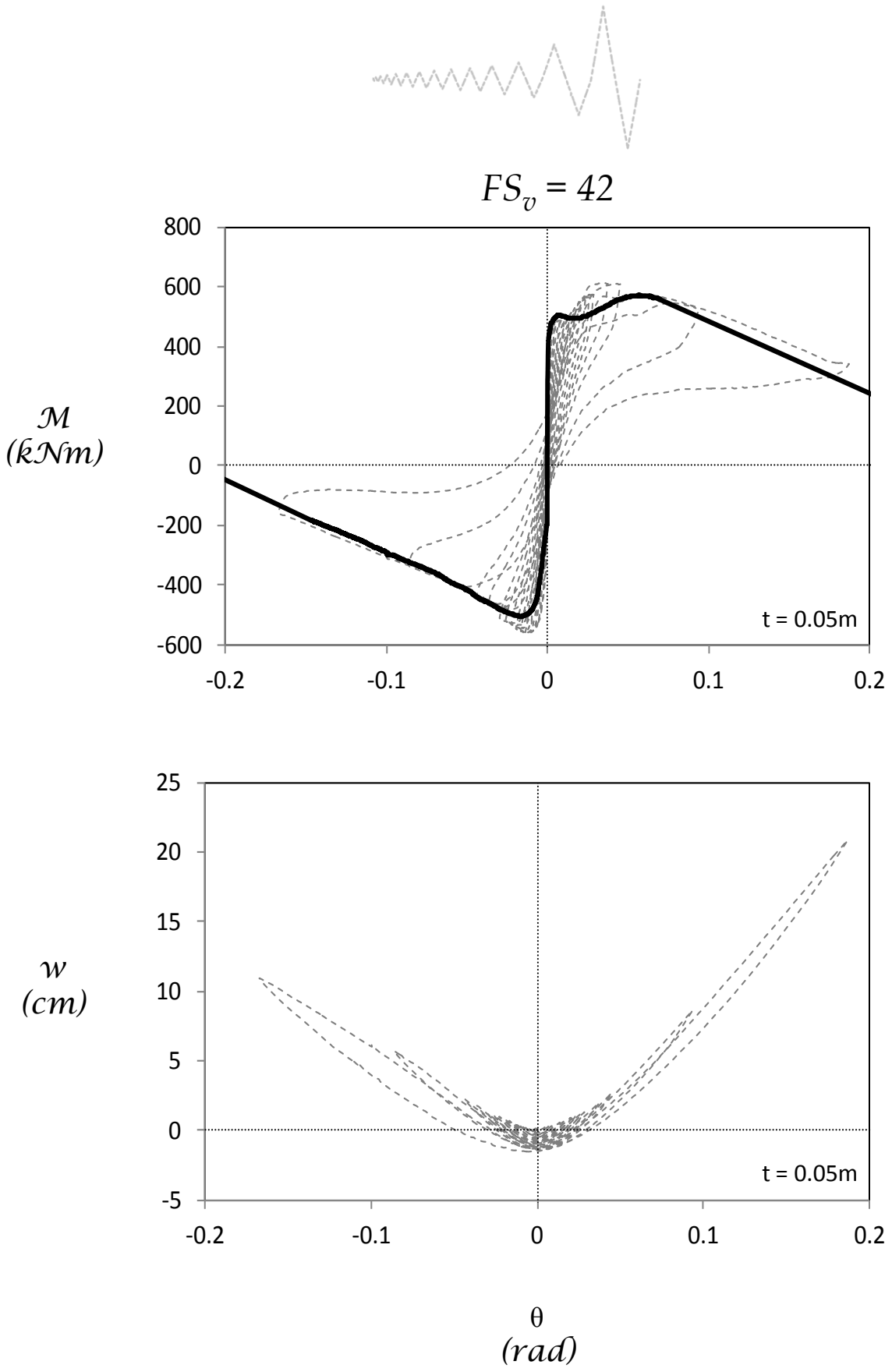

Figure 2.20 Diagrams of bending moment and settlement with respect to rotation angle derived from slow cyclic pushover testing for the hybrid footing with b = 3m and t = 0.05m. 44

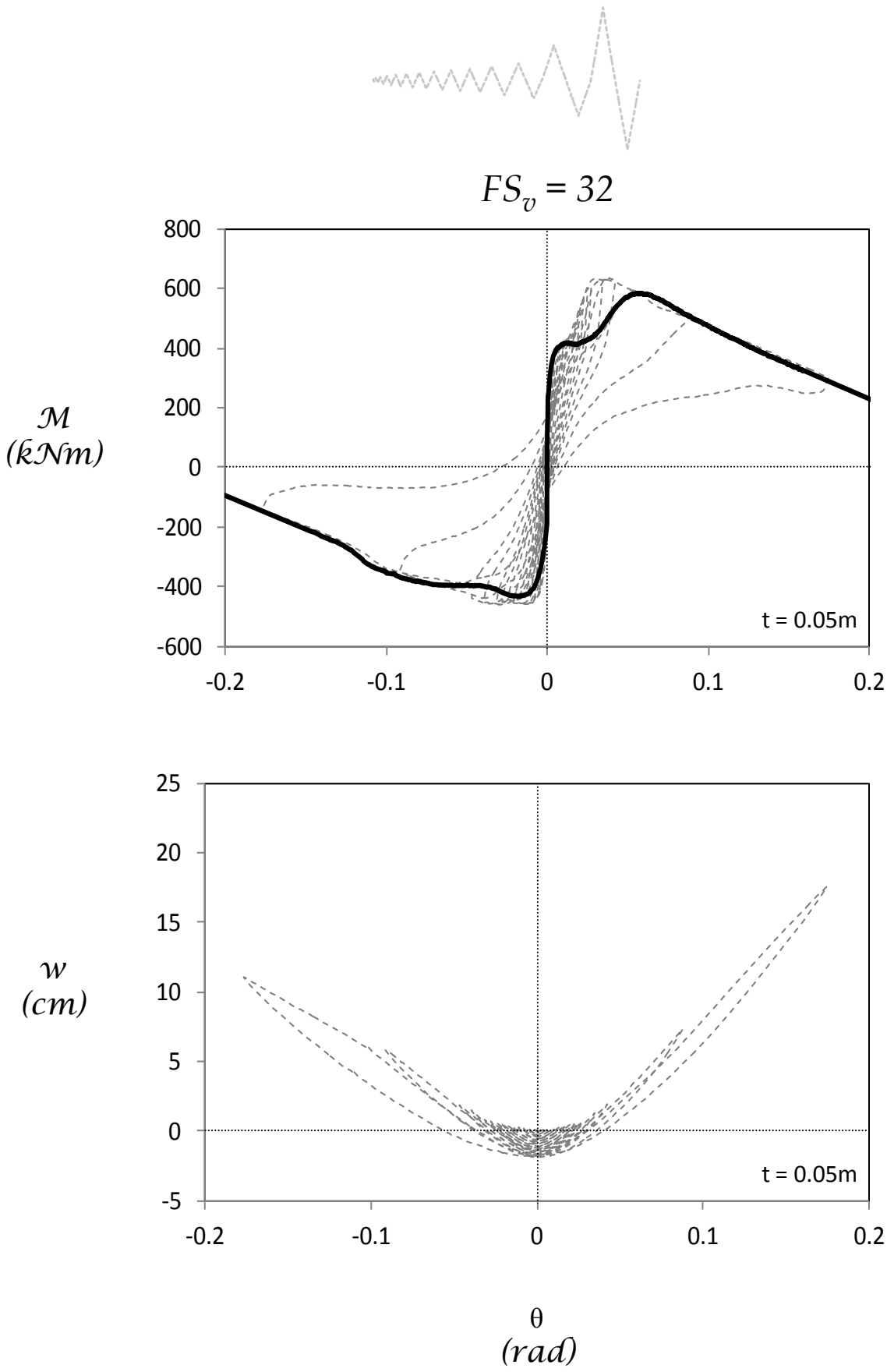

Figure 2.21 Diagrams of bending moment and settlement with respect to rotation angle derived from slow cyclic pushover testing for the hybrid footing with b = 2.5m and t = 0.05m.

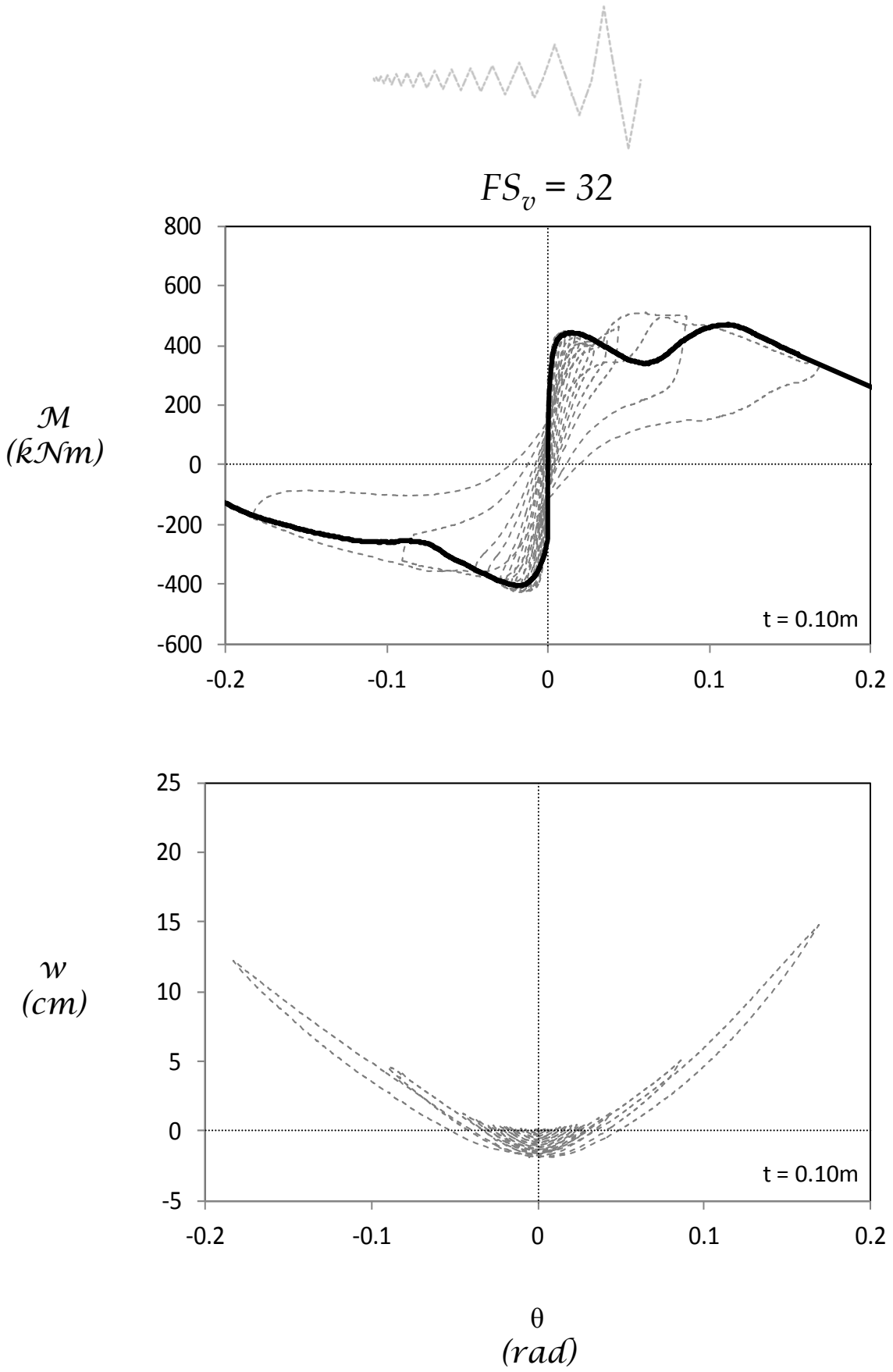

Figure 2.22 Diagrams of bending moment and settlement with respect to rotation angle derived from slow cyclic pushover testing for the hybrid footing with b = 2.5m and t = 0.10m.

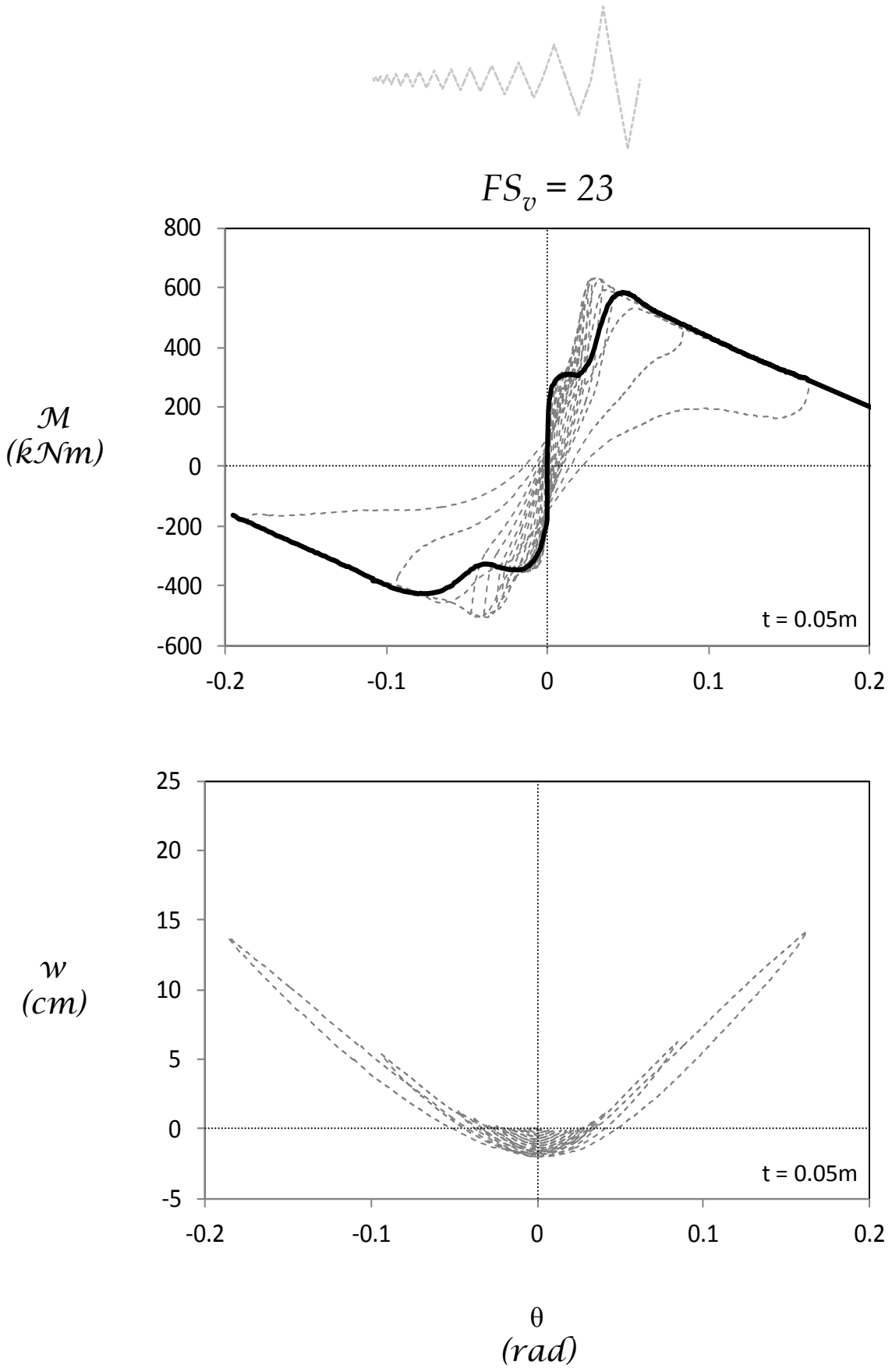

Figure 2.23 Diagrams of bending moment and settlement with respect to rotation angle derived from slow cyclic pushover testing for the hybrid footing with b = 2m and t = 0.05m.

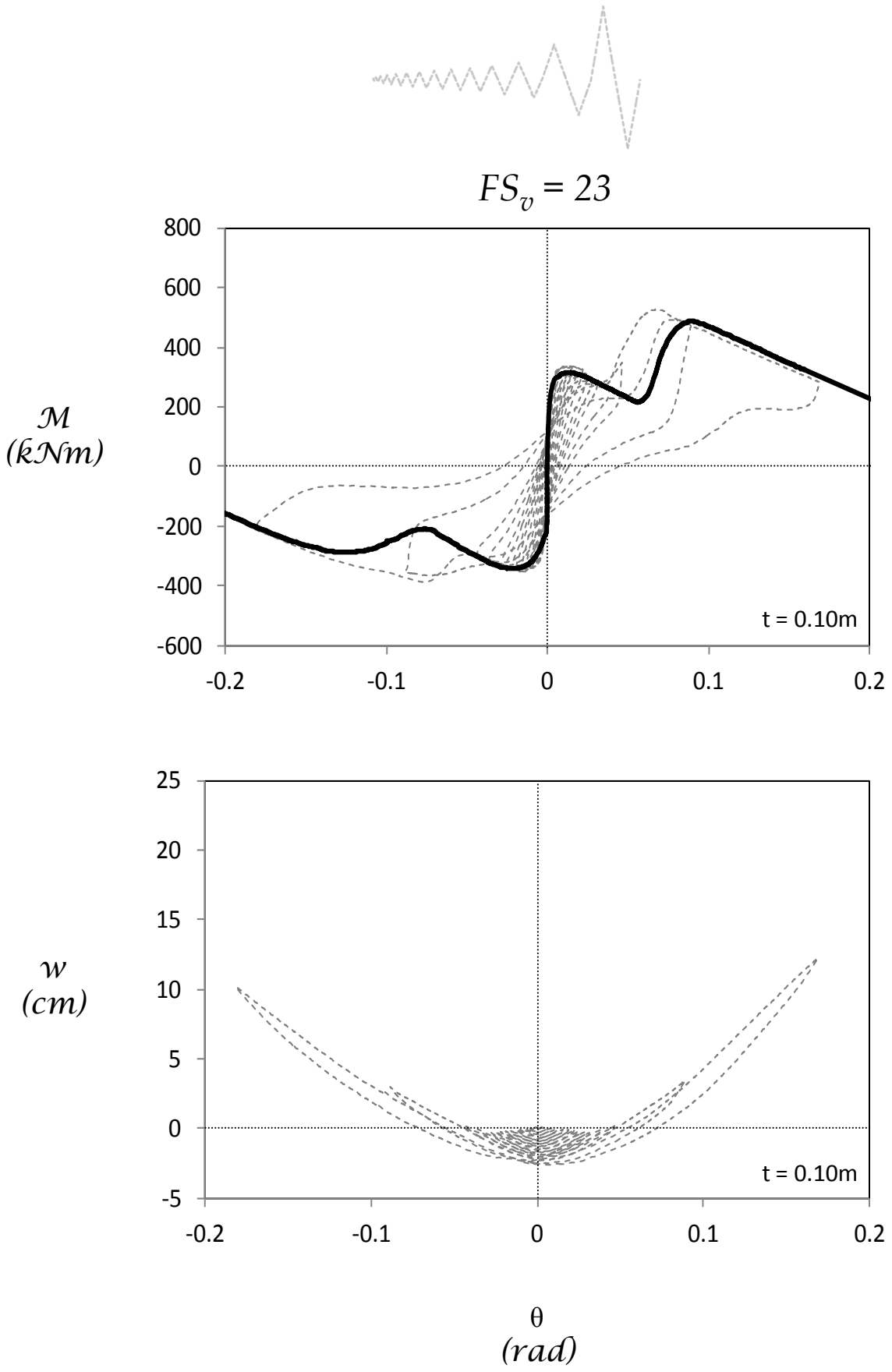

Figure 2.24 Diagrams of bending moment and settlement with respect to rotation angle derived from slow cyclic pushover testing for the hybrid footing with b = 2m and t = 0.10m.

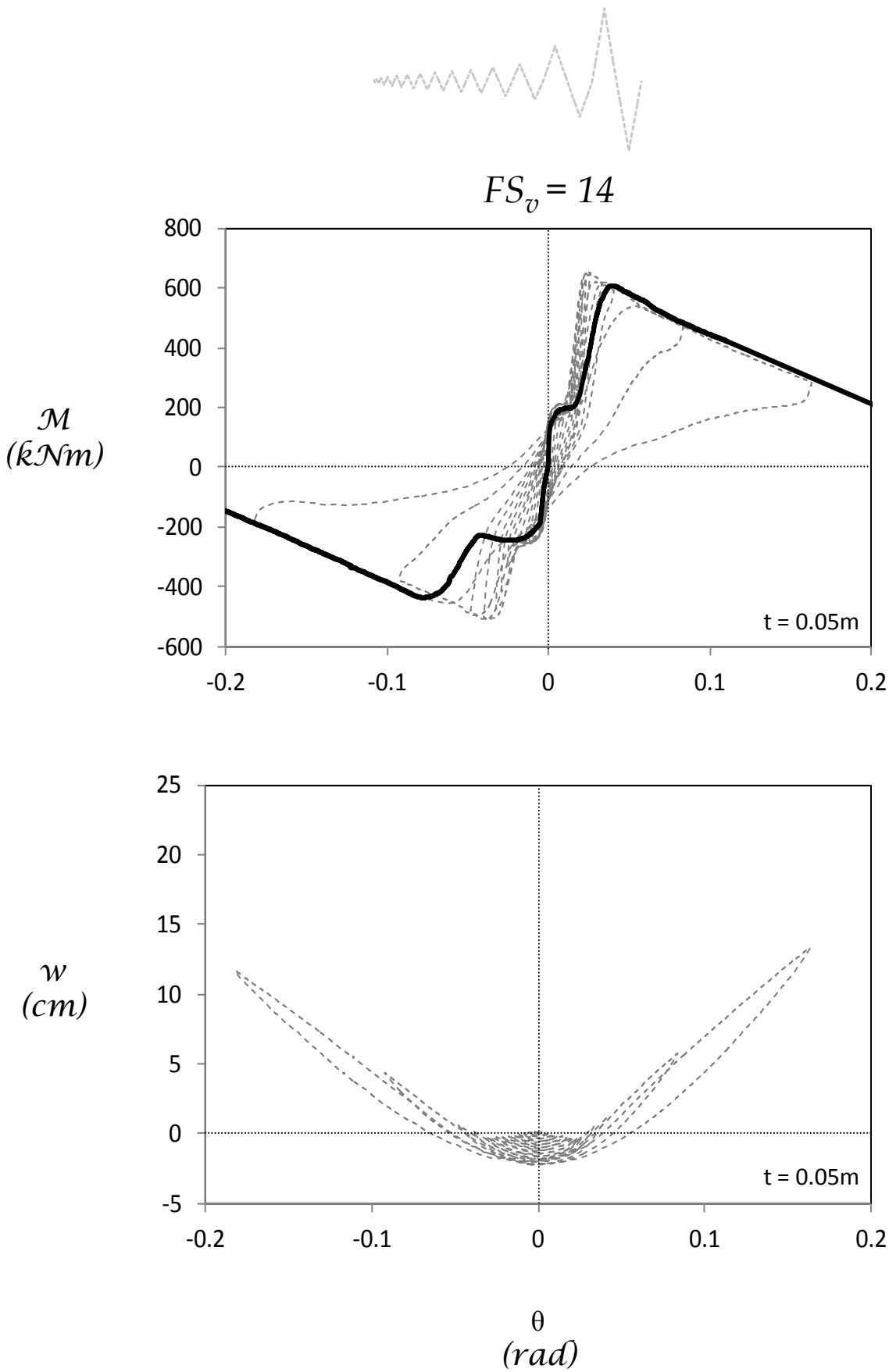

Figure 2.25 Diagrams of bending moment and settlement with respect to rotation angle derived from slow cyclic pushover testing for the hybrid footing with b = 1.5m and t = 0.10m.

3

Performance of the Original and Retrofitted Building

3. PERFORMANCE OF THE ORIGINAL AND THE RETROFITTED BUILDING

First, the cases of the building before and after being retrofitted with the RC wall are examined. The structure is subjected to a sequence of real seismic records and the results are presented in terms of measured acceleration and inter – storey differential displacement (drift and drift ratio). The results for the full sequence are presented in Appendix B for all the systems that are mentioned. The fact that the soil amplifies the imposed excitation was noticed and therefore the acceleration measured in a small depth from the surface of the soil is also displayed in all cases. It is worth mentioning that the SD spectra for the real seismic records and the accelerograms imposed by the shaking table were compared for all motions and the deviation was negligible.

3.1 Original Building

For the building prior to the retrofit the cases of the Aegion and the Lefkada 2003 records are selected as representative. Both records are of low to moderate intensity, but exceed the capacity of the structure. The failure mechanism is visible and, as expected; a soft storey is formed in the base storey as shown in Figure 3.1 that depicts the initial and deformed structure after being submitted to the record of Kalamata. That demonstrates the fact that the artificial plastic hinges were calibrated correctly and respond as desired.

Figures 3.2 and 3.3 depict the response of the building to the record of Aegion. It is clear that the displacement of the first storey is larger than those of the two other storeys, revealing that plastic deformation is localized in the first floor columns. The residual drift ratio of the first storey is approximately equal to 1 %, whereas the respective values for the second and third storey are 0.5 and 0 %.

Similarly, Figures 3.4 and 3.5 include the measured accelerograms and drifts for the record of Lefkada, with a maximum acceleration of 0.43g on the bedrock. The model could not

sustain this record and collapsed, having already accumulated deformations by the previously induced seismic records of Aegion and Kalamata. It is evident that the first storey displays an abrupt increase in displacement and the upper storeys follow as the building collapses. Unrealistically large values of acceleration were measured on the structure simultaneously to the sudden rise in drifts, due to the progressing failure.

The response of the foundation remained strictly elastic during the test, in accord with conventional capacity design principles (the foundation has to be stronger than the column). As a result, the settlement and rotation of all footings was practically negligible.

In accord with the SPEAR project, it is concluded that the original (un-retrofitted) structure is insufficient in terms of strength and ductility, being unable to survive even seismic motions of (relatively) moderate intensity. This conclusion is not only consistent with the SPEAR test results, confirming the equivalence of the reduced-scale model tested herein, but also compares well with reality: many such buildings sustained major damage or collapsed during the aforementioned (M ≈ 6) earthquakes in Greece. Retrofitting is therefore considered necessary, in order to increase its seismic resistance and increase the safety margins against collapse.

3.2 Retrofitted Building

3.2.1 *Performance under moderate seismic shaking*

As already mentioned, the selected way of retrofit is via a RC wall, added in the middle of the three – storey frame and along the height of the middle column. The retrofitting wall is designed according to Greek regulations (KAN.EPE.). A design coefficient A = 0.24 g is assumed as the retrofit target, yielding design acceleration Φ_d = 0.20 g assuming a behavior factor q = 3. The retrofitted structure is expected to sustain seismic motions of higher magnitude and simultaneously respond in a more ductile manner. Besides from the increase in strength and ductility, the addition of the shear wall will homogenize the lateral deformation of the structure (acting as a kinematic constraint), leading to a more uniform

damage distribution in all three storeys and prohibiting the development of a soft-storey collapse mechanism.

The strengthened frame is displayed in Figure 3.6, in its initial undeformed state as well as after being submitted to the record of Kalamata. The deformed shape of the building has altered completely, since it now follows the displacements of the shear wall, which is much stronger than the columns. As a result, the previously displayed, brittle soft storey collapse is prevented as desired.

Indeed, its response is very satisfactory, as is demonstrated by Figures 3.7 – 3.10 for the records of Aegion and Lefkada (2003). It is visible that the storey drifts are now almost identical and therefore a more uniforn distribution of strength and stiffness is achieved. Quantitatively, the response of the building has by far improved as is depicted in Figures 3.8 and 3.10 in terms of drifts. The maximum drift ratio during the record of Aegion has decreased significantly and the residual value is practically equal to zero. However, the successfulness of the retrofit is more apparent when it is subjected to the seismic record of Lefkada. The building not only sustains the motion that caused the original structure to collapse, but also responds with a residual value of drift ratio no more than 0.3 %. Consequently, it suffers no damage from the Greek moderate seismic records it was subjected to.

Additionally, both the existing foundation of the columns and the footing of the wall respond elastically in terms of settlement and rotation (*≈0*).

Therefore, the retrofit is considered to be efficient (Figure 3.11) and the model is from now on tested with the attached shear wall.

3.2.2 *Performance under strong seismic shaking*

After the successfulness of the retrofit was confirmed, the structure was further tested using high intensity seismic records in order to investigate its durability. The displayed diagrams are derived by subjecting the structure to a sequence of strong to very strong seismic

records as mentioned (Tables 1, 2), whereas the diagrams in Index B demonstrate the behavior of the building being submitted to the full sequence of motions.

The first strong seismic record to be applied is the JMA record from Kobe (1995), with a maximum value of acceleration equal to 0.82 g (PGA = 0.9 g, as measured in a small depth). As is shown in Figures 3.12 and 3.13, the structure reaches an acceleration of almost 1 g and a maximum residual drift ratio of almost 2.5 %. Therefore, it suffers from significant damage even though it does not collapse. Then the record of Rinaldi with $a_{max} \approx 0.84$ g (PGA = 1 g) from the earthquake of Northridge (1994) is simulated and imposed on the model. The response is satisfactory (Figures 3.14 – 3.15) but the structure has already accumulated deformation and finally collapses during the very strong record of Takatori (Kobe, 1995) with a maximum acceleration of 0.61 g (PGA = 0.95 g)and several cycles.

Even in these cases of high intensity motions, the response of the foundation remains insignificant with negligible values of residual settlement and rotation. However, the footing of the shear wall slides significantly after the plastic hinge at the base of the wall is formed. That was predicted by the pushover test performed previously.

Figures of Chapter 3

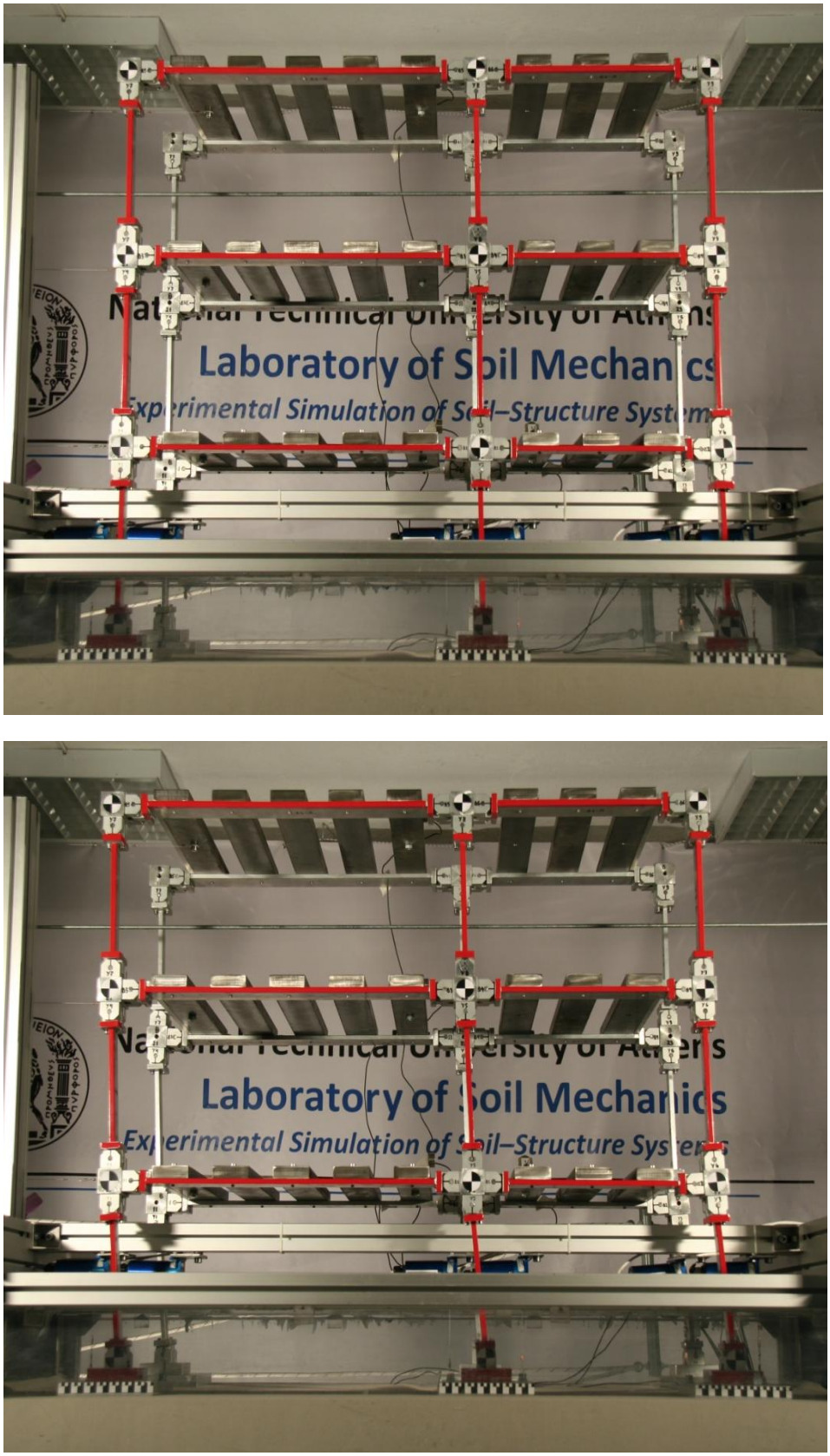

Figure 3.1 Photographs of original building before and after being submitted to a moderate intensity record (Kalamata).

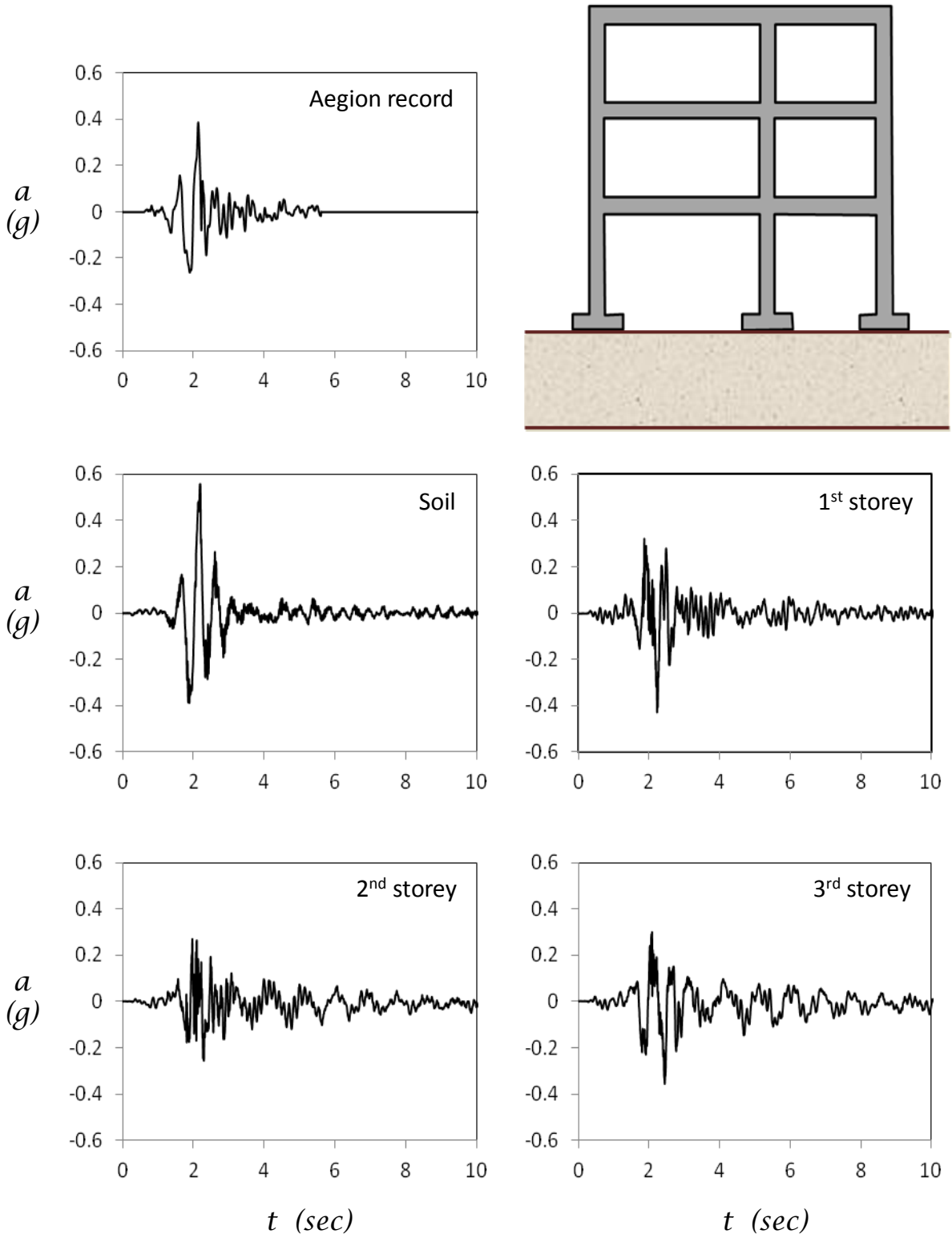

Figure 3.2 Acceleration time histories measured on the original building while submitted to the record of Aegion.

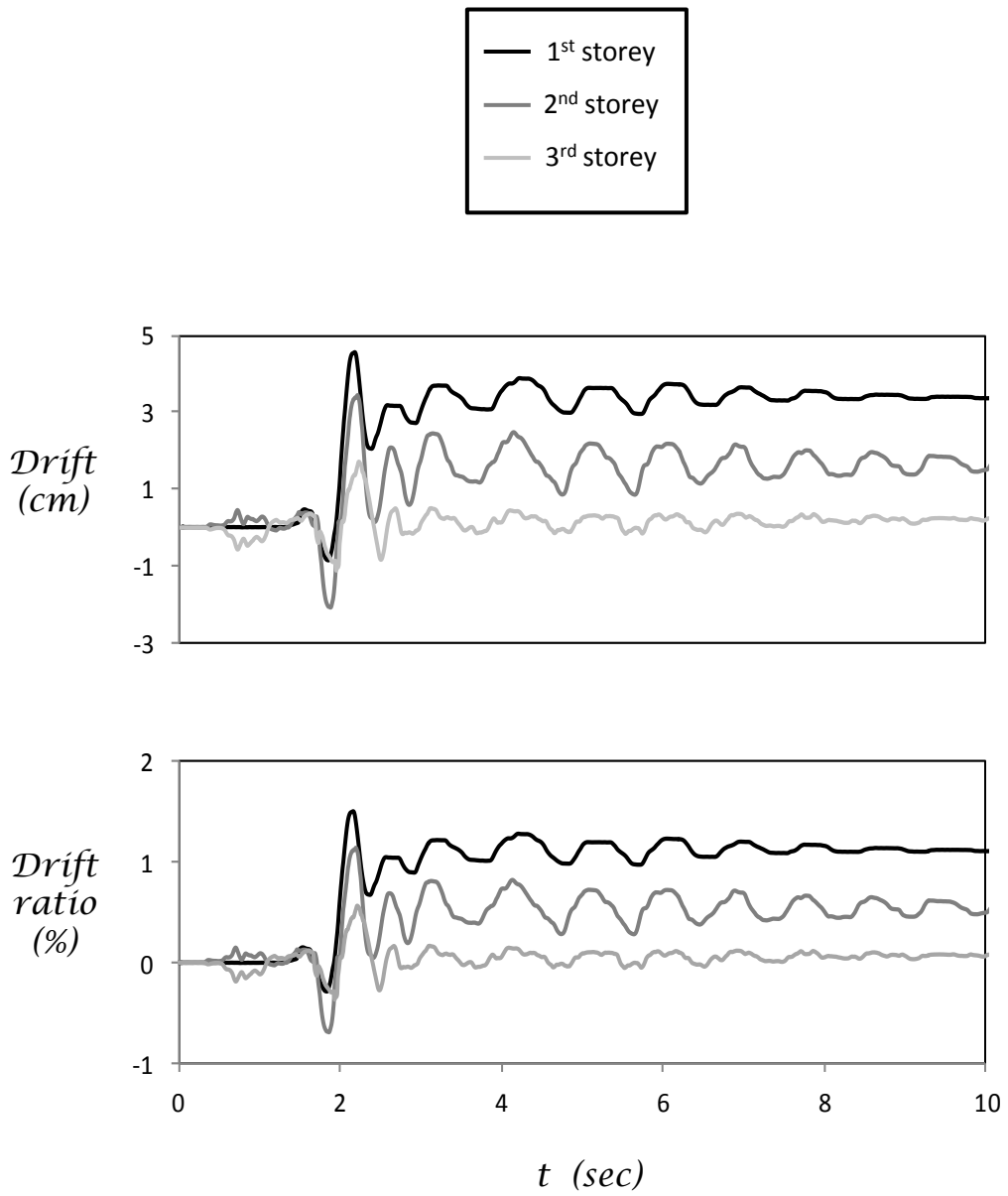

Figure 3.3 Time histories of storey drift and drift ratio of original building while submitted to the record of Aegion.

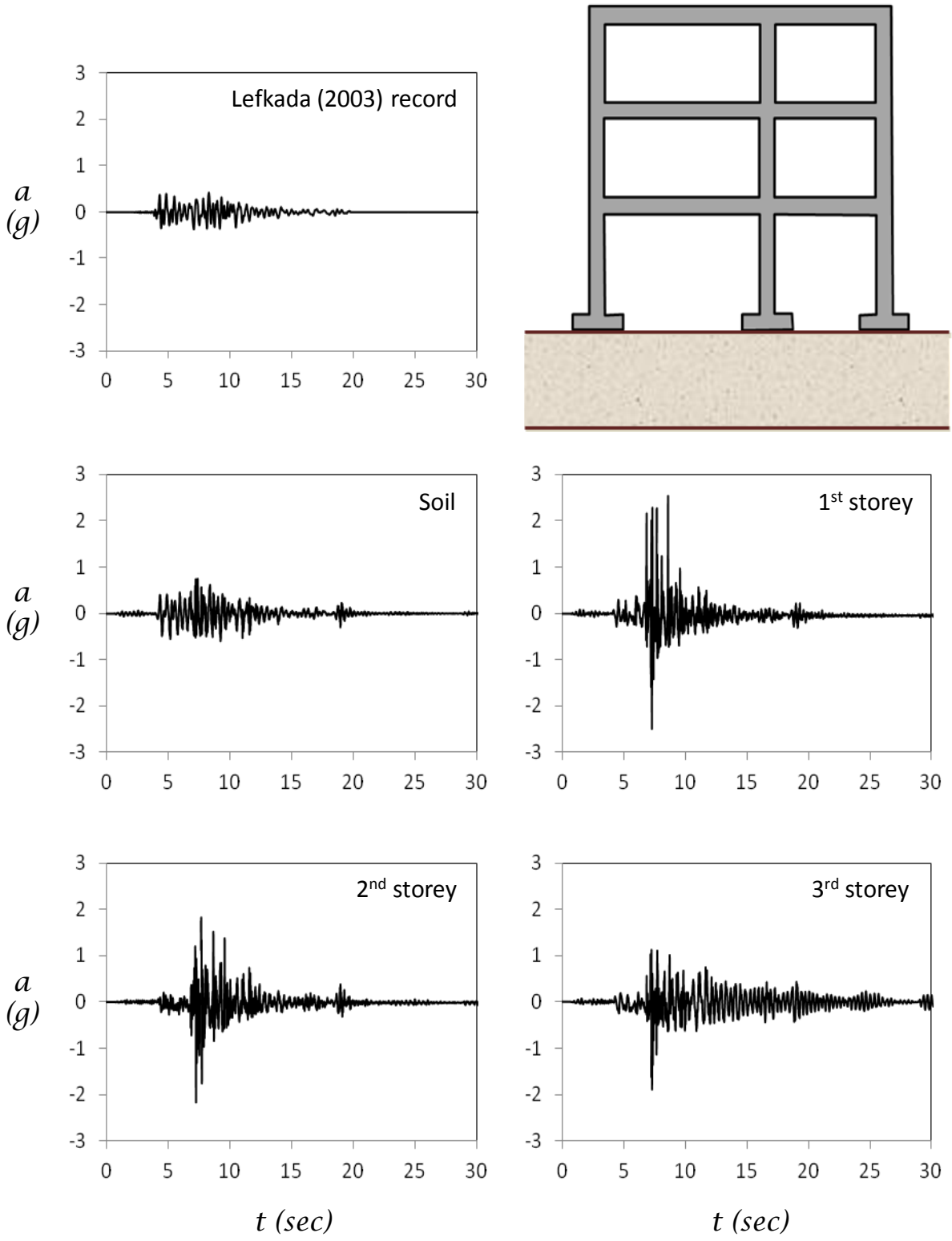

Figure 3.4 Acceleration time histories measured on the original building while submitted to the record of Lefkada (2003).

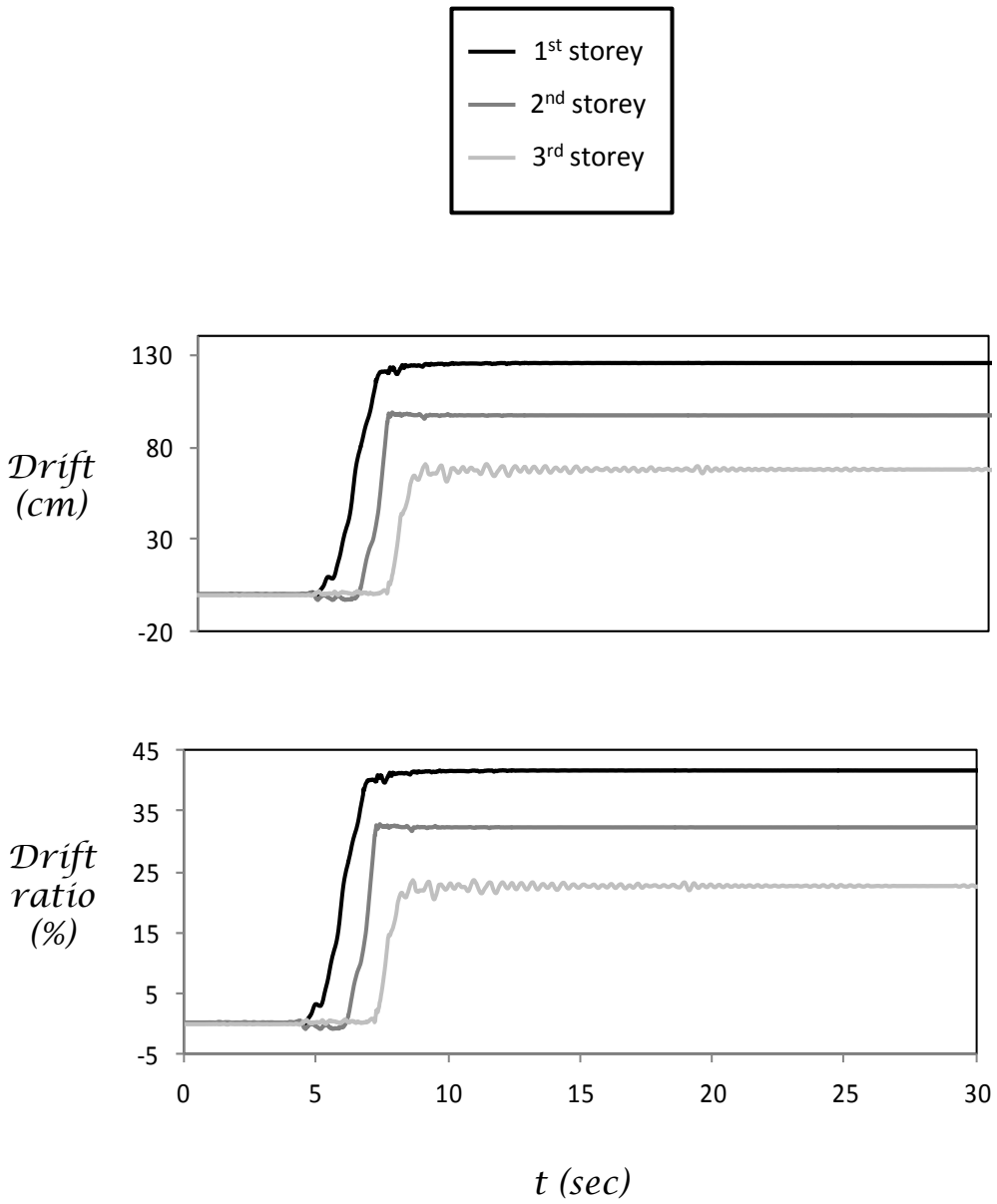

Figure 3.5 Time histories of storey drift and drift ratio of original building while submitted to the record of Lefkada (2003).

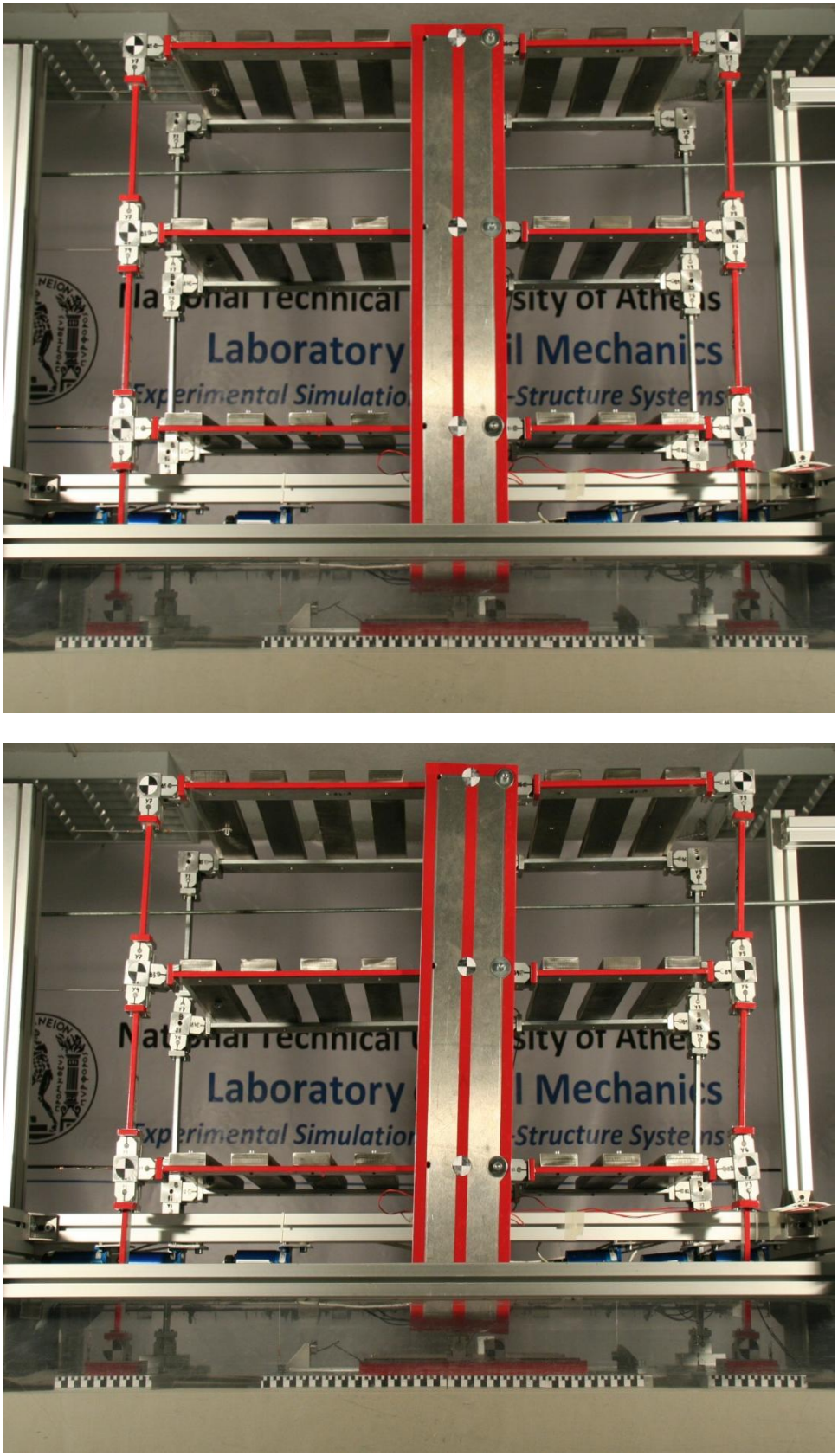

Figure 3.6 Photographs of retrofitted building with conventional wall foundation (B = 6m) before and after being submitted to a moderate intensity record (Kalamata).

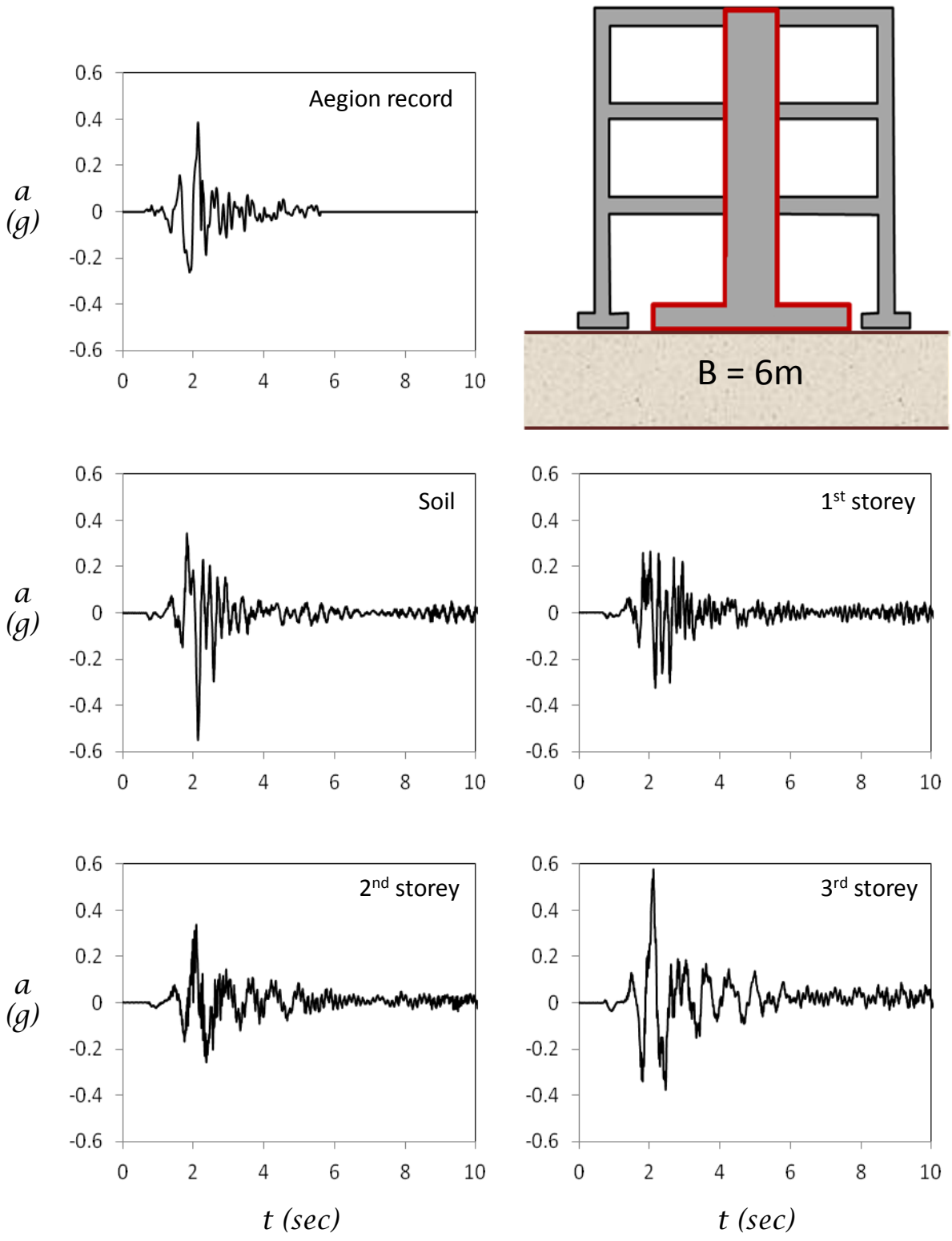

Figure 3.7 Acceleration time histories measured on the retrofitted building with conventional wall foundation (B = 6m) while submitted to the record of Aegion.

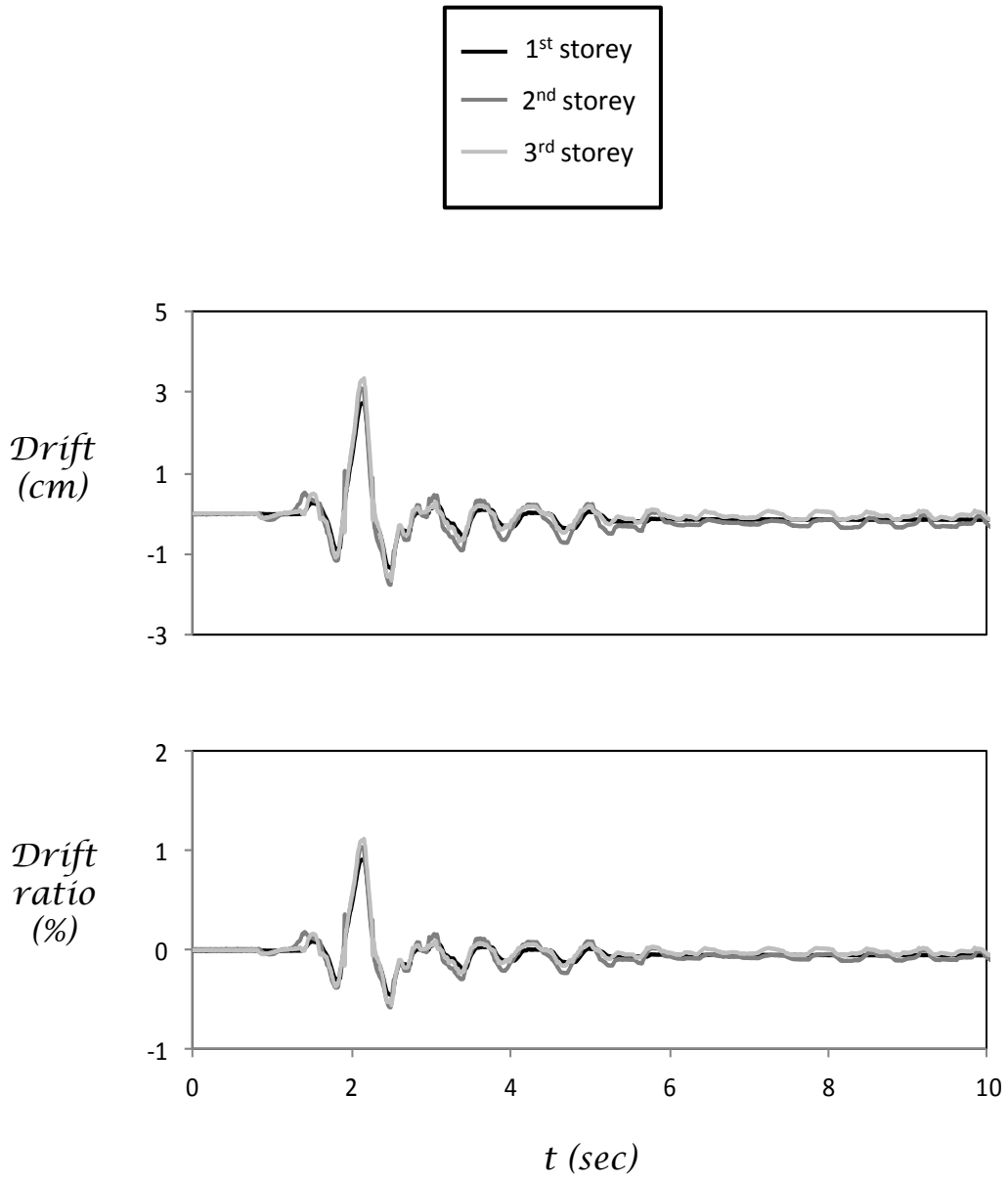

Figure 3.8 Time histories of storey drift and drift ratio of retrofitted building with conventional wall foundation (B = 6m) while submitted to the record of Aegion.

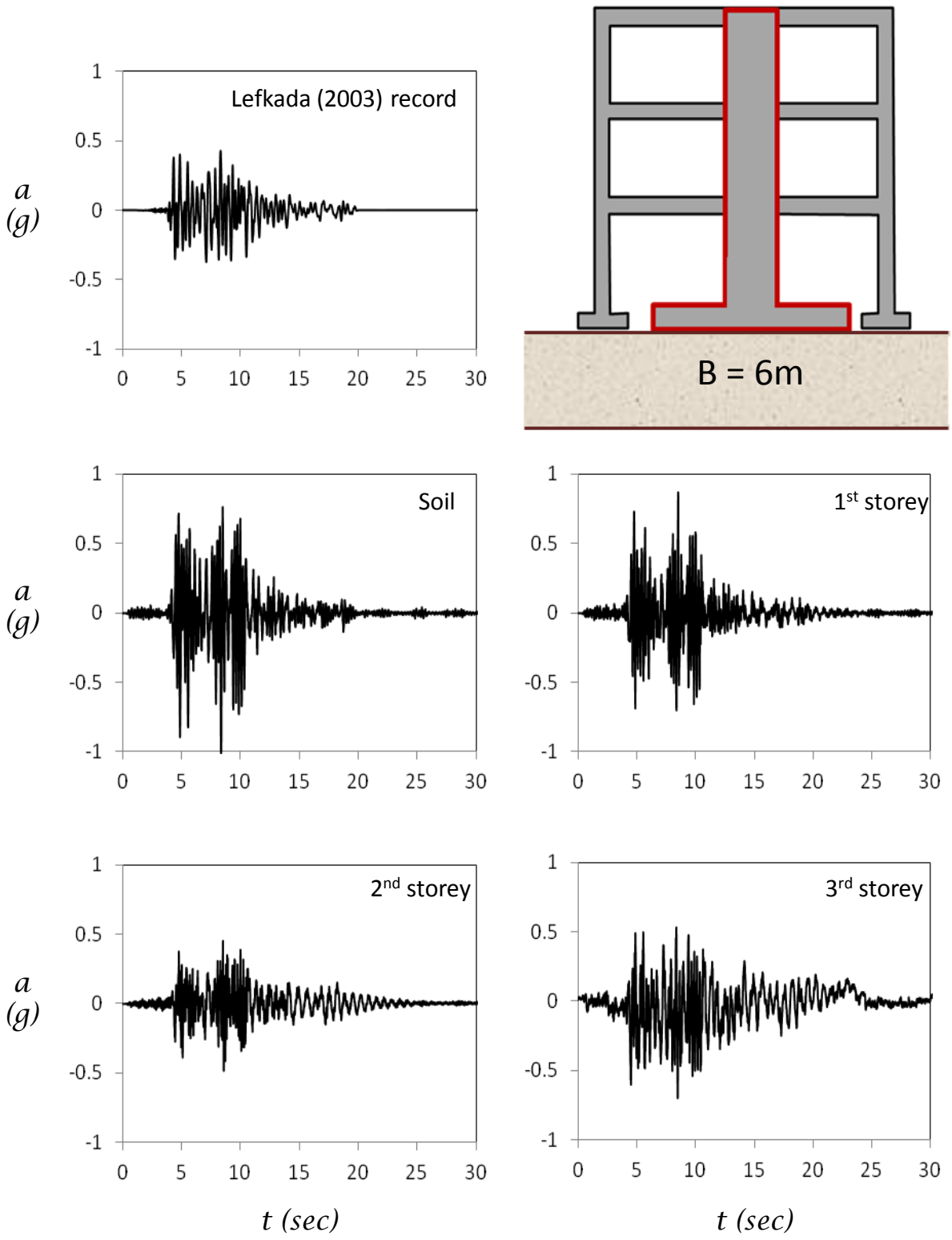

Figure 3.9 Acceleration time histories measured on the retrofitted building with conventional wall foundation (B = 6m) while submitted to the record of Lefkada (2003).

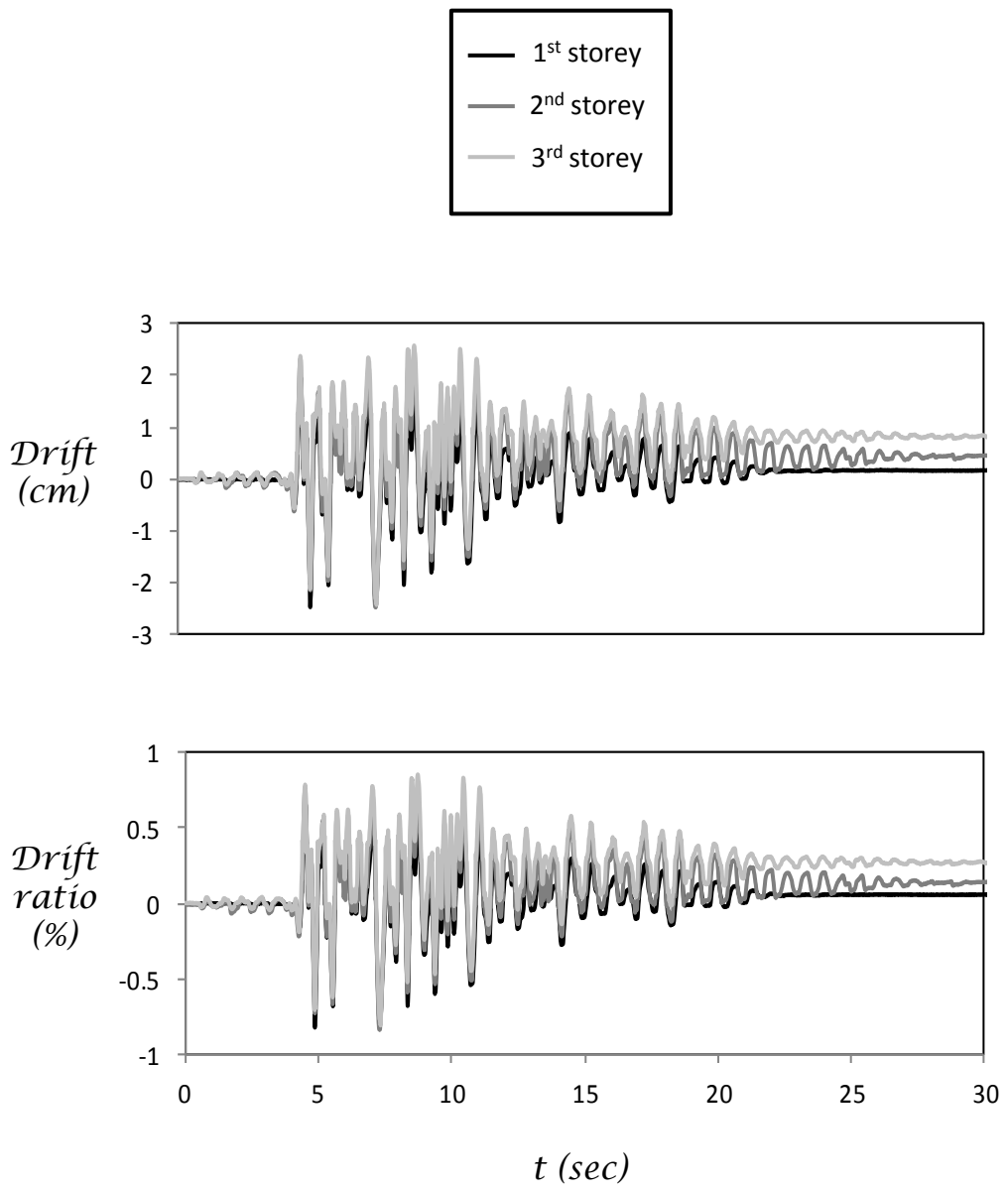

Figure 3.10 Time histories of storey drift and drift ratio of retrofitted building with conventional wall foundation (B = 6m) while submitted to the record of Lefkada (2003).

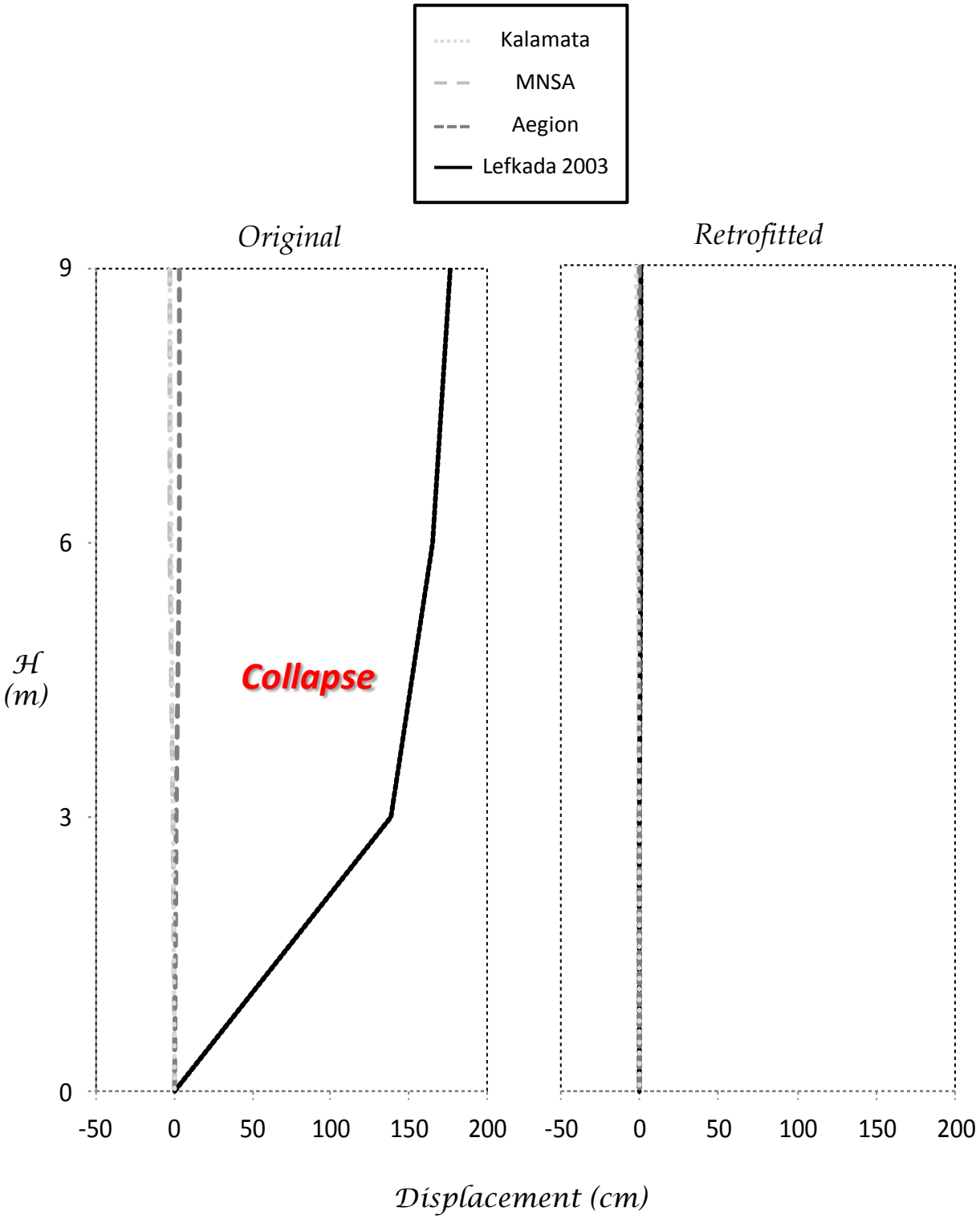

Figure 3.11 Comparison of displacement distribution with height between original and retrofitted building with conventional wall foundation (B = 6m) after being submitted to Greek seismic records of moderate intensity.

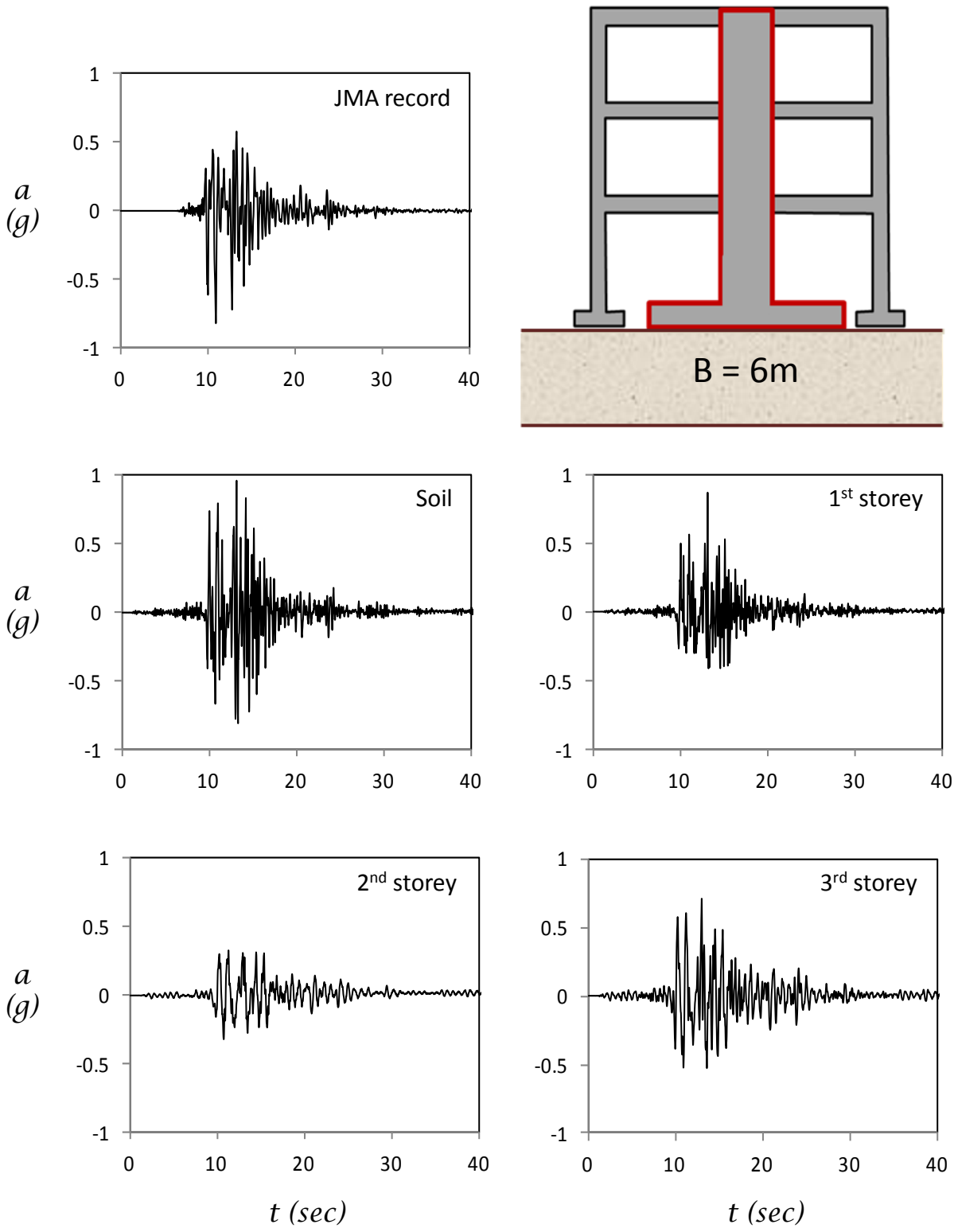

Figure 3.12 Acceleration time histories measured on the retrofitted building with conventional wall foundation (B = 6m) while submitted to the record of JMA.

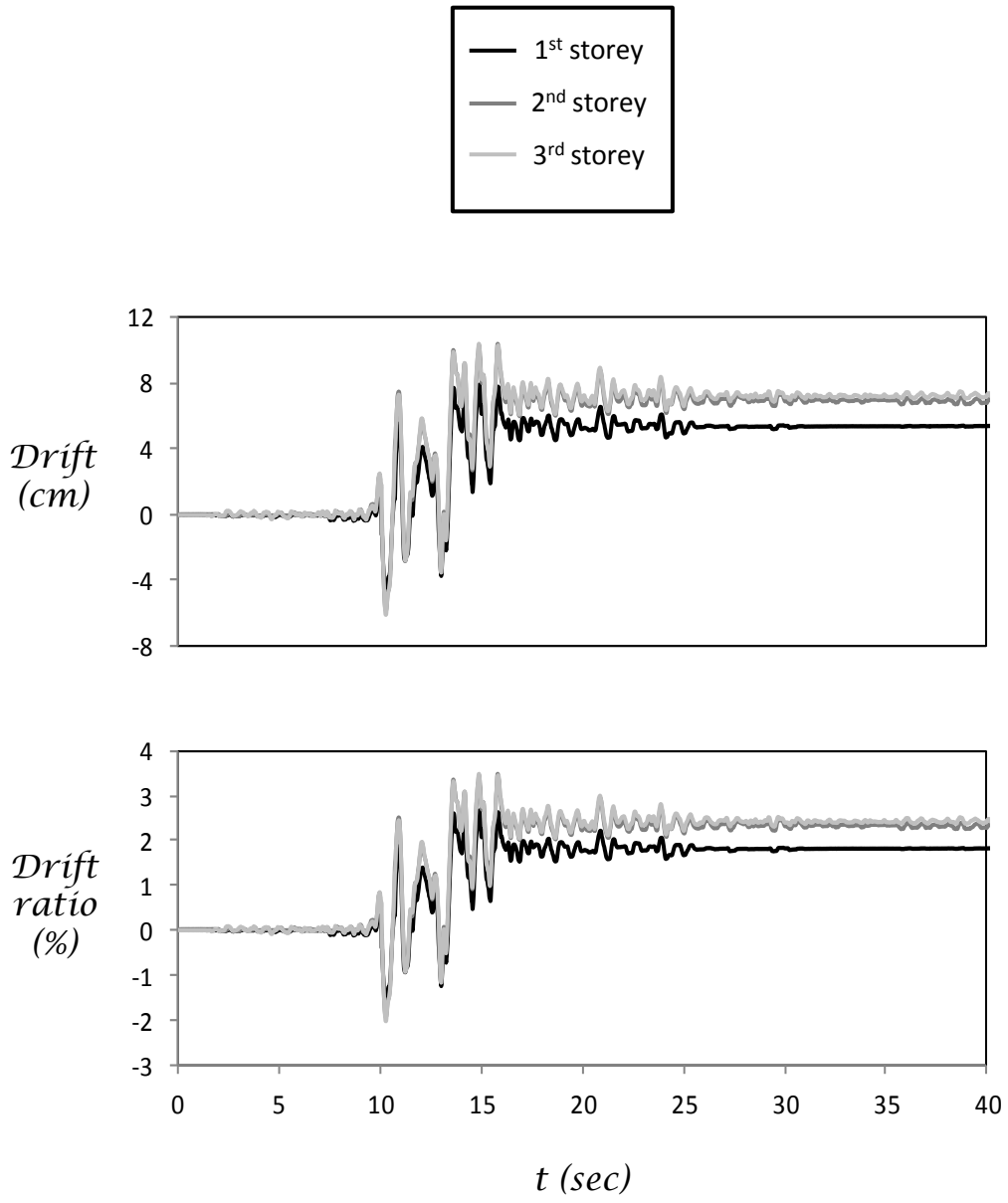

Figure 3.13 Time histories of storey drift and drift ratio of retrofitted building with conventional wall foundation (B = 6m) while submitted to the record of JMA.

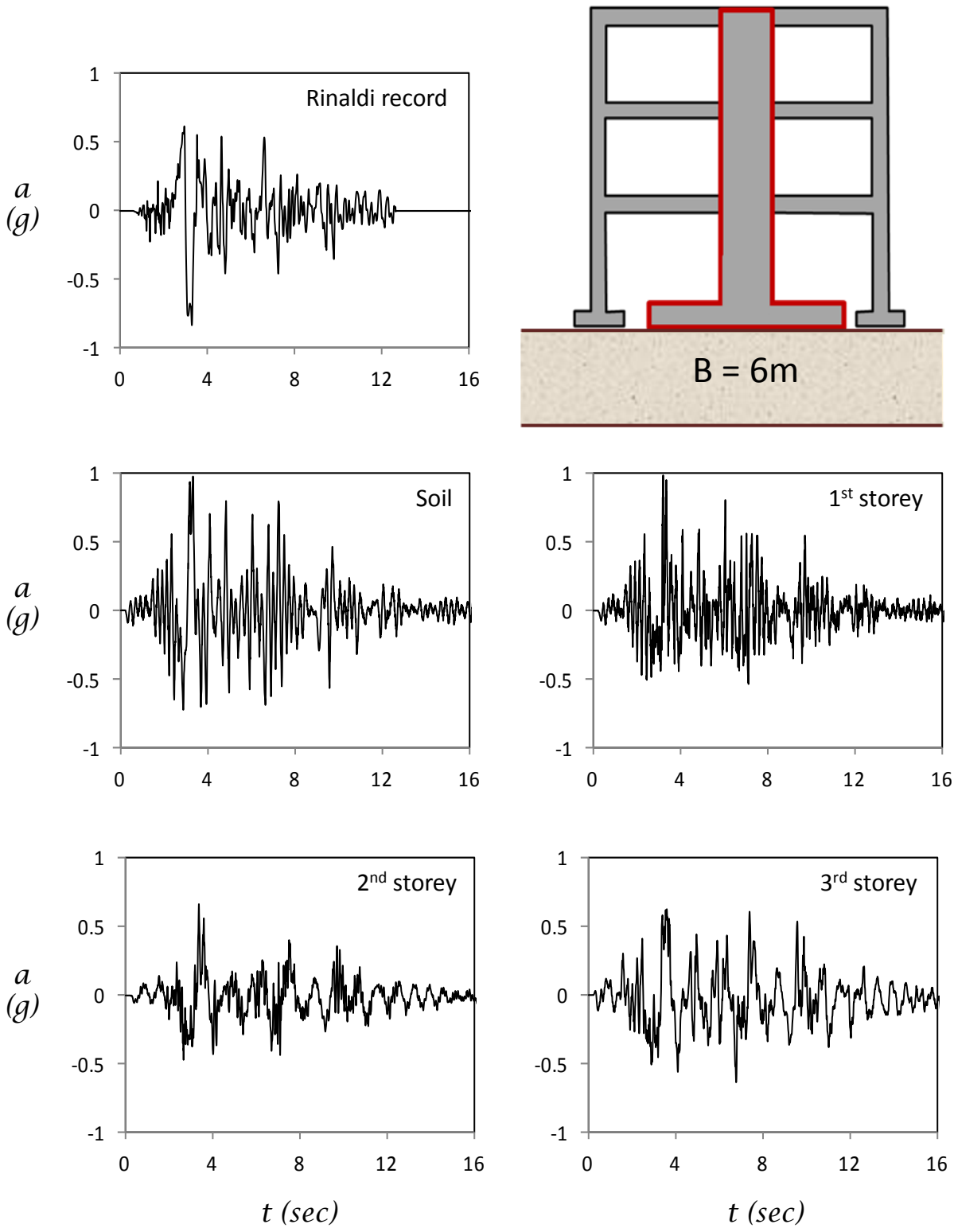

Figure 3.14 Acceleration time histories measured on the retrofitted building with conventional wall foundation (B = 6m) while submitted to the record of Rinaldi.

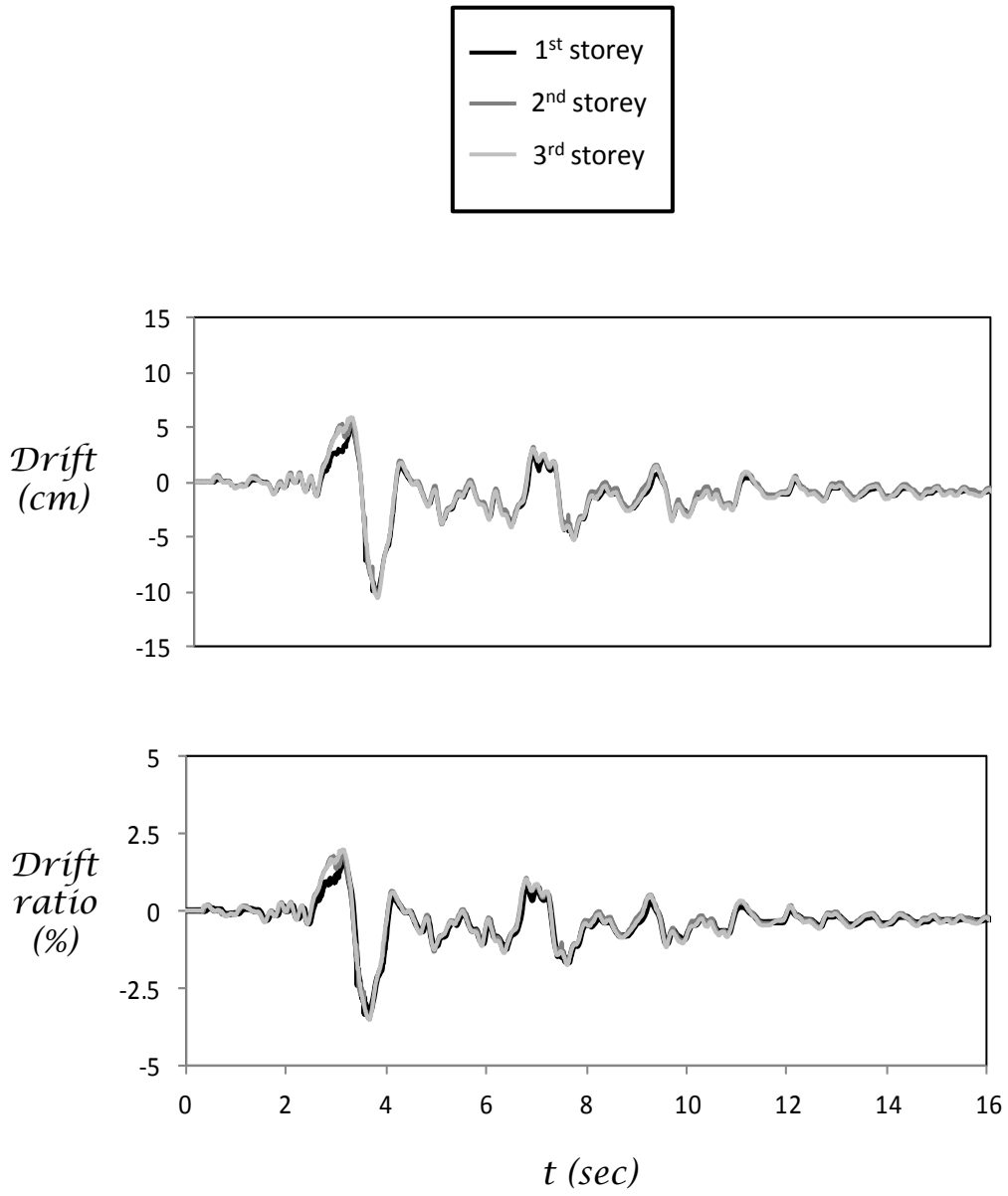

Figure 3.15 Time histories of storey drift and drift ratio of retrofitted building with conventional wall foundation (B = 6m) while submitted to the record of Rinaldi.

4

Performance of the Rocking Isolated Alternative

4. PERFORMANCE OF THE ROCKING ISOLATED ALTERNATIVE

Further improvement is attempted through the reduction of width of the conventionally designed shear wall foundation. The alternative is tested under the same conditions and the results are then compared.

4.1 Reduction of Shear Wall Foundation

As already described, the conventional footing of the retrofitting wall is of 6 m width. In this alternative solution the footing's width is reduced in almost half (B = 3.5 m), thus achieving a system with bending strength of the foundation significantly lower than that of the shear wall. Figure 4.1 illustrates the deformation of the building after being submitted to the record of Kalamata. Qualitatively, the deformed shape remains the same, with the wall homogenizing the inter - storey drifts. However, the difference is visible at the base of the wall, where the wall – foundation system appears to have rotated as a whole, as opposed to the conventionally designed system, where the bending deformation of the wall was already apparent.

4.1.1 *Performance under moderate seismic shaking*

More specifically, Figures 4.2 and 4.3 demonstrate the response of this system to the Lefkada (2003) record. In terms of drifts, the reduction of the foundation width does not appear to have affected the structure significantly, as the maximum residual drift ratio is lower than 0.2 %.

The comparison between the two retrofitting solutions for moderate intensity seismic motions is summarized in Figure 4.4, in the form of displacements measured per storey with regard to the height of storey. It can be concluded that both alternatives are equally satisfactory and able to sustain a typical spectrum of seismic records. Indeed, research has

proved that rocking isolation is mostly beneficial for structures under strong seismic shaking [Anastasopoulos et al., 2010; Gelagoti, 2010].

4.1.2 *Performance under strong seismic shaking*

In the following, the performance of the rocking isolated alternative when subjected to the same strong seismic records is evaluated.

As shown in Figures 4.5 and 4.6, the response of the model is by far improved for the record of JMA, with a residual value of drift ratio no more than 0.9%. Hence, it does not suffer serious damage, unlike the conventional solution. Figure 4.7 depicts the comparison between the two retrofitted structures in terms of displacement time history on the top of the wall and settlement with regard to rotation angle of the foundation. The first part of the Figure shows the total displacement on the top of the wall during the shaking (δ_{tot}), together with the displacement caused by flexural distortion of the wall (δ_f) and the displacement caused by the rotation of the wall's footing (δ_r). So, apart from the decrease in maximum and residual displacement, the rocking isolation achieves a significant reduction in the flexural distortion of the wall. Specifically, the conventional system fully responds to the seismic shaking by deforming at the base of the RC wall. As illustrated by Figure 4.7 a, the time history of δ_r remains equal to 0. On the other hand, the alternative divides the deformation between the bending of the wall and the rotation of the footing. Therefore, rocking proves beneficial in two ways. The residual settlement and rotation in this case are the small price to pay (Figure 4.7 b), while the settlement of the conventional system is negligible as previously mentioned.

Similarly, the two systems are compared for the seismic record of Rinaldi. The performance is quite comparable in terms of residual drift ratio and settlement (Figures 4.9, 4.10). Yet the difference lies not in the magnitude but in the way that the two alternatives have deformed. Figure 4.10 demonstrates that the conventional footing does not rotate, whereas the reduced footing rocks achieving zero flexural distortion of the wall.

For the record of Takatori, the superiority of the rocking isolated alternative is evident in the Figures that follow. While the conventional system displays large displacements and collapses, the alternative manages to survive the strong shaking. The residual displacement at the top of the wall due to the rotation of the foundation is significant but the flexural displacement of the wall is practically zero. Moreover, the residual settlement is no more than 2 cm. The $w - \vartheta$ curve for the conventional system (Figure 4.11 b) is misleading, as the settlement of the system was in fact negligible. The value of settlement depicted is caused by the faulty measurement of the vertical displacement due to the large sliding that occurred during the collapse of the building.

It is worth noticing that the maximum displacement at the top of the wall (or inter – storey drift) does not differ significantly between the two alternatives. The difference in the residual values is achieved thanks to the rocking mechanism that enables the structure to "return" by taking advantage of gravity. Figure 4.12 depicts the overall performance of the two systems under strong seismic shaking. In summary, the rocking isolated alternative performs in a much more satisfactory manner.

4.2 Hybrid Foundation

In this paragraph, the application of "hybrid" foundation to the shear wall is investigated. All examined systems were quite satisfactory when subjected to moderate seismic shaking (Index B), without requiring the top wider component to mobilize its strength and ductility. For that reason, only their performance under strong shaking is studied herein. Each of the corresponding Figures (4.13 - 4.16) depicts the performance of footings with same width b but different height t of the added plate under shaking with the records of JMA and Rinaldi and can be compared to Figures 4.7 and 4.10 that were discussed previously.

Comparison of Hybrid systems under strong seismic shaking

JMA seismic record

The first figure depicts the performance of systems with b = 2.5 m when subjected to the record of JMA. The two systems respond similarly, with the first footing (t = 0.05 m) performing slightly better. Both alternatives display significant deformation of the wall – foundation system due to the rotation of the footing but no flexural distortion of the shear wall. The value of the residual settlement is relatively small in both cases (≈ 2 cm). The upper part of the footing did not come to touch the soil since the residual rotation angle is also minor. That explains the similar behavior of the two systems.

Figure 4.14 shows the same curves for the hybrids with b = 2 m. The difference between the two is more noticeable, as the residual displacement at the top of the wall is approximately 50 % larger for the second system (t = 0.10 m). However, the bending distortion of the shear wall is again negligible for both alternatives. Due to the smaller value of b in this case senario the rotation angle required for the upper component to touch the soil is smaller while the settlement and rotation caused by shaking are larger. In reality, the first footing (t = 0.05 m) comes to contact the soil with its top part and thus benefits from the increase in strength and ductility, whereas the second one (t = 0.10 m) does not.

Rinaldi seismic record

The next figure illustrates the performance of the previous hybrid footings (b = 2.5 m with t = 0.05 m and 0.10 m respectively) during the seismic record of Rinaldi. The displacement time history as well as the $w - \vartheta$ curve for the hybrid with the smaller gap (t = 0.05 m) are almost identical with the respective curves for the system with the 3.5 m wide footing (Figure 4.10), with the residual displacement on top of the wall being practically equal to zero. That confirms the fact that the upper part of the footing (B = 3.5 m) has come to touch the soil during the shaking and has therefore contributed with its strength and ductility. However, the hybrid with the larger gap (t = 10 cm) from the soil surface behaves quite differently, displaying significant residual displacement on the top of the wall along with settlement and rotation of the footing. Apparently, the top part of the hybrid is not in contact with the soil

and the bending strength of the bottom part is not sufficient to withstand this motion without significant damage (residual drift ratio ≈ 2 %). It can be assumed that a footing with a width of 2.5 m would not be a satisfactory enough solution. It is worth mentioning that the pushover test for this case demonstrated that the soil – foundation system did not benefit in terms of maximum bending strength, even when the top footing was fully mobilized, but it gained in terms of ductility (Figure 2.16).

The last case scenario included in this chapter is the alternative with b = 2 m being submitted to the record of Rinaldi as well (Figure 4.16). The curves for the hybrid with the smaller gap (t = 0.05 m) are almost identical to the respective curves of Figure 4.15, since the top part has also begun to mobilize its strength during the shaking. The second hybrid of same width but a thicker bottom part appears to have performed less satisfyingly, because its top component was not mobilized. On the other hand, the residual δ_{tot} is equal to the respective value for the hybrid with the same t but larger b, while the residual values of w and θ are lower (Figure 4.15). This was expected, since this footing settled and rotated significantly during the seismic record of JMA and was therefore able to activate its top component during shaking with the record of Rinaldi, which was imposed afterwards.

The values of δ_f were negligible in all cases, since the wall is "protected" from flexural damage by rocking, which is allowed in the foundation. The comparison of hybrid systems of same width but different thickness under strong seismic shaking is summarized in Figures 4.17 and 4.18. The alternatives of both b = 2.5 and 2 m and small thickness of bottom component performed equally well during this series.

Figures of Chapter 4

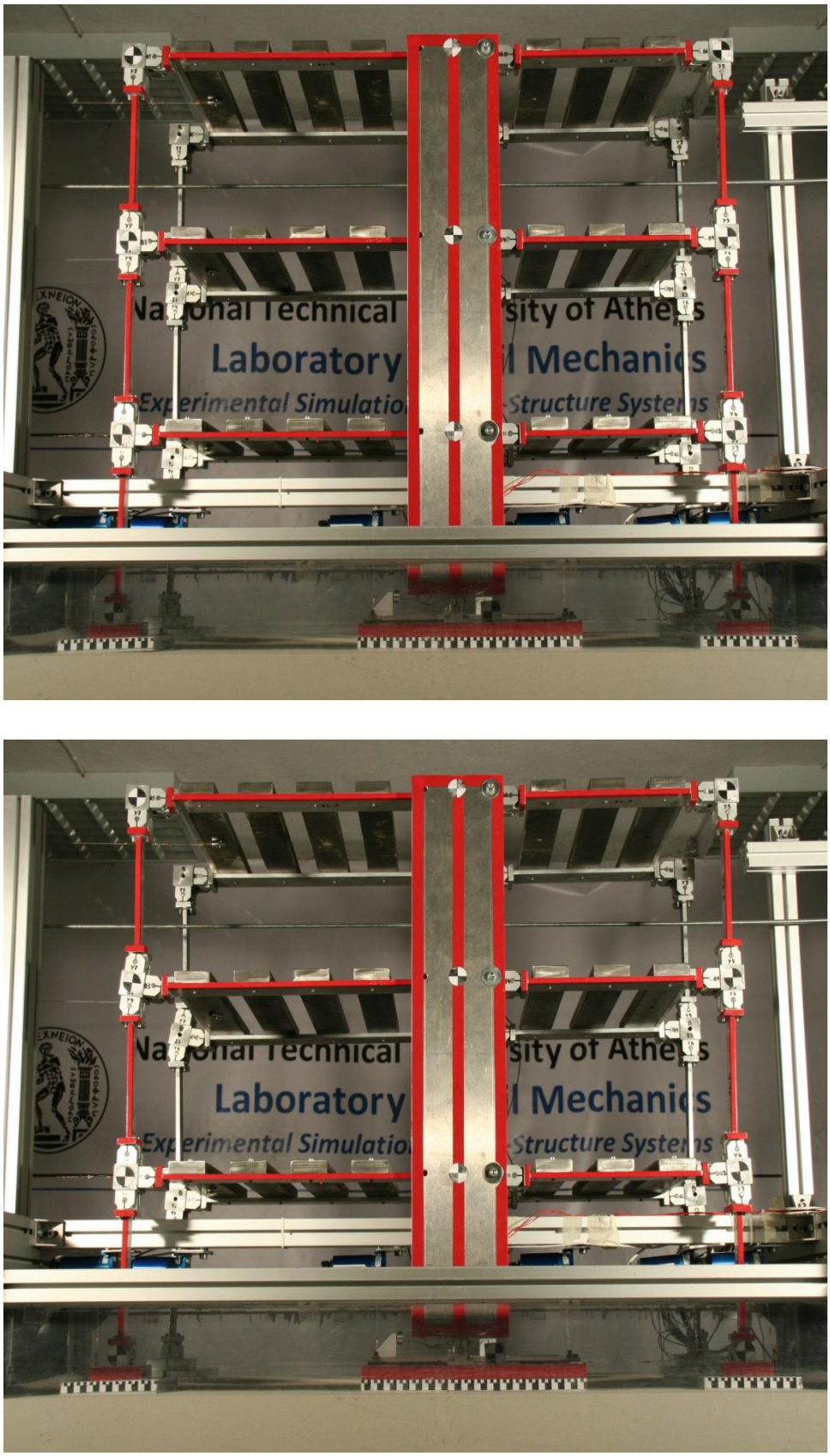

Figure 4.1 Photographs of retrofitted building with rocking isolation (B = 3.5m) before and after being submitted to a moderate intensity record (Kalamata).

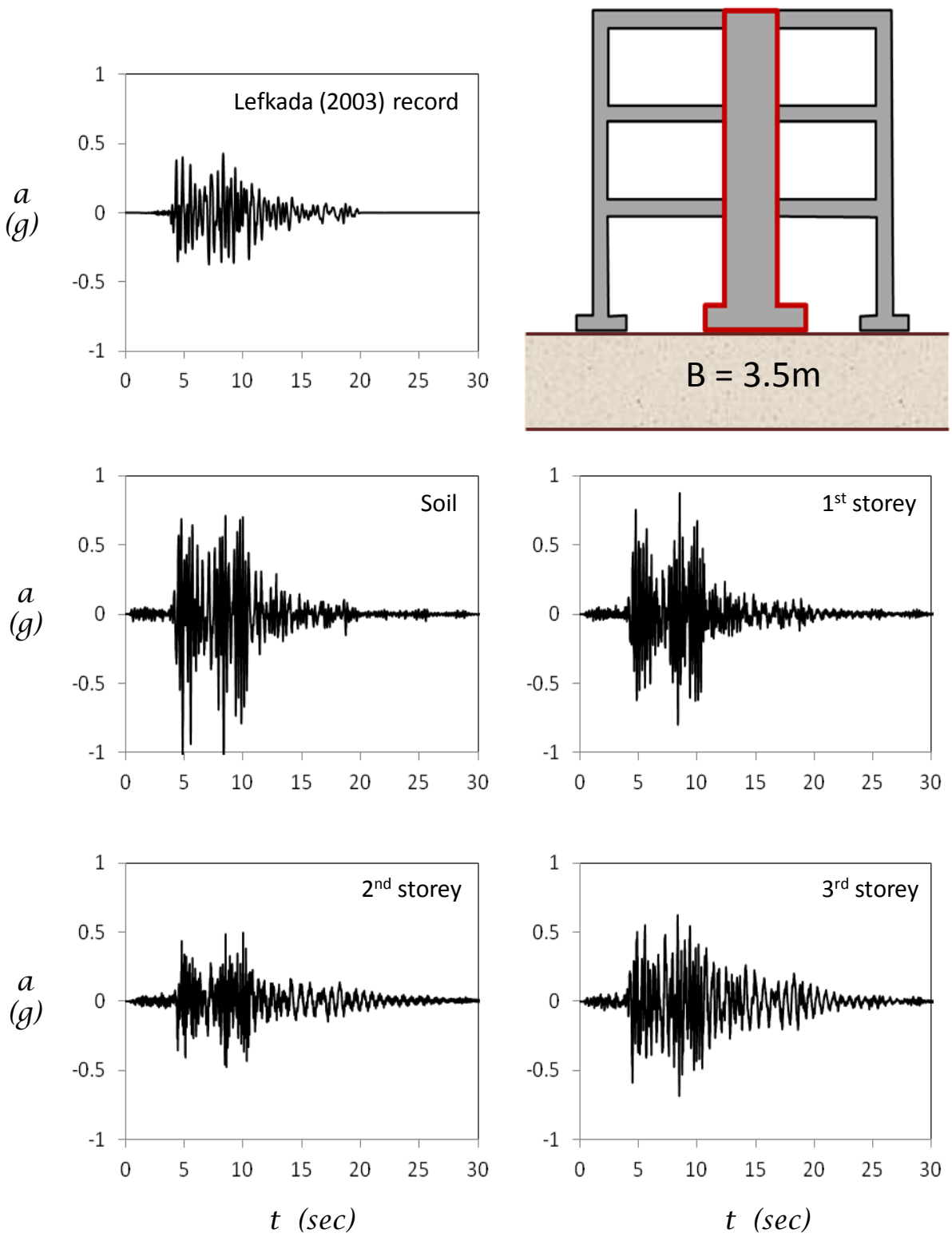

Figure 4.2 Acceleration time histories measured on the retrofitted building with rocking isolation (B = 3.5m) while submitted to the record of Lefkada (2003).

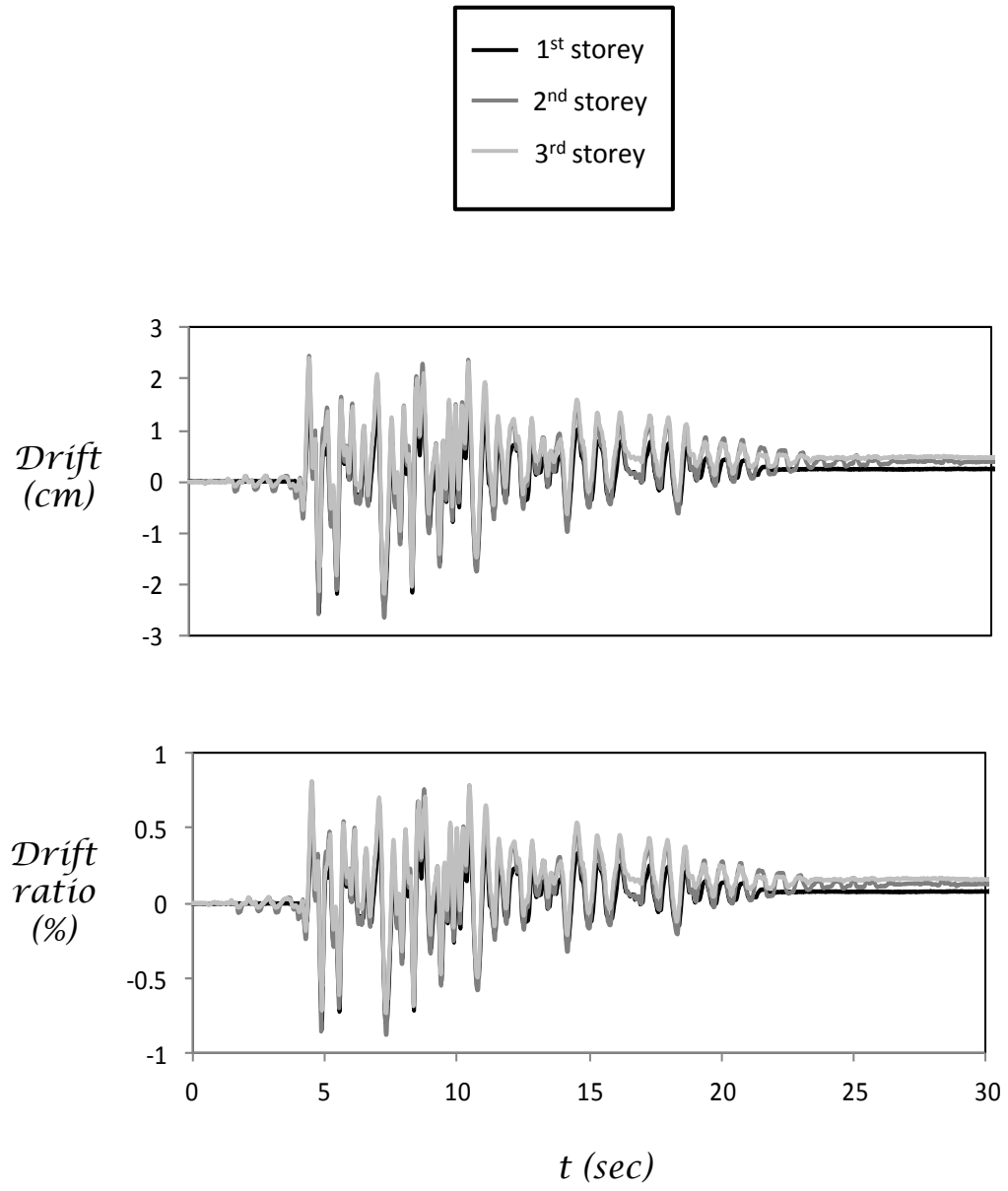

Figure 4.3 Time histories of storey drift and drift ratio of retrofitted building with rocking isolation (B = 3.5m) while submitted to the record of Lefkada (2003).

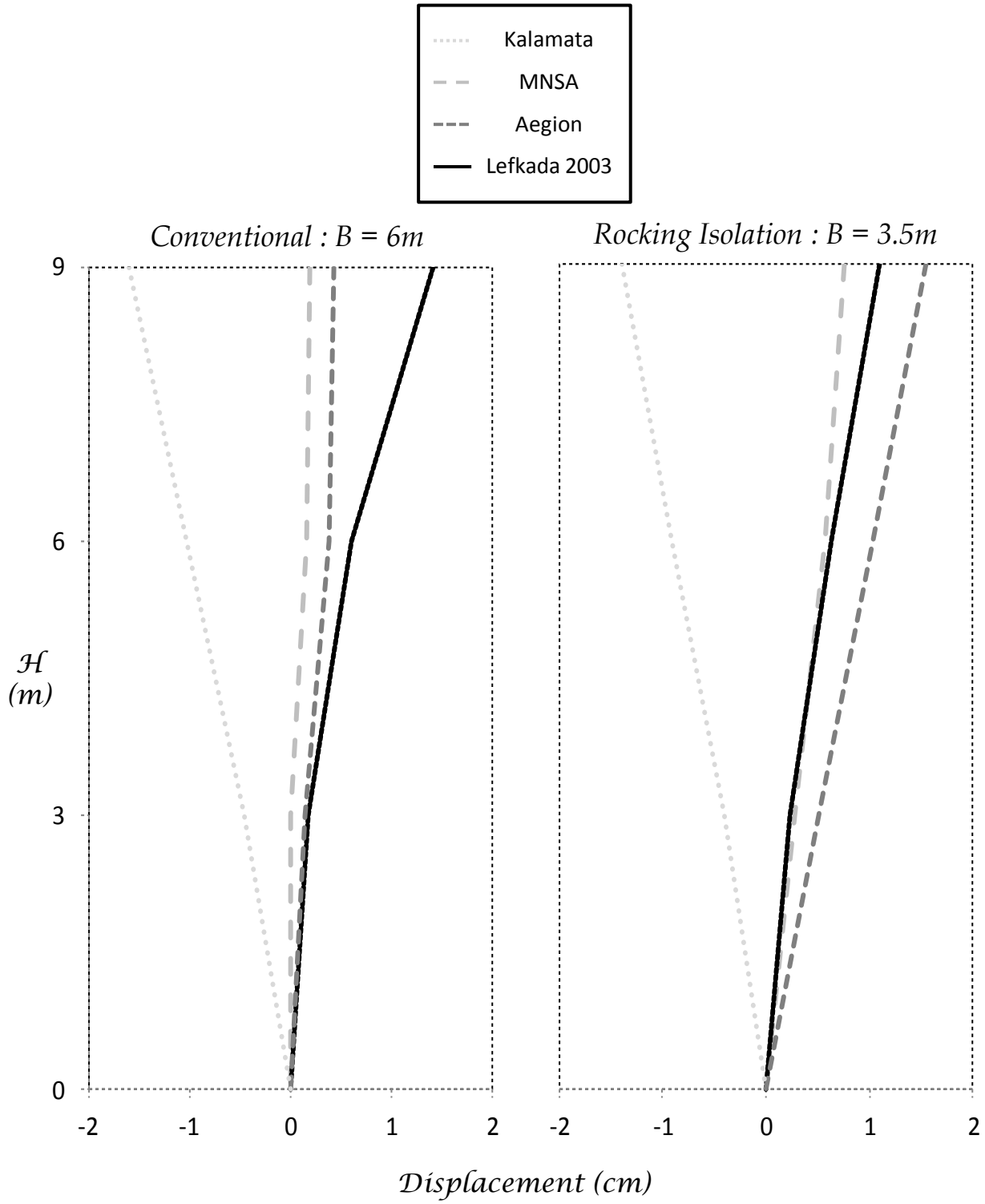

Figure 4.4 Comparison of displacement distribution with height between retrofitted building with conventional wall foundation (B = 6m) and rocking isolation (B = 3.5m) after being submitted to Greek seismic records of moderate intensity.

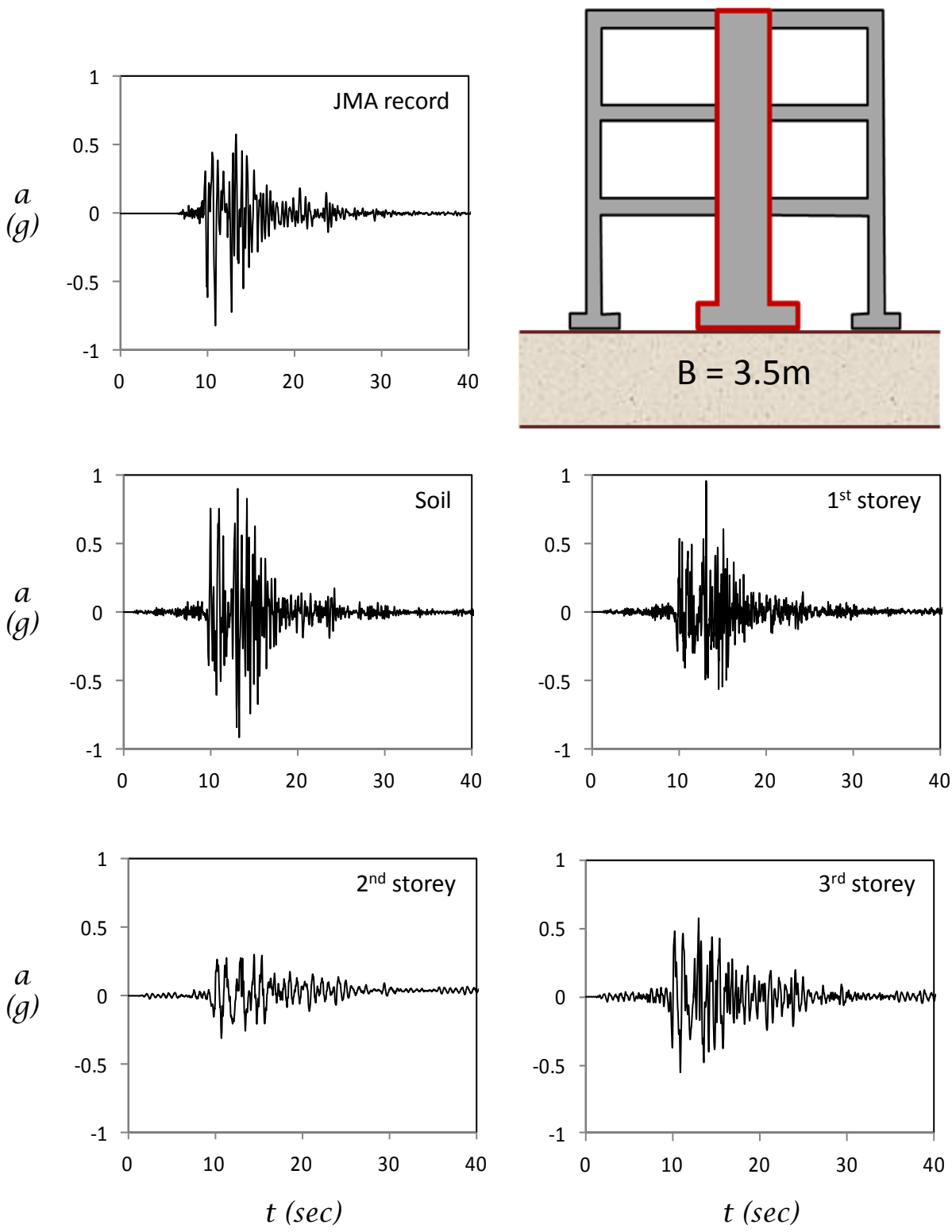

Figure 4.5 Acceleration time histories measured on the retrofitted building with rocking isolation (B = 3.5m) while submitted to the record of JMA.

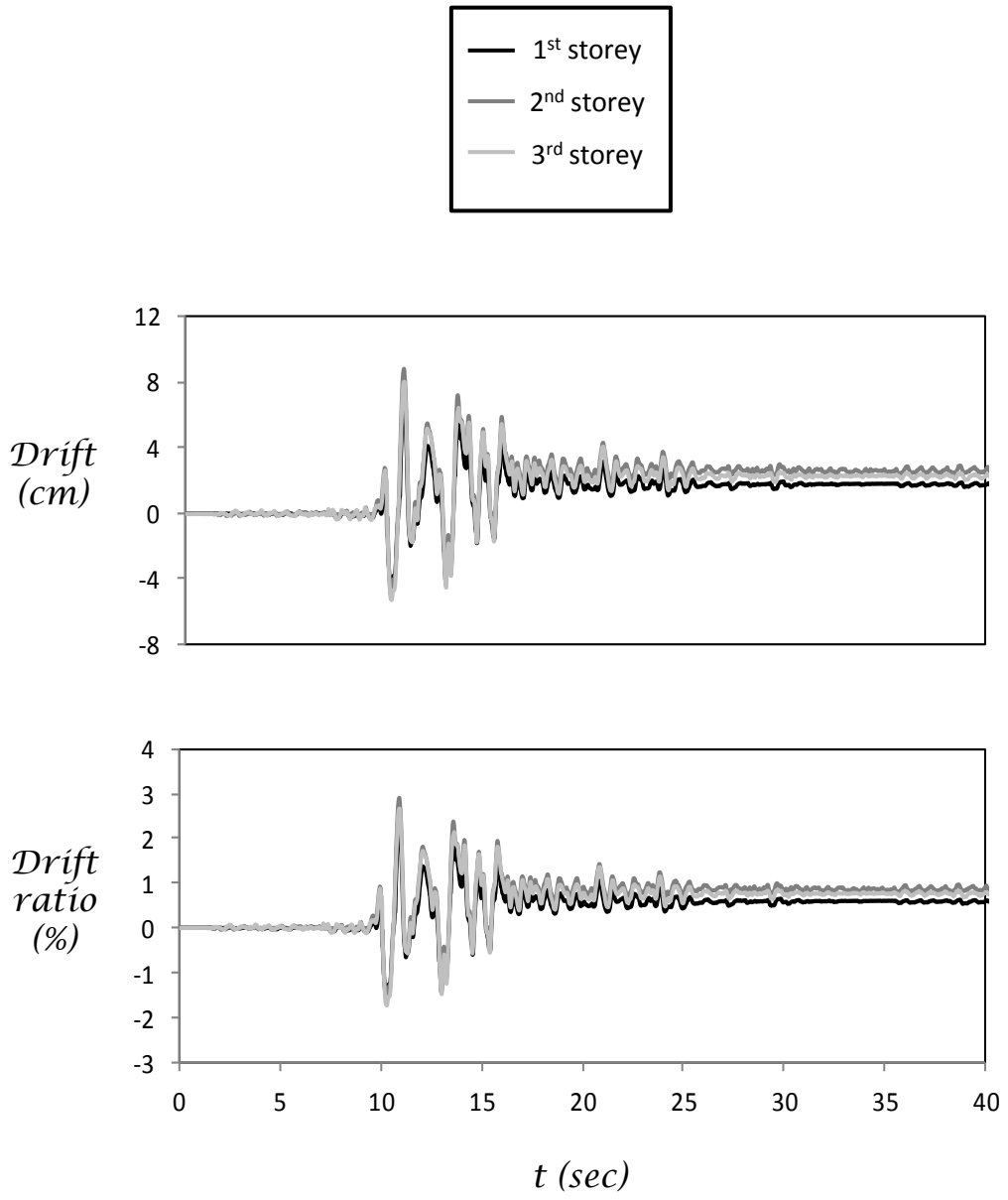

Figure 4.6 Time histories of storey drift and drift ratio of retrofitted building with rocking isolation (B = 3.5m) while submitted to the record of JMA.

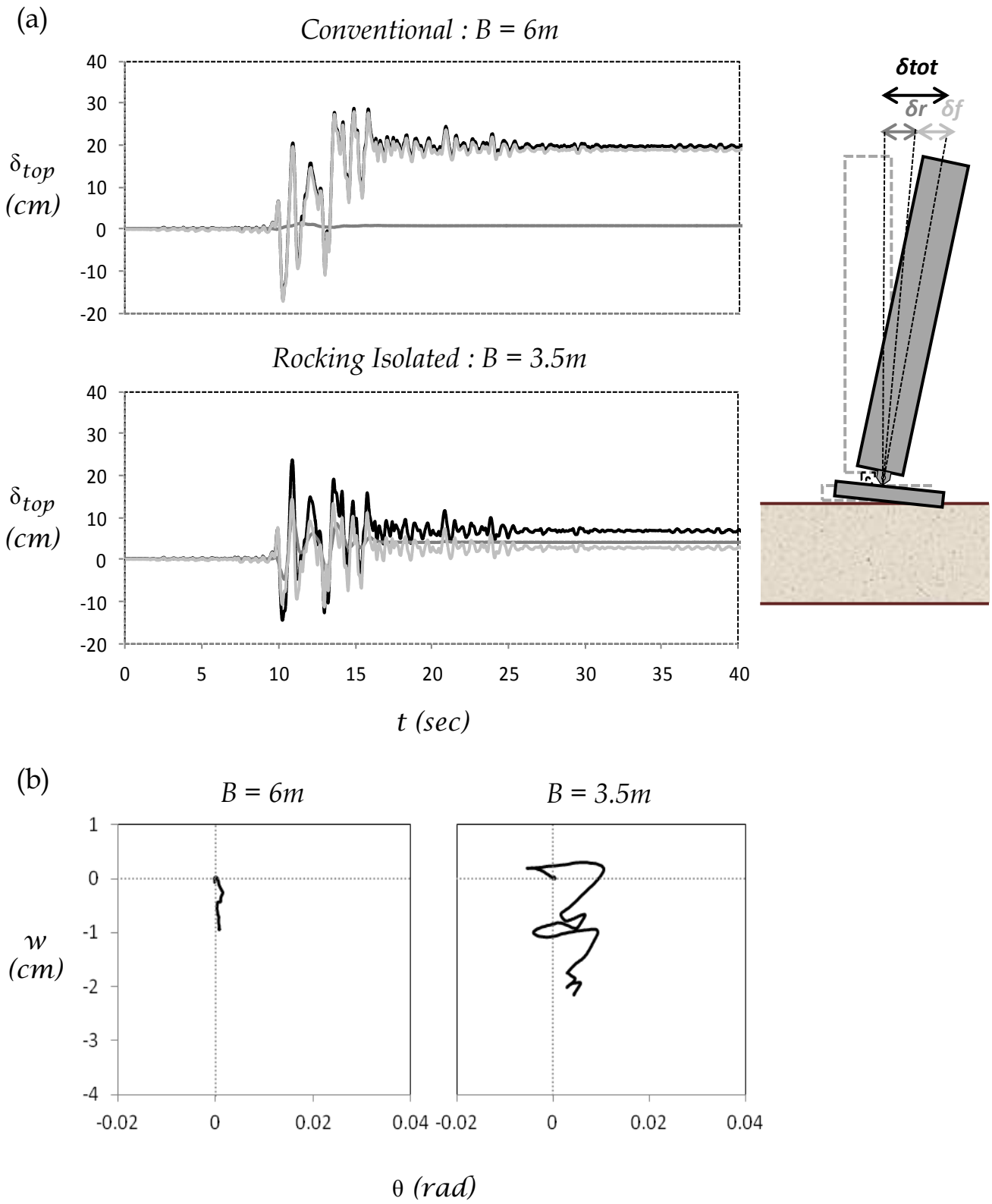

Figure 4.7 (a) Time history of displacement at the top of the shear wall and **(b)** settlement with regard to rotation angle of shear wall foundation, for retrofitted building with conventional wall foundation (B = 6m) and rocking isolation (B = 3.5m) while submitted to the record of JMA.

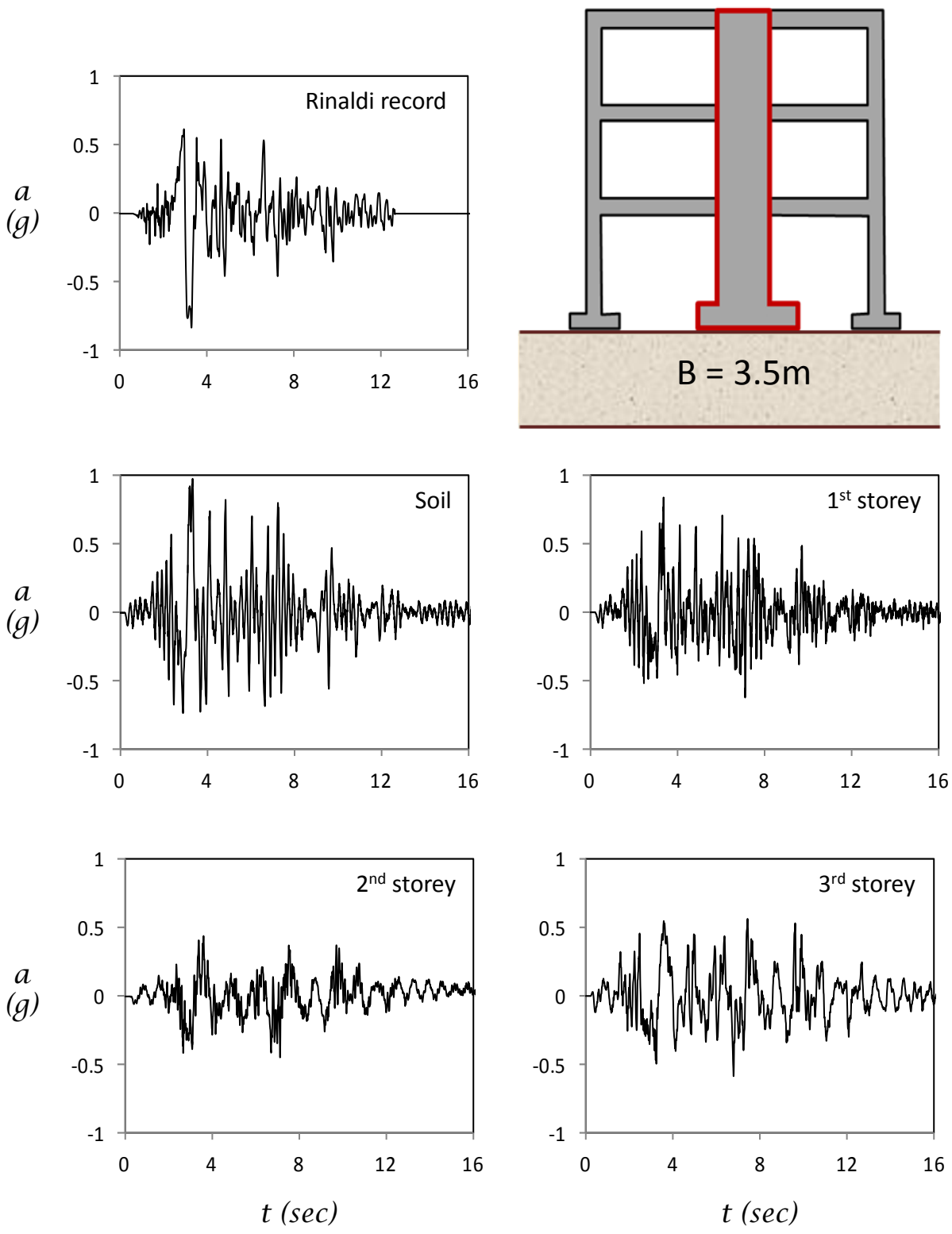

Figure 4.8 Acceleration time histories measured on the retrofitted building with rocking isolation (B = 3.5m) while submitted to the record of Rinaldi.

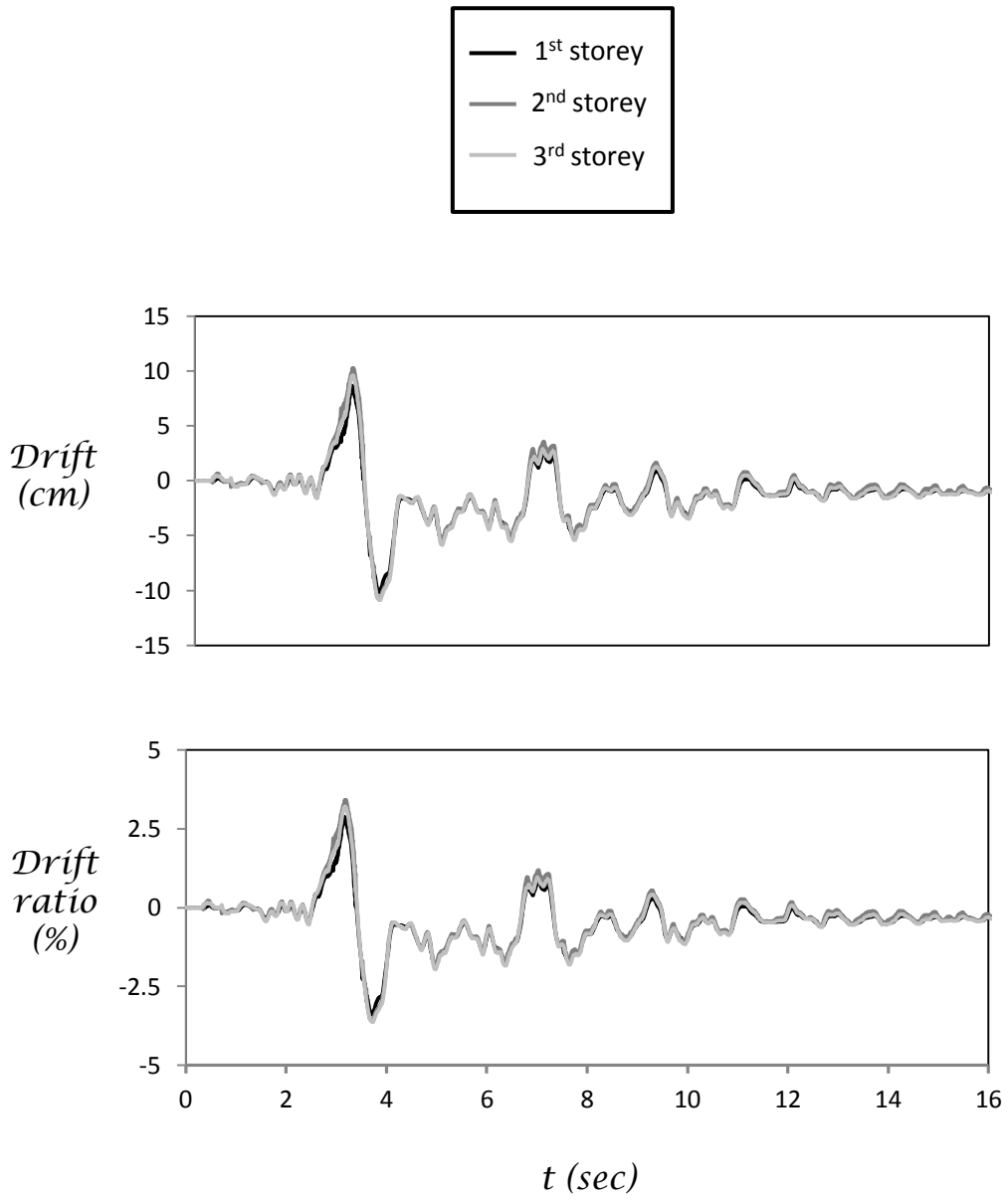

Figure 4.9 Time histories of storey drift and drift ratio of retrofitted building with rocking isolation (B = 3.5m) while submitted to the record of Rinaldi.

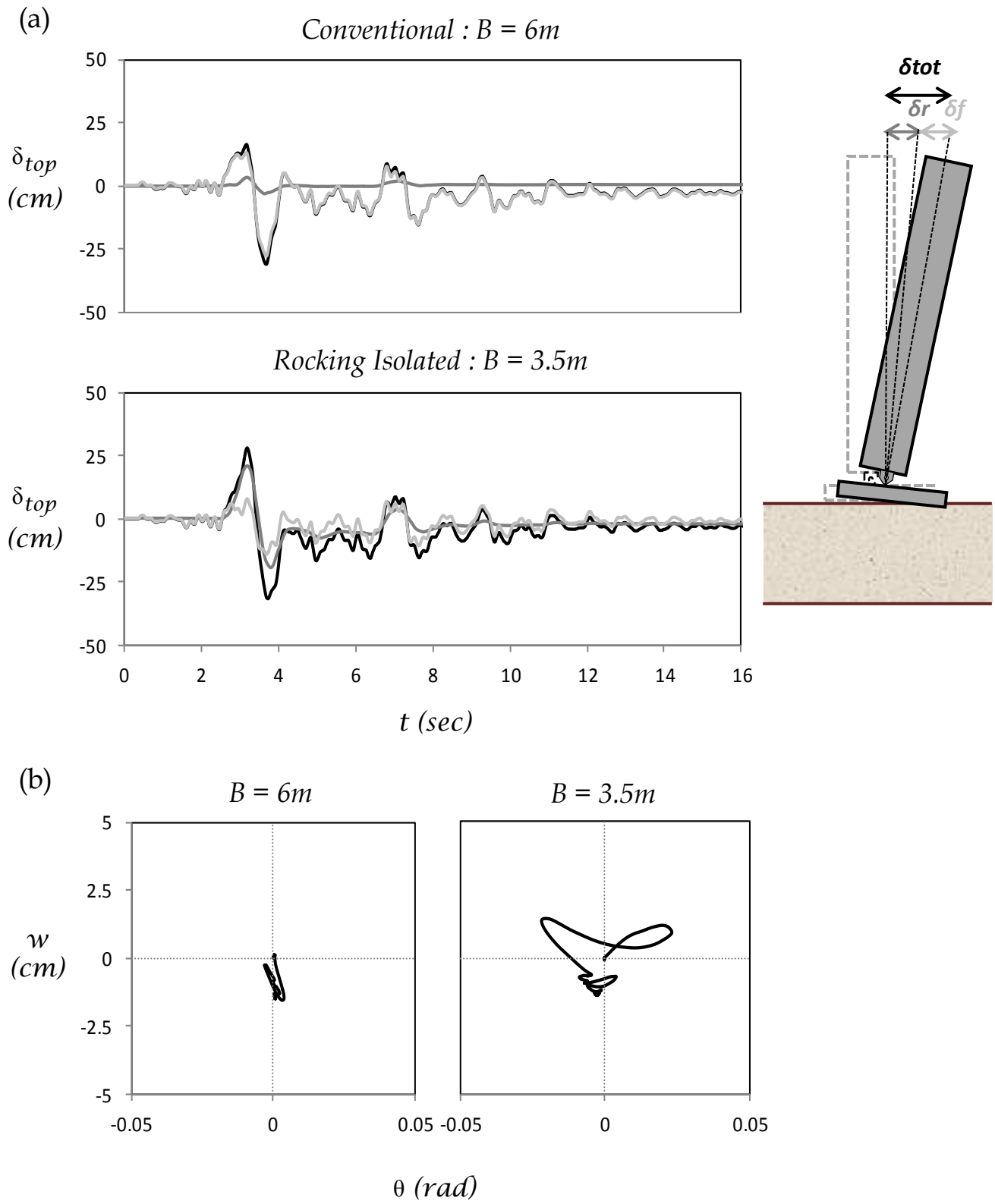

Figure 4.10 (a) Time history of displacement at the top of the shear wall and **(b)** settlement with regard to rotation angle of shear wall foundation, for retrofitted building with conventional wall foundation (B = 6m) and rocking isolation (B = 3.5m) while submitted to the record of Rinaldi.

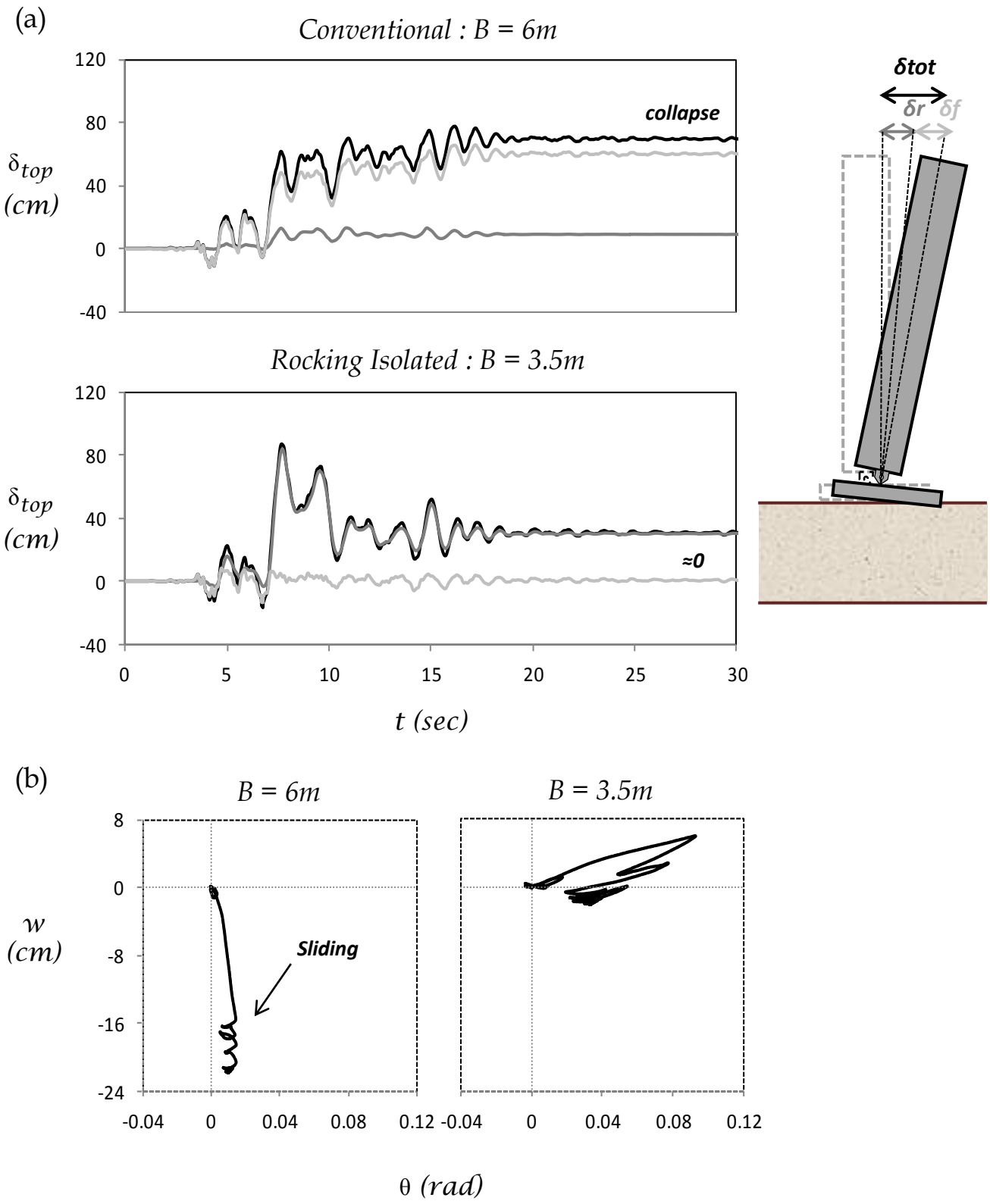

Figure 4.11 (a) Time history of displacement at the top of the shear wall and **(b)** settlement with regard to rotation angle of shear wall foundation, for retrofitted building with conventional wall foundation (B = 6m) and rocking isolation (B = 3.5m) while submitted to the record of Takatori.

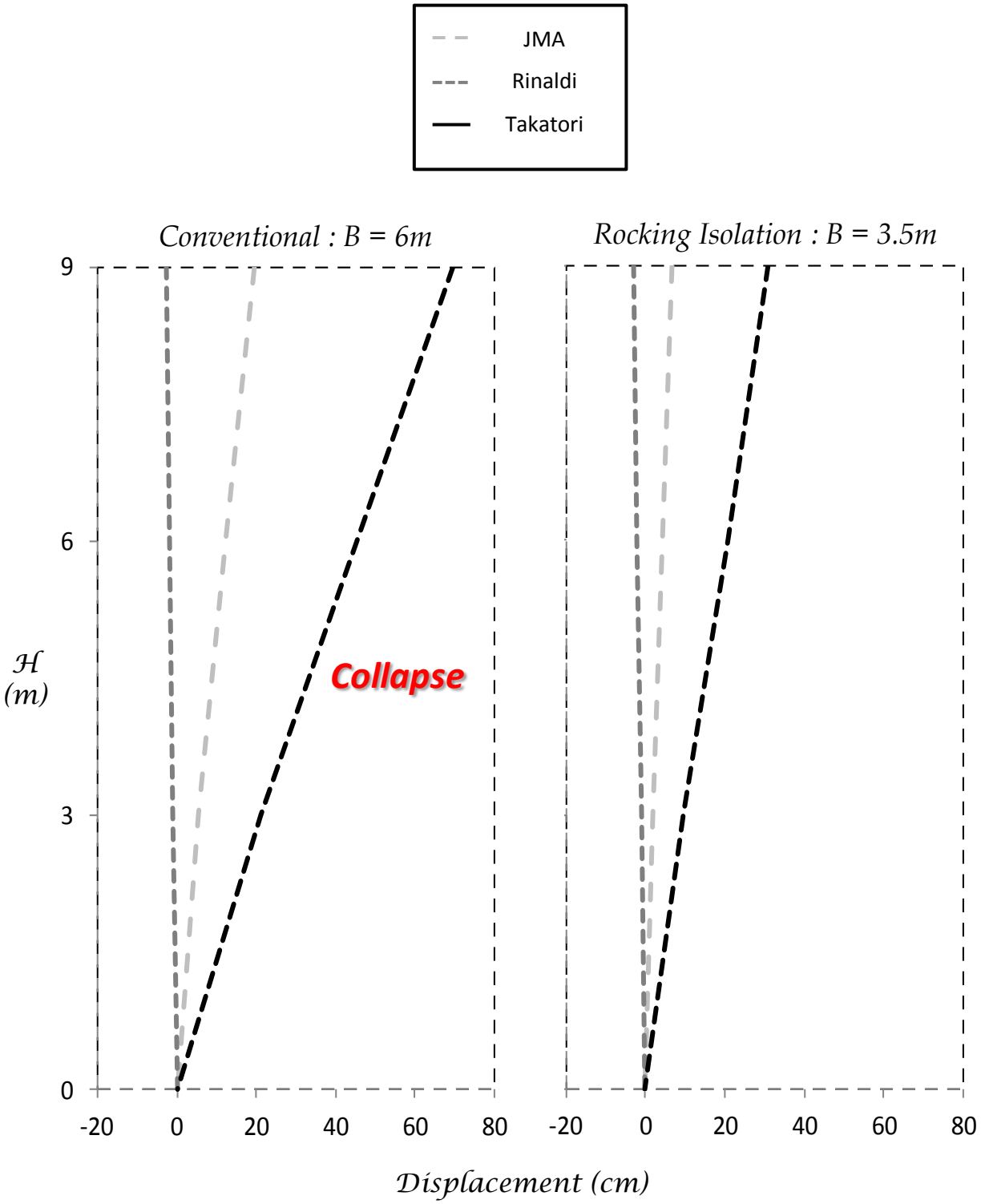

Figure 4.12 Comparison of displacement distribution with height between retrofitted building with conventional wall foundation (B = 6m) and rocking isolation (B = 3.5m) after being submitted to seismic records of high intensity.

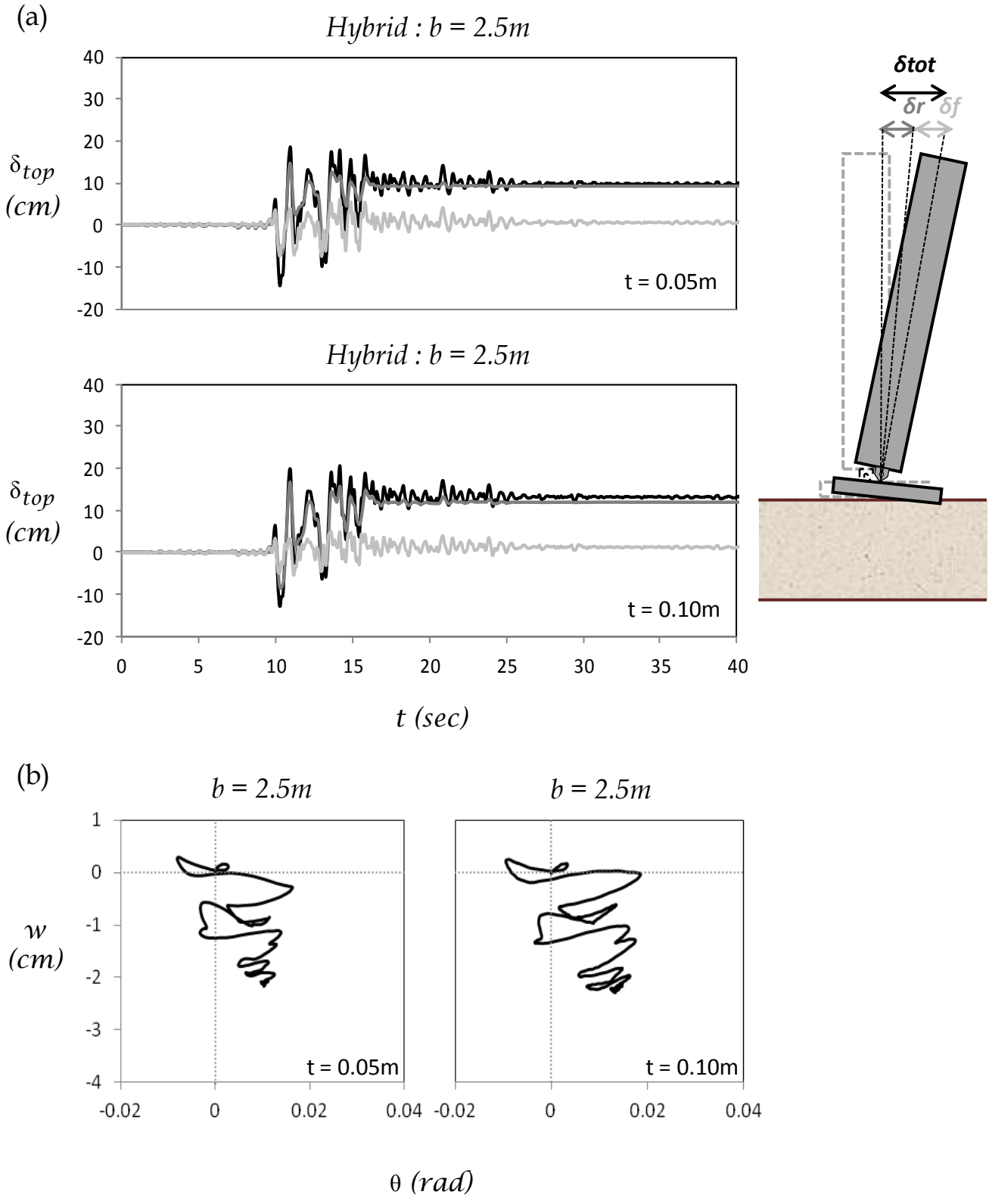

Figure 4.13 (a) Time history of displacement at the top of the shear wall and **(b)** settlement with regard to rotation angle of shear wall foundation, for retrofitted building with rocking isolation (b = 2.5m) while submitted to the record of JMA.

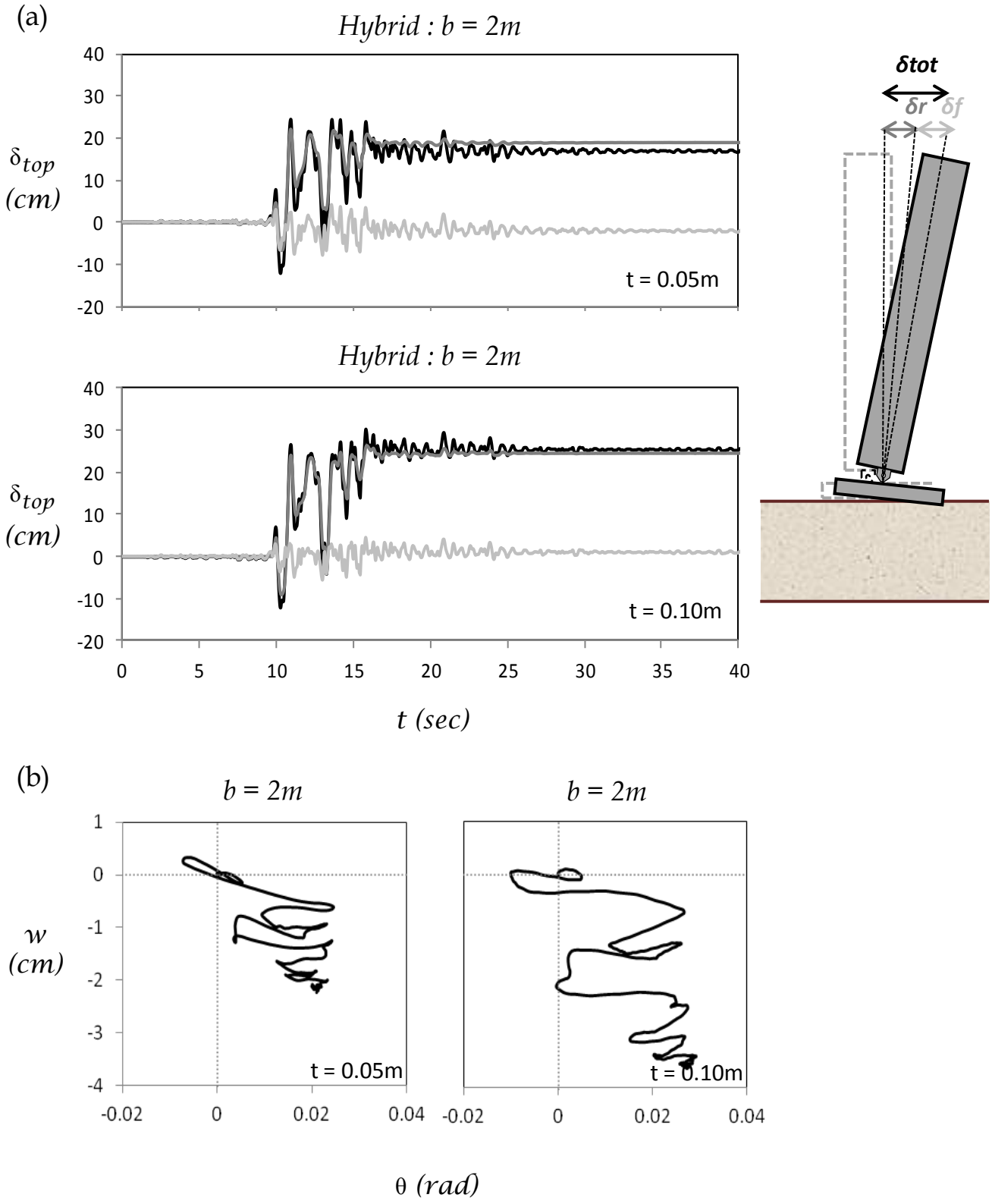

Figure 4.14 (a) Time history of displacement at the top of the shear wall and **(b)** settlement with regard to rotation angle of shear wall foundation, for retrofitted building with rocking isolation (b = 2m) while submitted to the record of JMA.

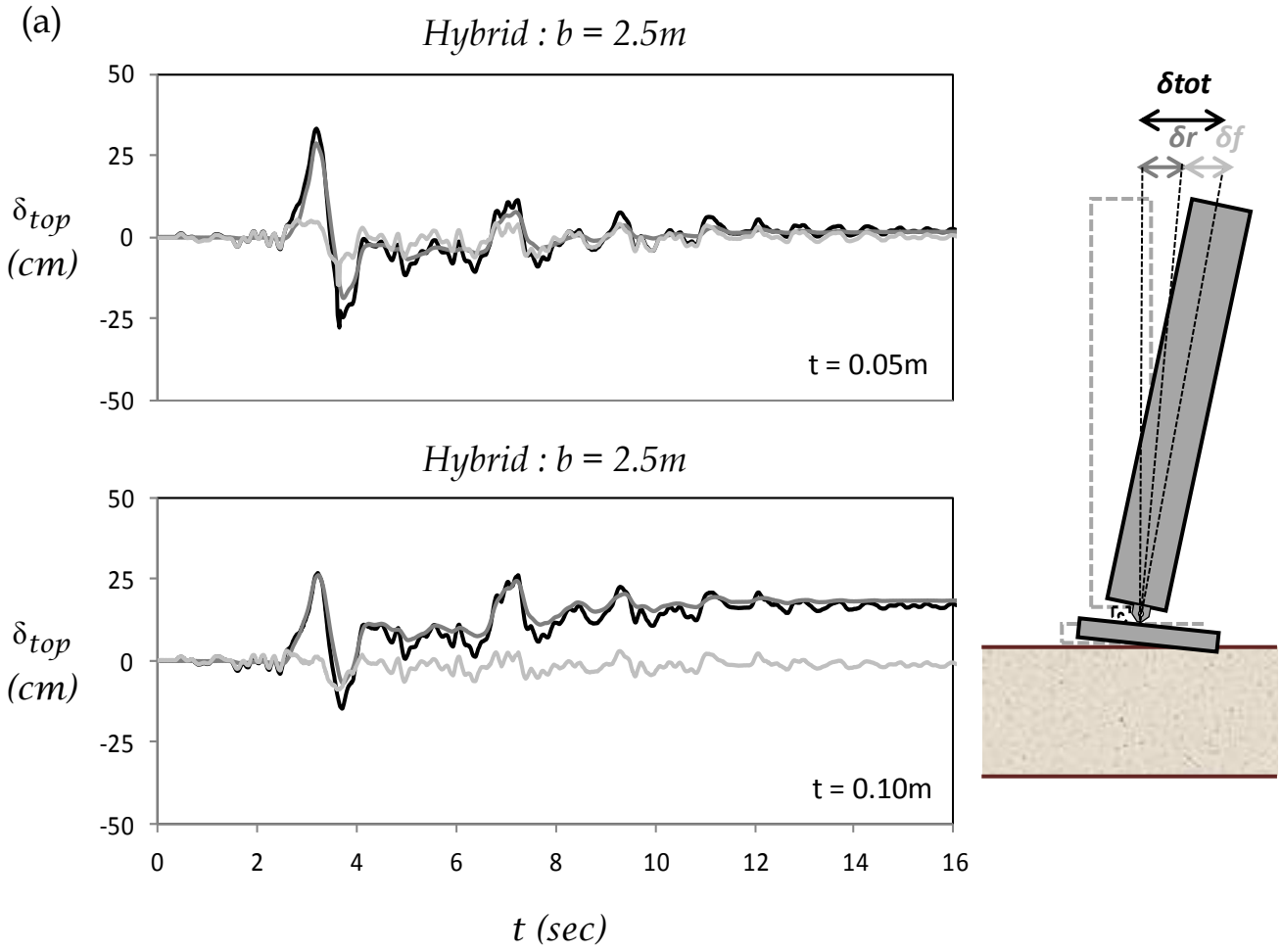

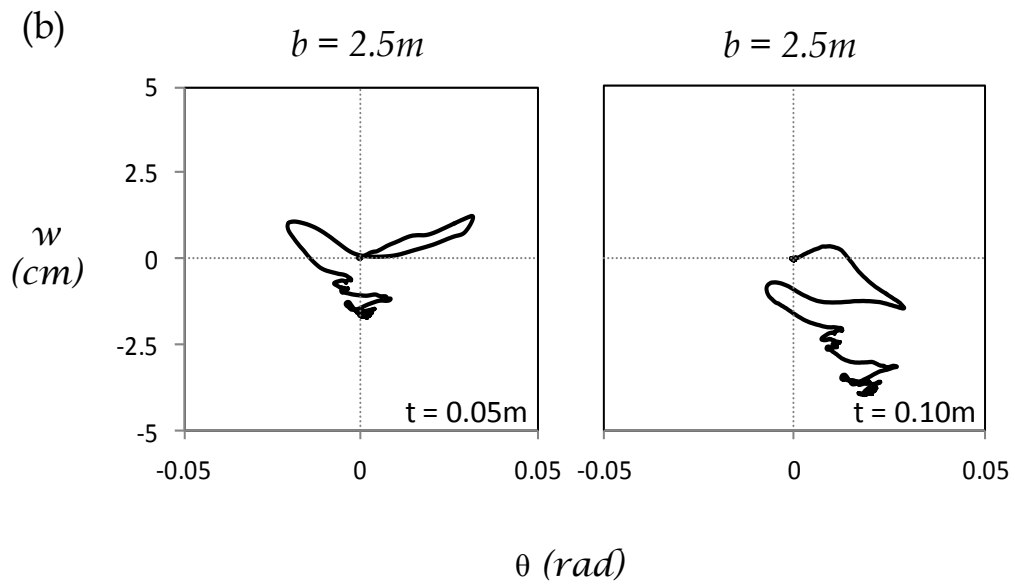

Figure 4.15 (a) Time history of displacement at the top of the shear wall and **(b)** settlement with regard to rotation angle of shear wall foundation, for retrofitted building with rocking isolation (b = 2.5m) while submitted to the record of Rinaldi.

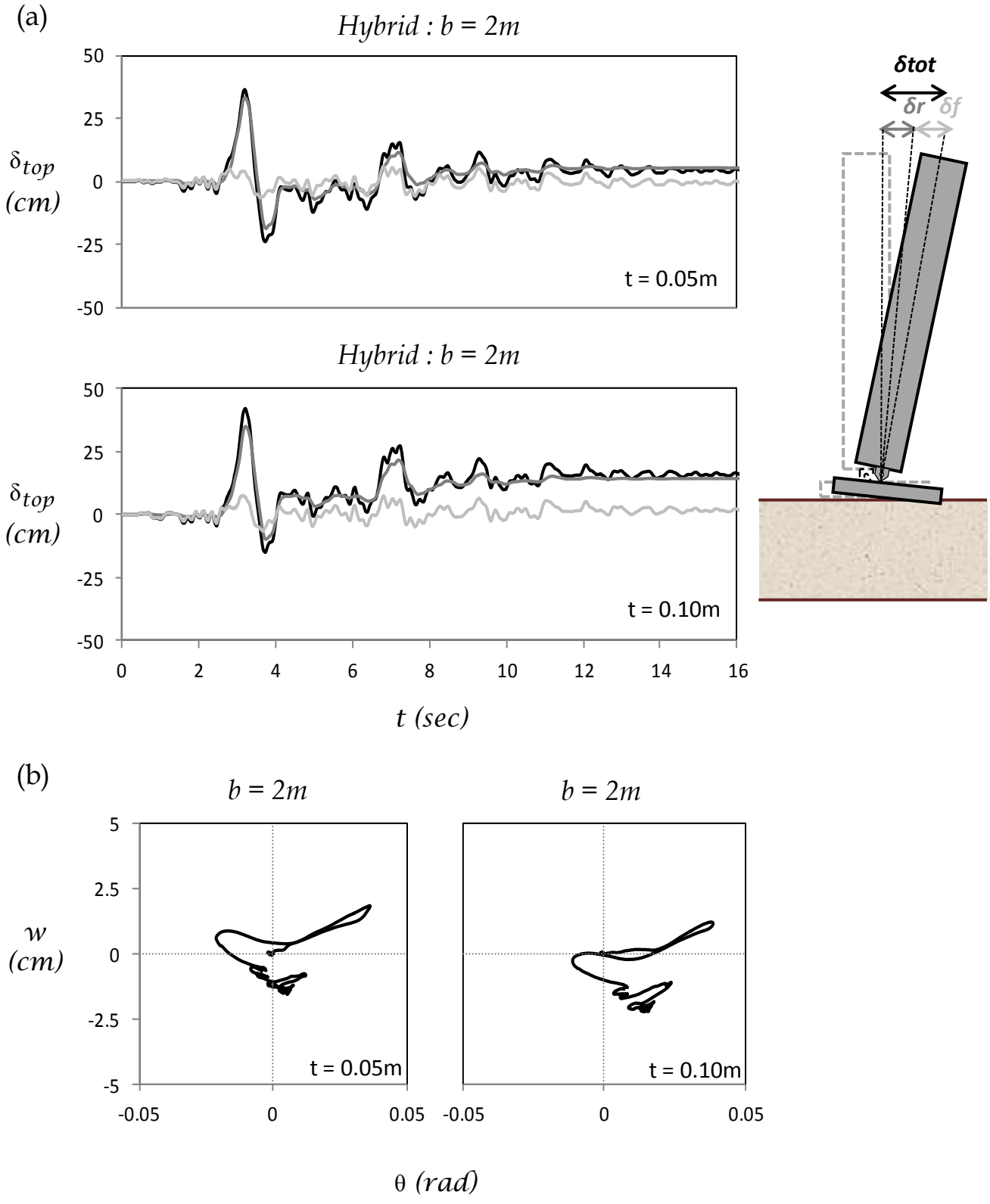

Figure 4.16 (a) Time history of displacement at the top of the shear wall and **(b)** settlement with regard to rotation angle of shear wall foundation, for retrofitted building with rocking isolation (b = 2m) while submitted to the record of Rinaldi.

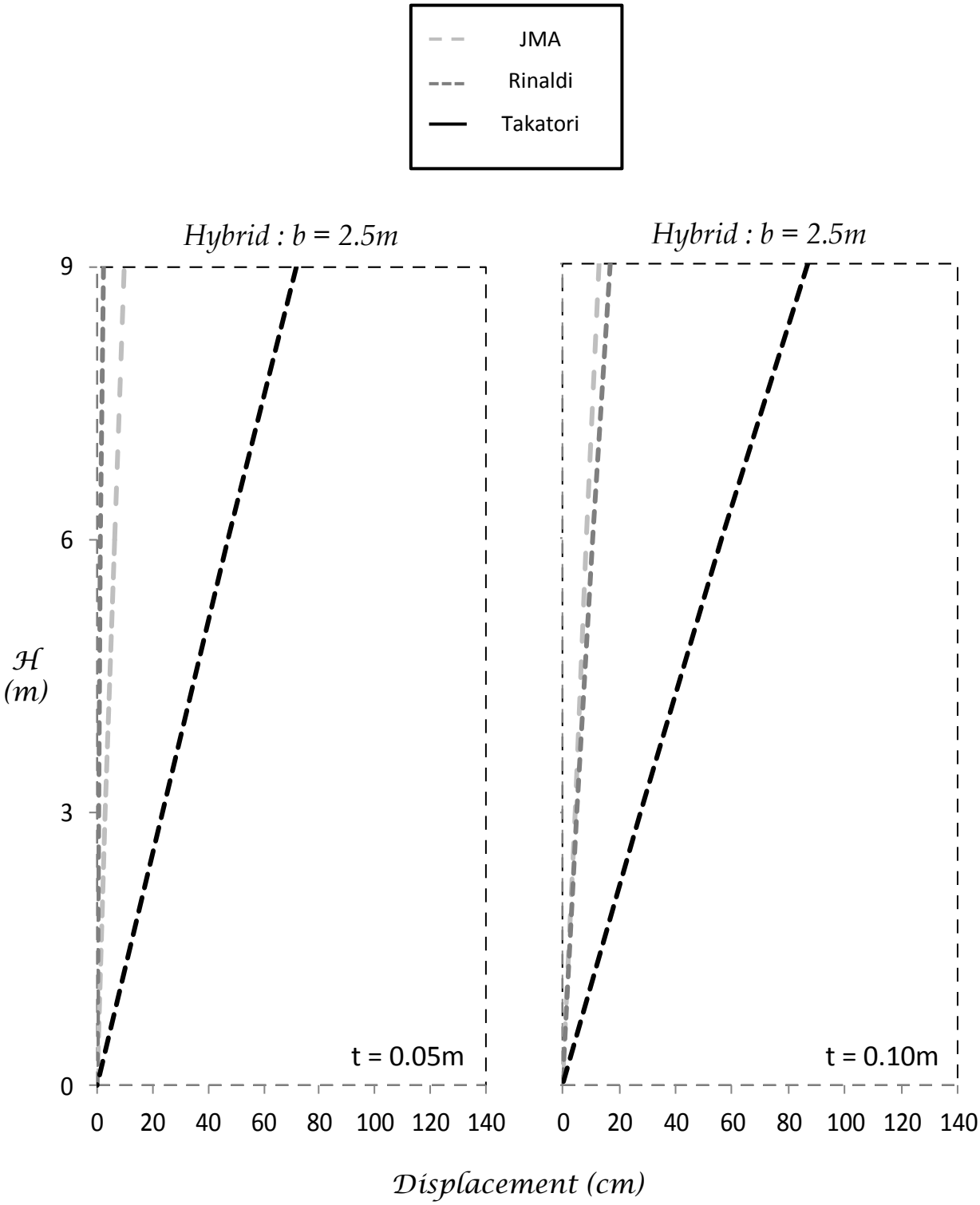

Figure 4.17 Comparison of displacement distribution with height between retrofitted building with rocking isolation (b = 2.5m) after being submitted to seismic records of high intensity.

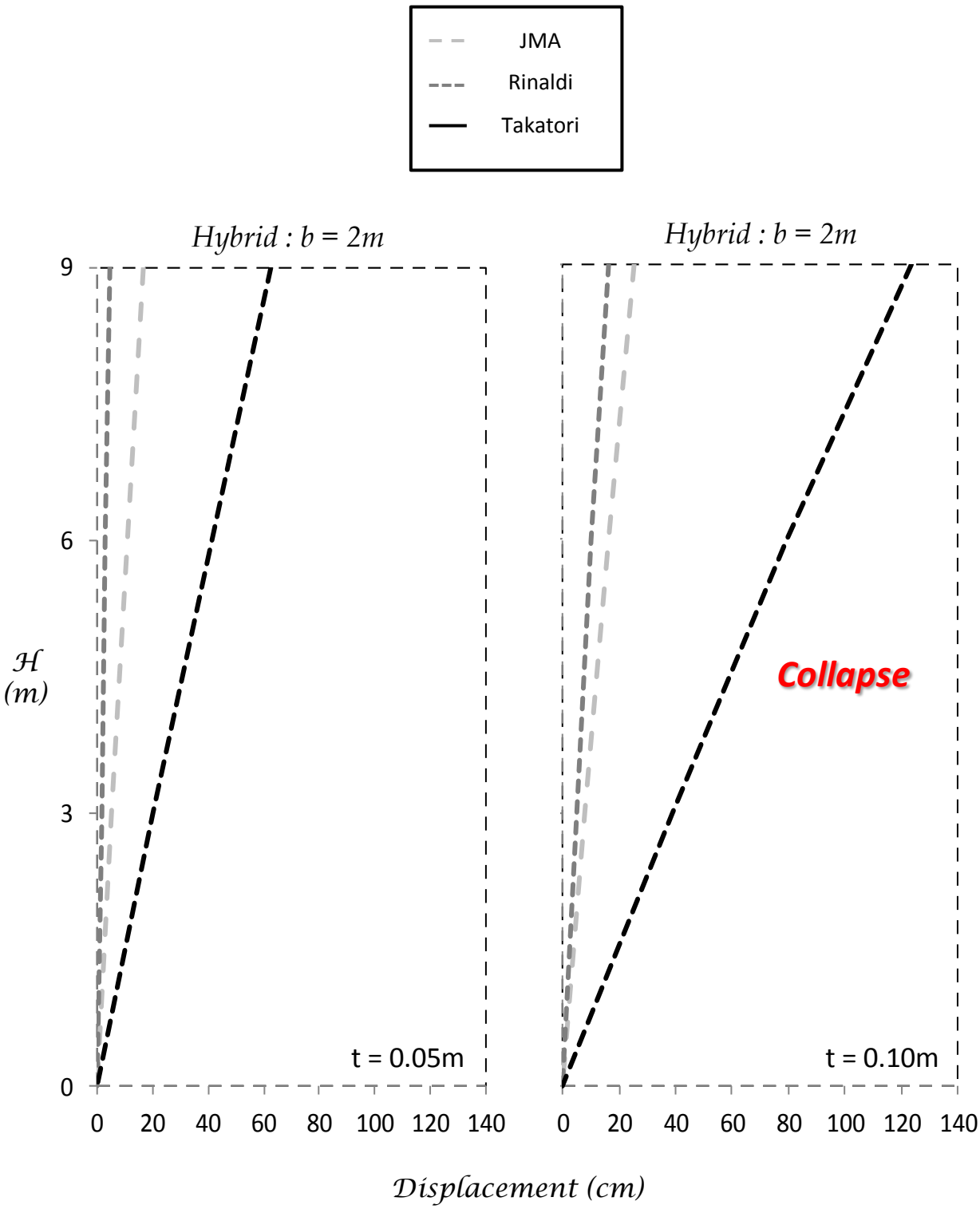

Figure 4.18 Comparison of displacement distribution with height between retrofitted building with rocking isolation (b = 2m) after being submitted to seismic records of high intensity.

5

Addition of Tie Beams

5. ADDITION OF TIE BEAMS

An issue that was faced during this thesis was the significant sliding of particular rocking isolated alternatives under strong seismic shaking. As already explained, the under - designed central footing tends to mobilize its soil failure mechanisms in order to isolate the superstructure. Nevertheless, the existing footings of the columns are conventionally designed and their behavior remains elastic, thus guiding failure to the base of the columns. Yet when soil failure occurs in the shear wall footing and the seismic shaking continues, it sometimes tends to slide - dragging along the failed prism of soil. This happens especially in cases where the footing rocks but does not settle largely. Once this occurs, the differential horizontal displacement between the central and the lateral footings becomes significant, as they remain “fixed”. As a result, the structure collapses. For this reason, the addition of tie beams was examined as a solution.

One extreme case was studied extensively in an attempt to cure this problem (Figures 5.1 – 5.2). The hybrid footing with b = 3 m and t = 0.05 m performs very well while being submitted to the record of JMA, with residual drift ratio of 1.1 %, same as the alternative with b = 2.5 m and the same thickness. Though the latter went on to settle significantly, the first displayed minor settlement and the tendency to slide during the record of Rinaldi. Therefore, even though it appears to perform satisfyingly in terms of drifts (residual drift ratio ≈ 0.4 %), Figure 5.2 is misleading due to the large sliding that the footing displayed (≈ 17 cm), while the column footings practically remained fixed. Figure 5.3 illustrates the collapse of the model during shaking with the record of Takatori (residual drift ratio ≈ 9 %).

5.1 Fixed Tie Beams

The addition of tie beams with fixed edges between the shear wall footing and the column footings should prevent the differential horizontal displacement of the footings. The performance of this alternative for the same seismic record (Rinaldi) is depicted in Figures 5.4 – 5.5 and the two are compared in Figure 5.6. Apparently, the tie beams are not entirely fixed, as the foundation is able to rotate and part of the displacement at the top of the wall

is caused by it. Although the residual displacement is negligible and sliding is almost entirely prevented, the displacement of the shear wall top has more than doubled. In terms of residual drift ratio, in the latter case it is equal to 1 % as opposed to merely 0.4% for the previous system. In conclusion, the addition of fixed – end tie beams is not a satisfactory solution; a fact that becomes more obvious by the building's collapse during the Takatori record, depicted in Figure 5.7 (residual drift ratio ≈ 12 %) .

5.2 Hinged Tie Beams

The solution studied in this paragraph is the addition of hinged – end beams between the footings of the frame. This alternative proves successful in that it reduces sliding significantly, while simultaneously allowing the shear wall hybrid footing to rock freely. As a result, residual drifts decrease with the price of a small increase in residual sliding. Figure 5.10 compares this solution with the alternative without tie beams in terms of displacement at the top of the wall and settlement with regard to rotation angle of the wall foundation during application of the Rinaldi record. The superiority of the hybrid system with unconventional, hinged tie beams is visible.

Figure 5.11 demonstrates that the latter system achieves to survive the Takatori record with significant damage (residual drift ratio ≈ 5 %). Quantitatively, the two solutions using tie beams are compared for the same record in Figure 5.12. Indeed, the fixed tie beams cancel the beneficial effect of the rocking isolation, causing the retrofitting wall to deform flexurally and fail while its foundation suffers zero settlement. On the other hand, the hinged tie beams allow the wall footing to rock, thus completely protecting the superstructure from flexural distortion while suffering minor residual settlement (< 1 cm). Maximum uplift reaches the value of 6 cm.

The comparison between the three alternatives under strong seismic shaking is summarized in Figures 5.13 – 5.14.

Figures of Chapter 5

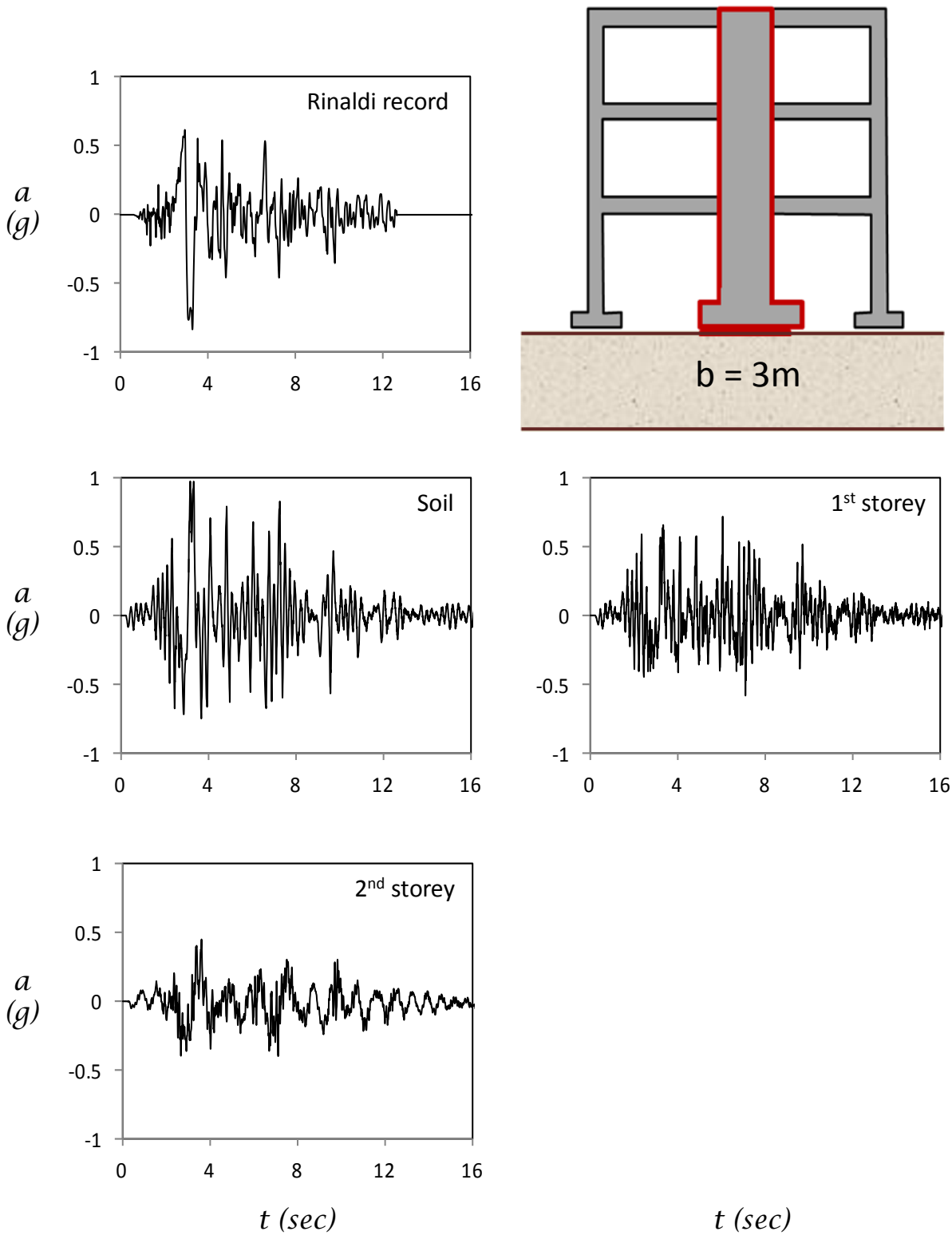

Figure 5.1 Acceleration time histories measured on the retrofitted building with hybrid foundation (b = 3m , t = 0.05m) while submitted to the record of Rinaldi.

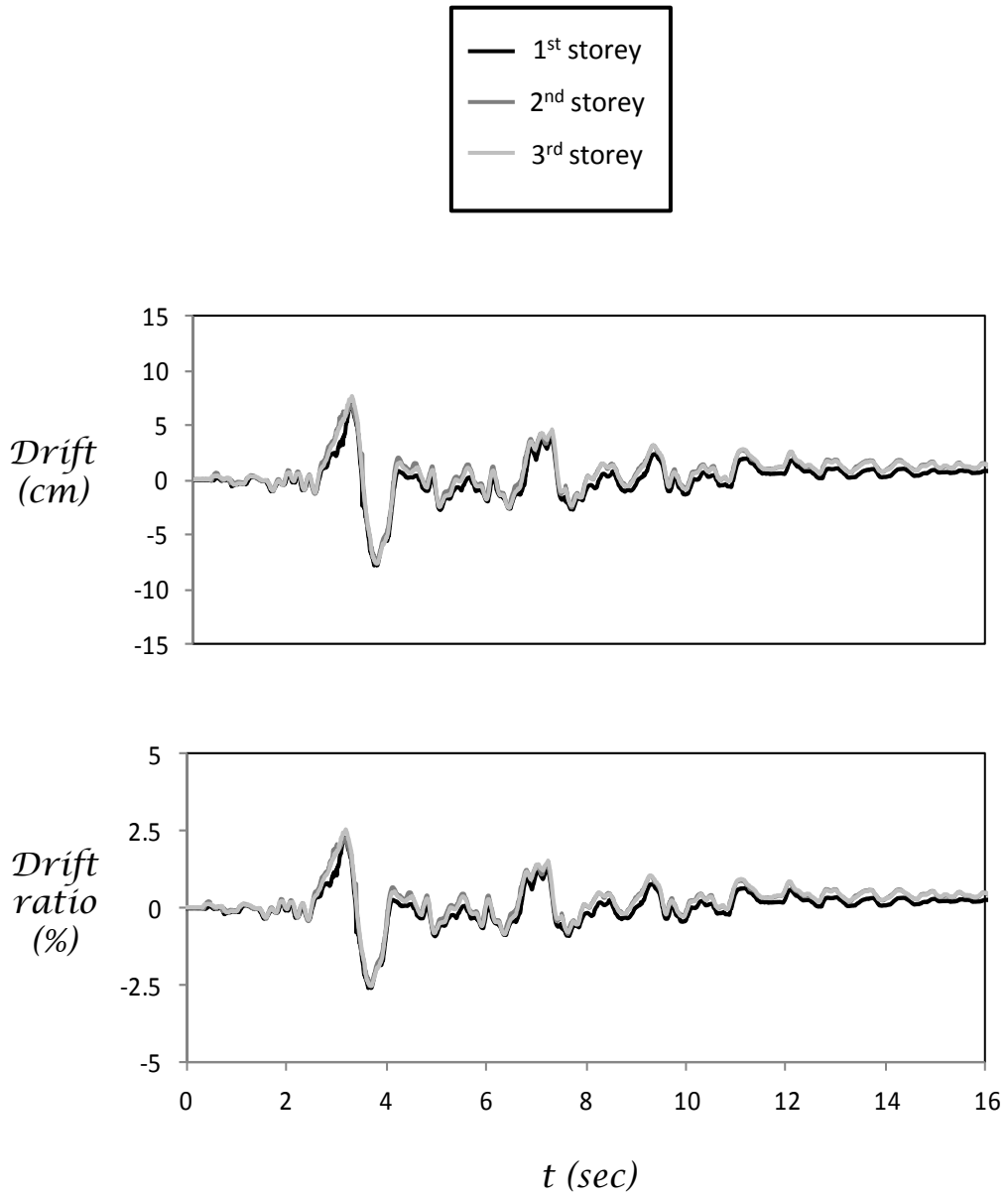

Figure 5.2 Time histories of storey drift and drift ratio of retrofitted building with hybrid foundation (b = 3m , t = 0.05m) while submitted to the record of Rinaldi.

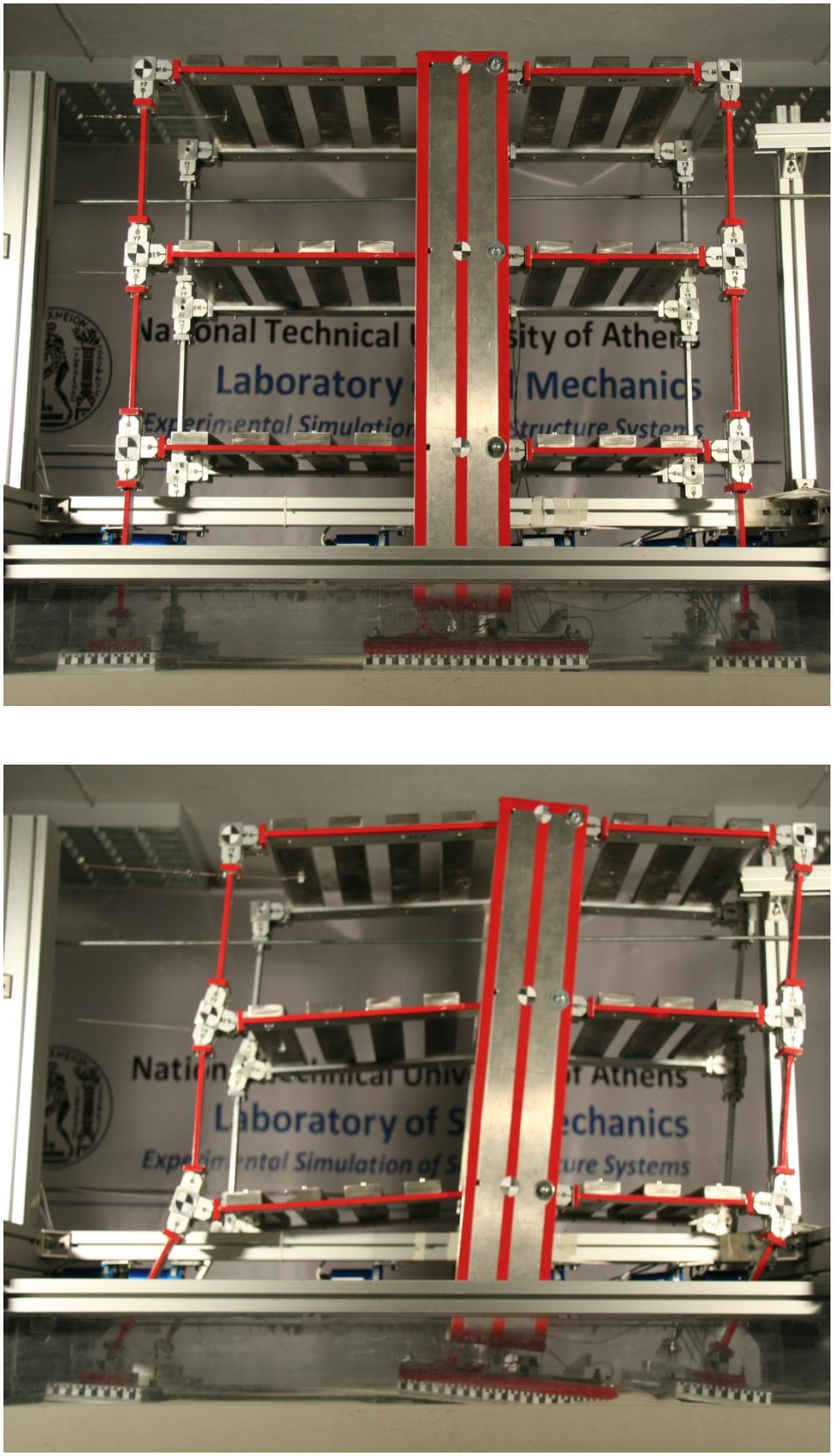

Figure 5.3 Photographs of retrofitted building with hybrid foundation (b = 3m , t = 0.05m) before and after being submitted to a high intensity record (Takatori).

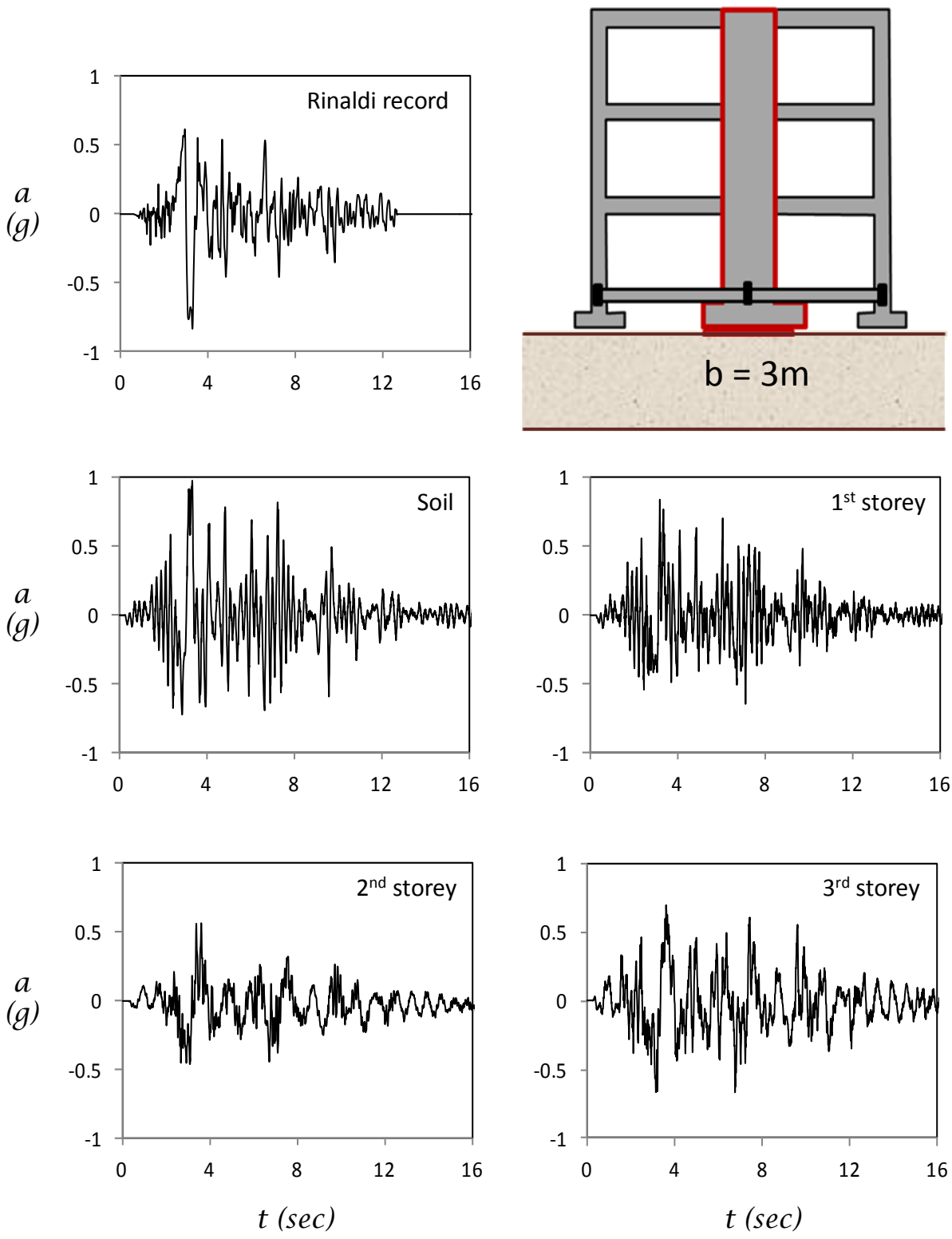

Figure 5.4 Acceleration time histories measured on the retrofitted building with hybrid foundation (b = 3m , t = 0.05m) and fixed tie beams while submitted to the record of Rinaldi.

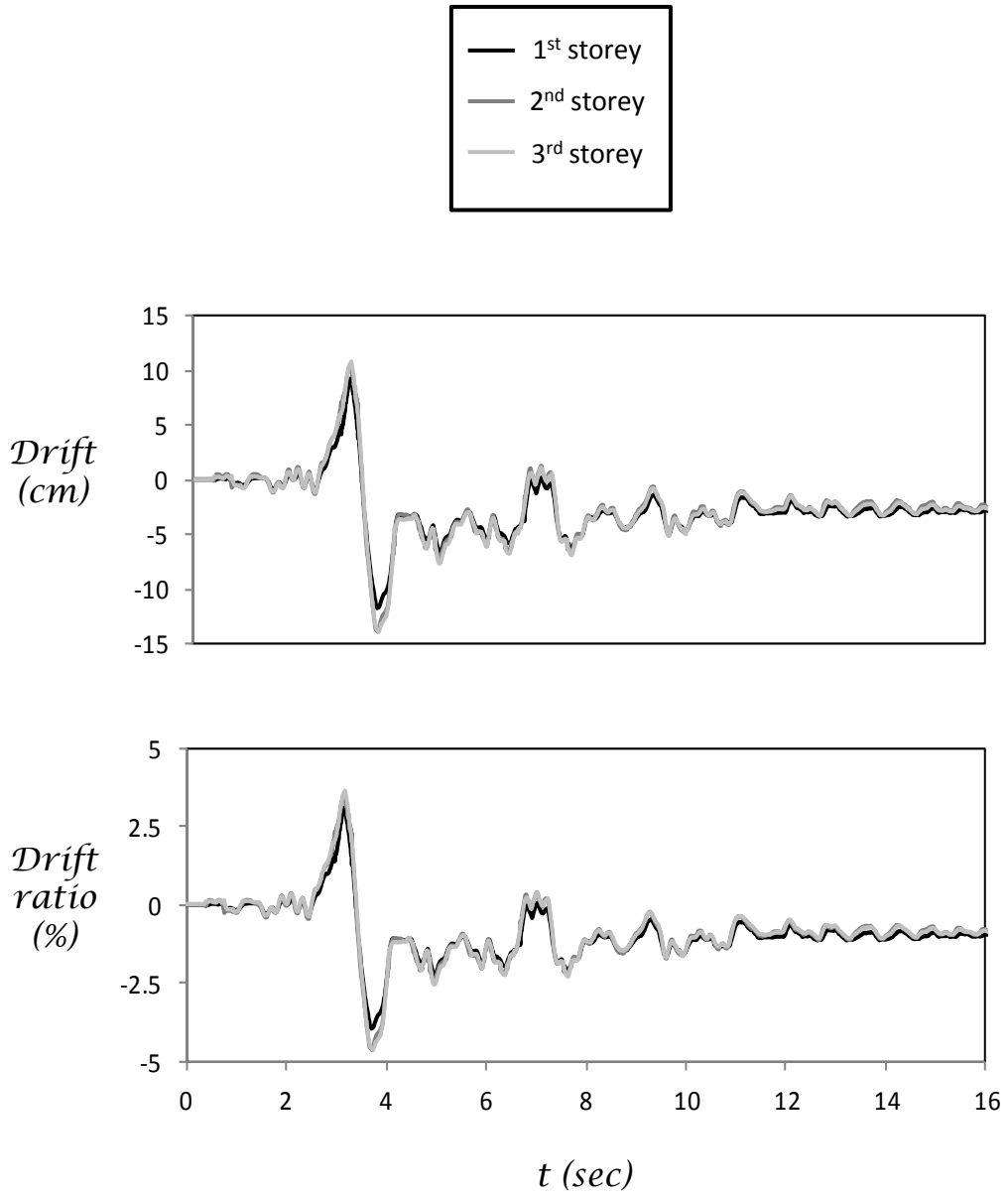

Figure 5.5 Time histories of storey drift and drift ratio of retrofitted building with hybrid foundation (b = 3m , t = 0.05m) and fixed tie beams while submitted to the record of Rinaldi.

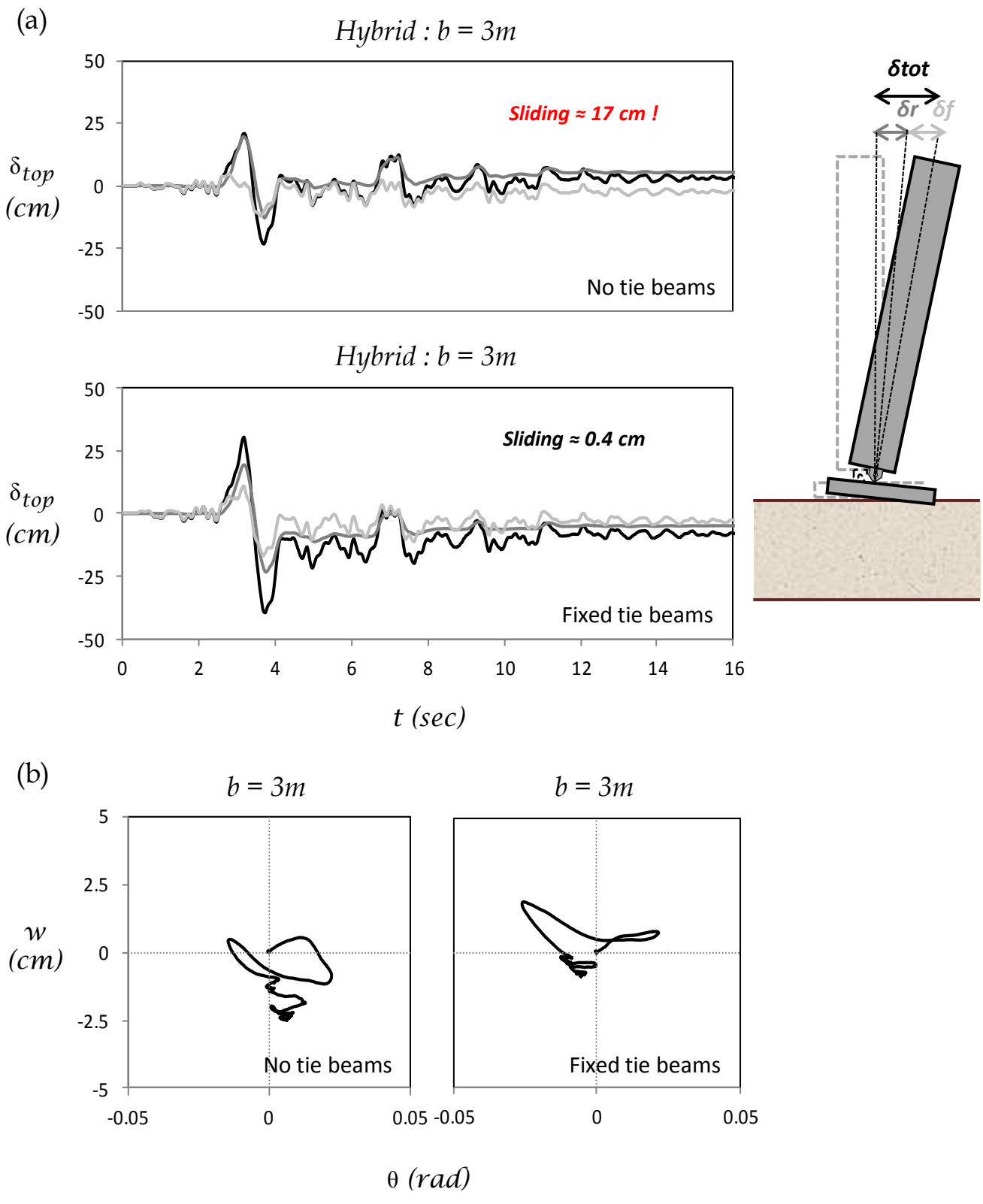

Figure 5.6 (a) Time history of displacement at the top of the shear wall and **(b)** settlement with regard to rotation angle of shear wall foundation, for retrofitted building with hybrid foundation (b = 3m , t = 0.05m) and with fixed tie beams while submitted to the record of Rinaldi.

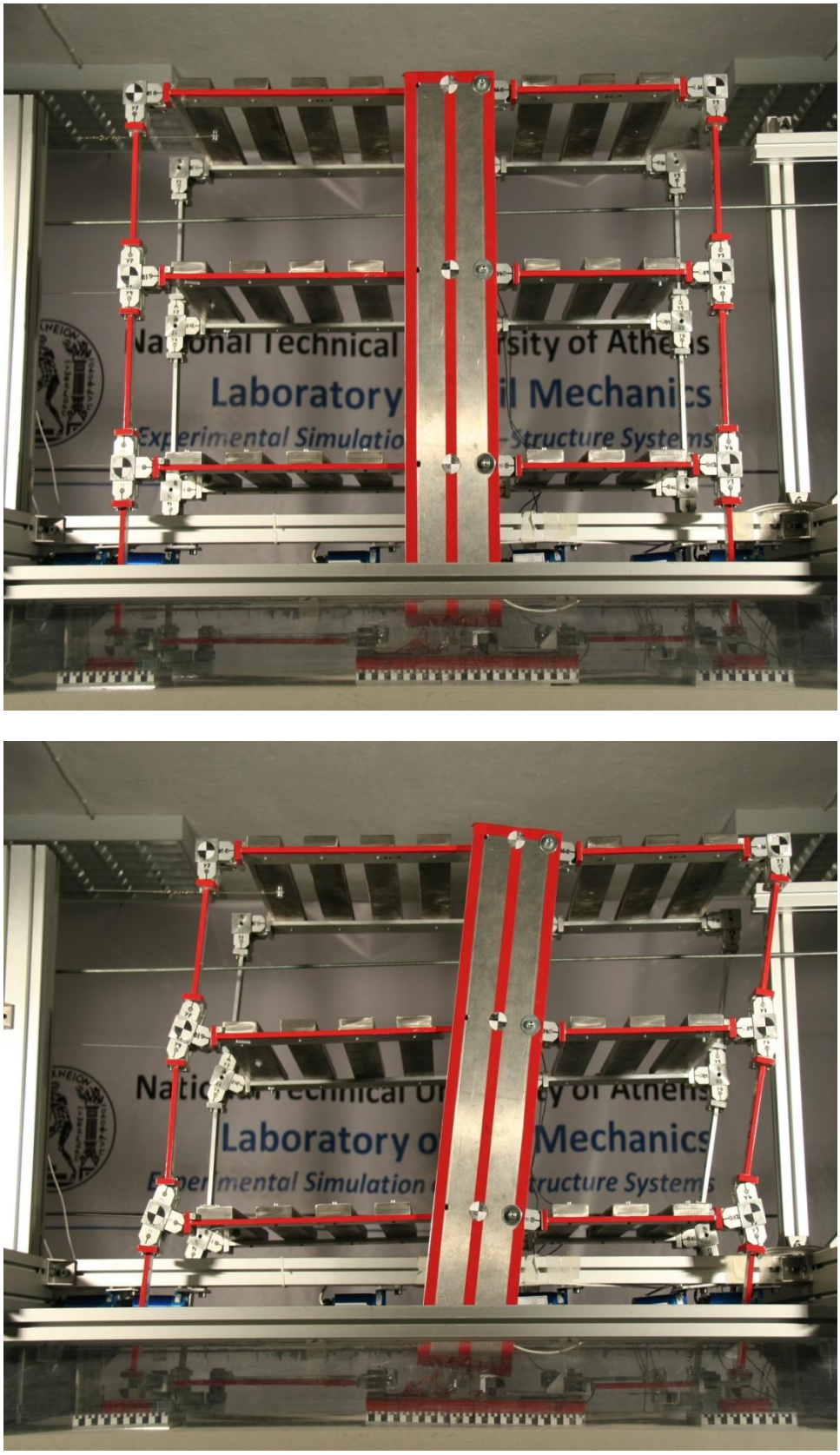

Figure 5.7 Photographs of retrofitted building with hybrid foundation (b = 3m , t = 0.05m) and fixed tie beams before and after being submitted to a high intensity record (Takatori).

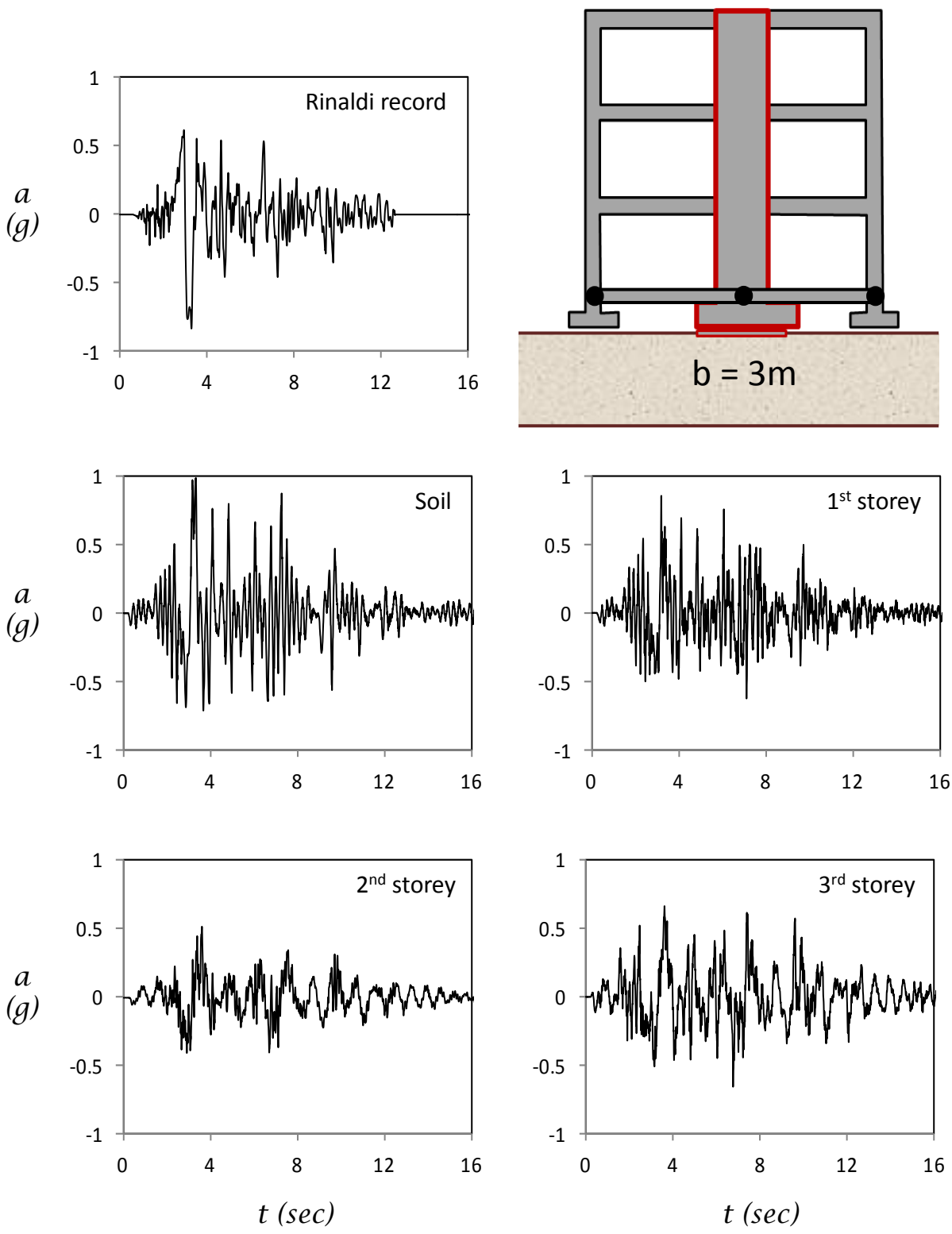

Figure 5.8 Acceleration time histories measured on the retrofitted building with hybrid foundation (b = 3m , t = 0.05m) and hinged tie beams while submitted to the record of Rinaldi.

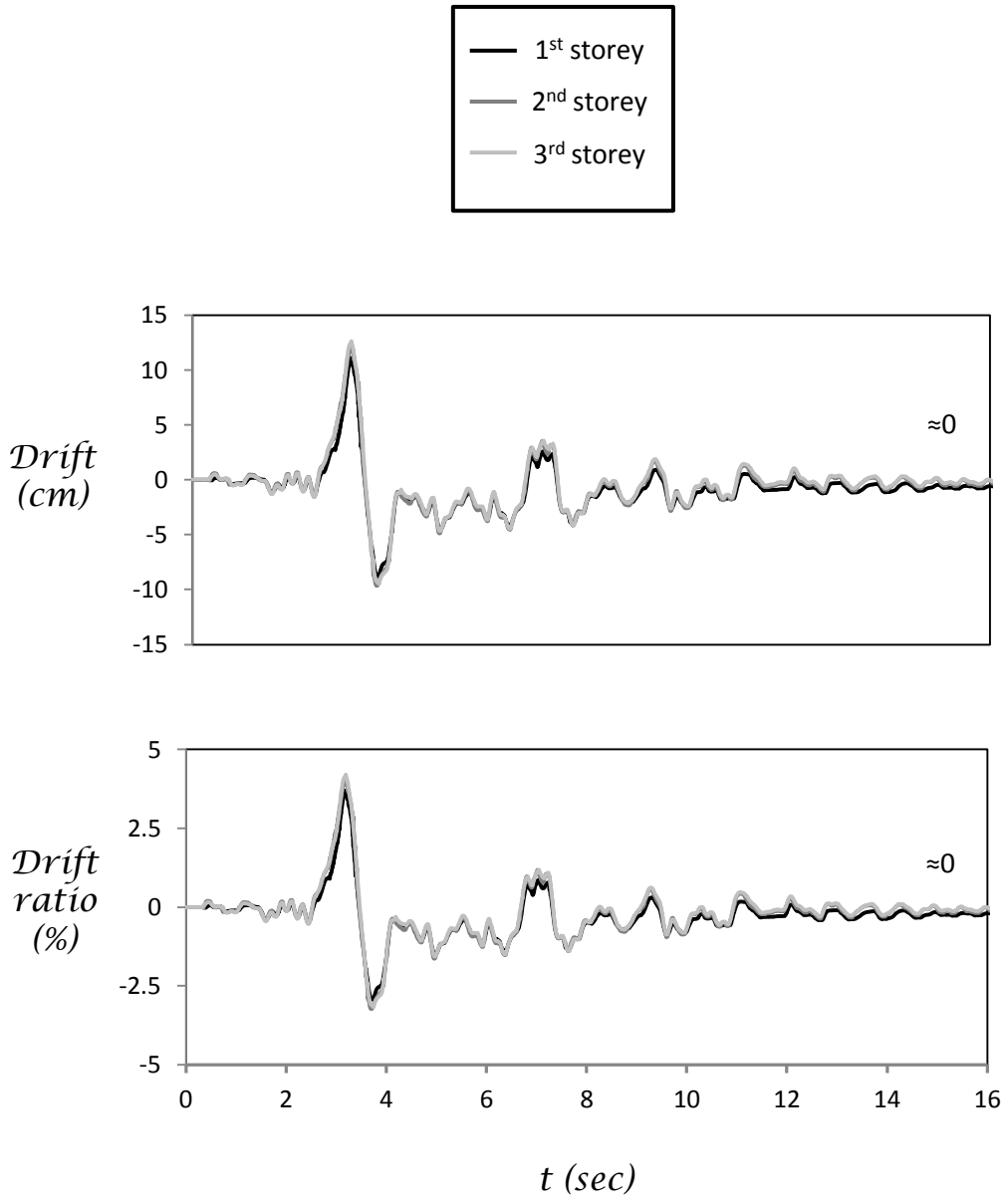

Figure 5.9 Time histories of storey drift and drift ratio of retrofitted building with hybrid foundation (b = 3m , t = 0.05m) and hinged tie beams while submitted to the record of Rinaldi.

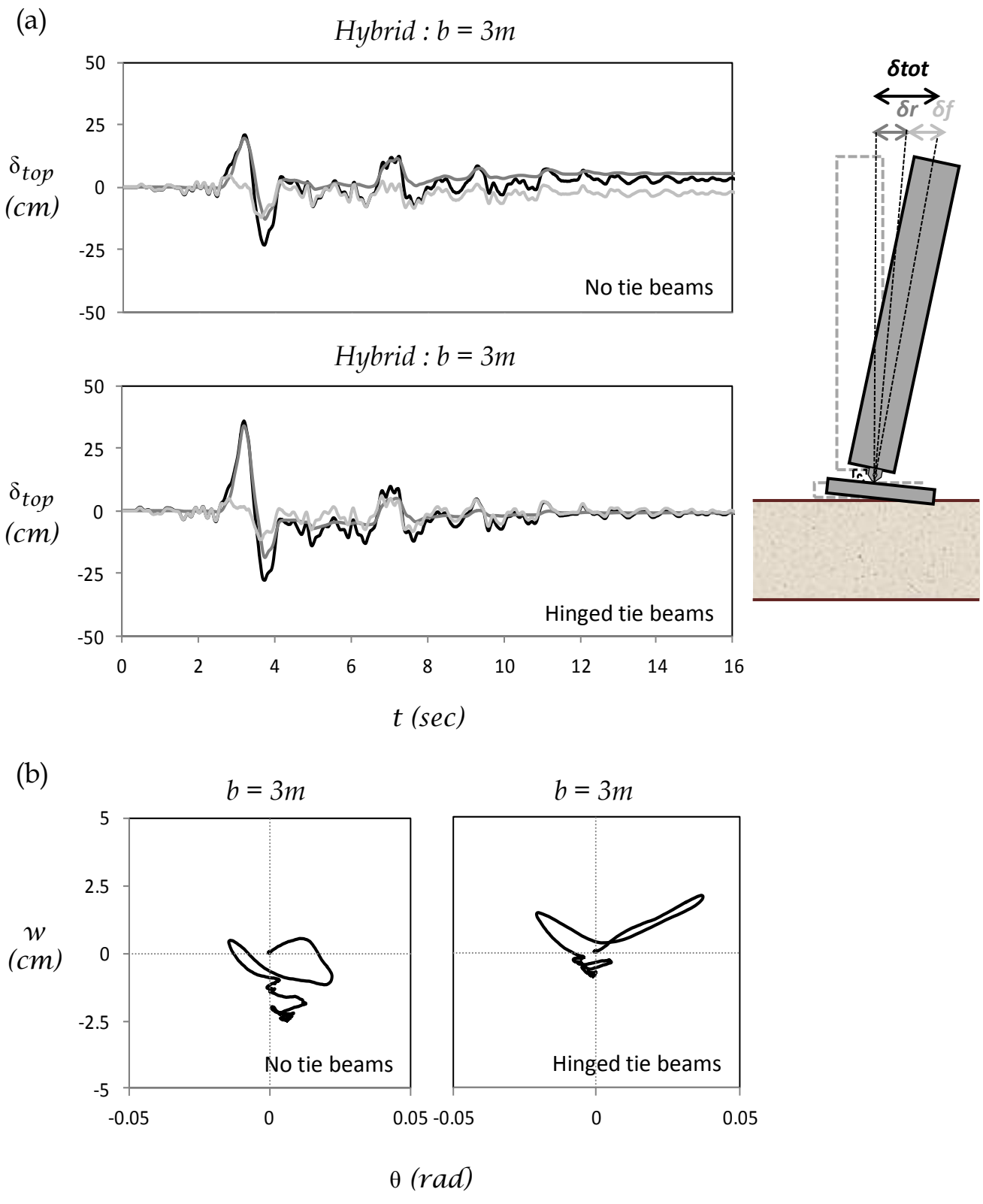

Figure 5.10 (a) Time history of displacement at the top of the shear wall and **(b)** settlement with regard to rotation angle of shear wall foundation, for retrofitted building with hybrid foundation (b = 3m , t = 0.05m) and with hinged tie beams while submitted to the record of Rinaldi.

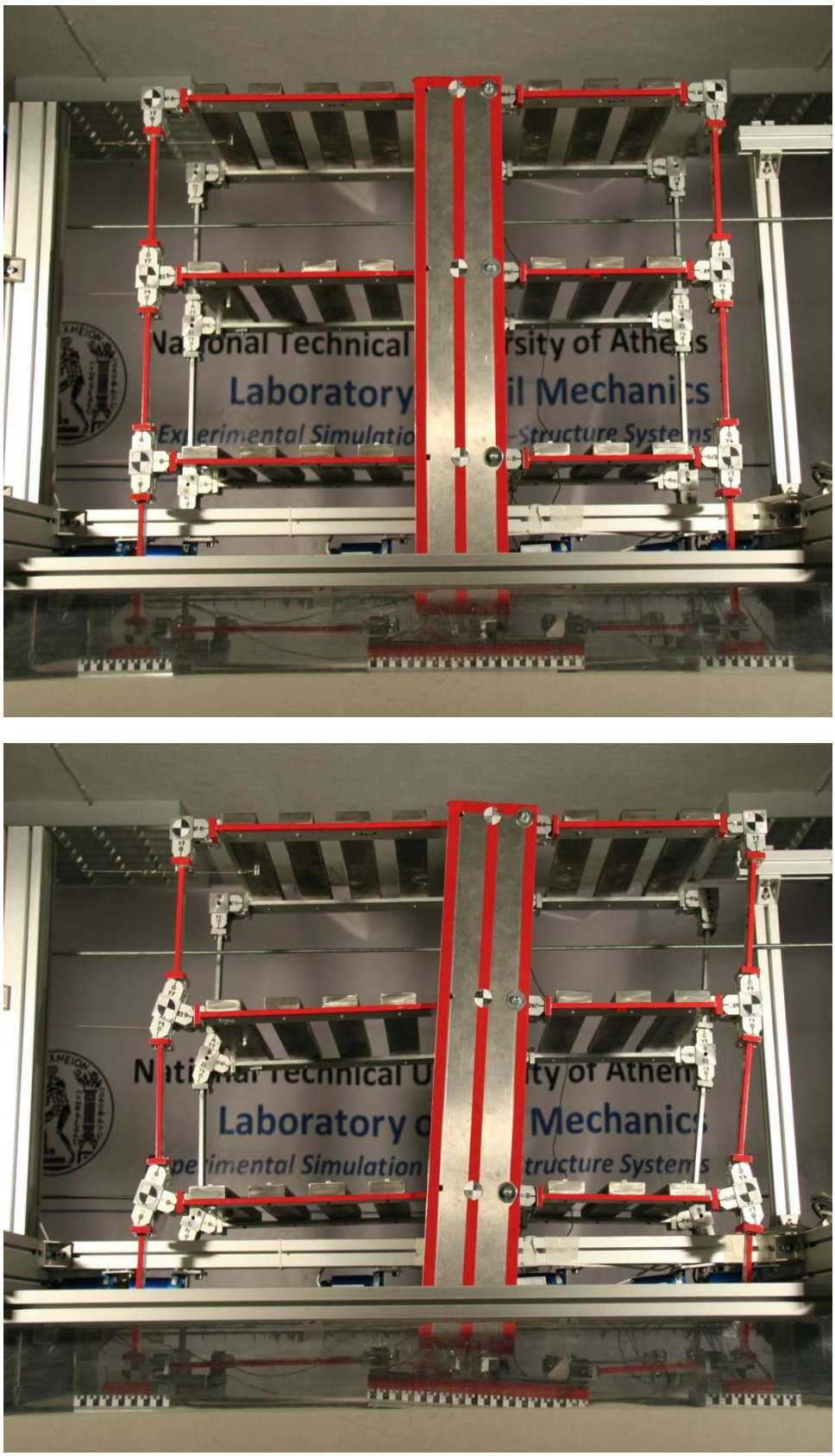

Figure 5.11 Photographs of retrofitted building with hybrid foundation (b = 3m , t = 0.05m) and hinged tie beams before and after being submitted to a high intensity record (Takatori).

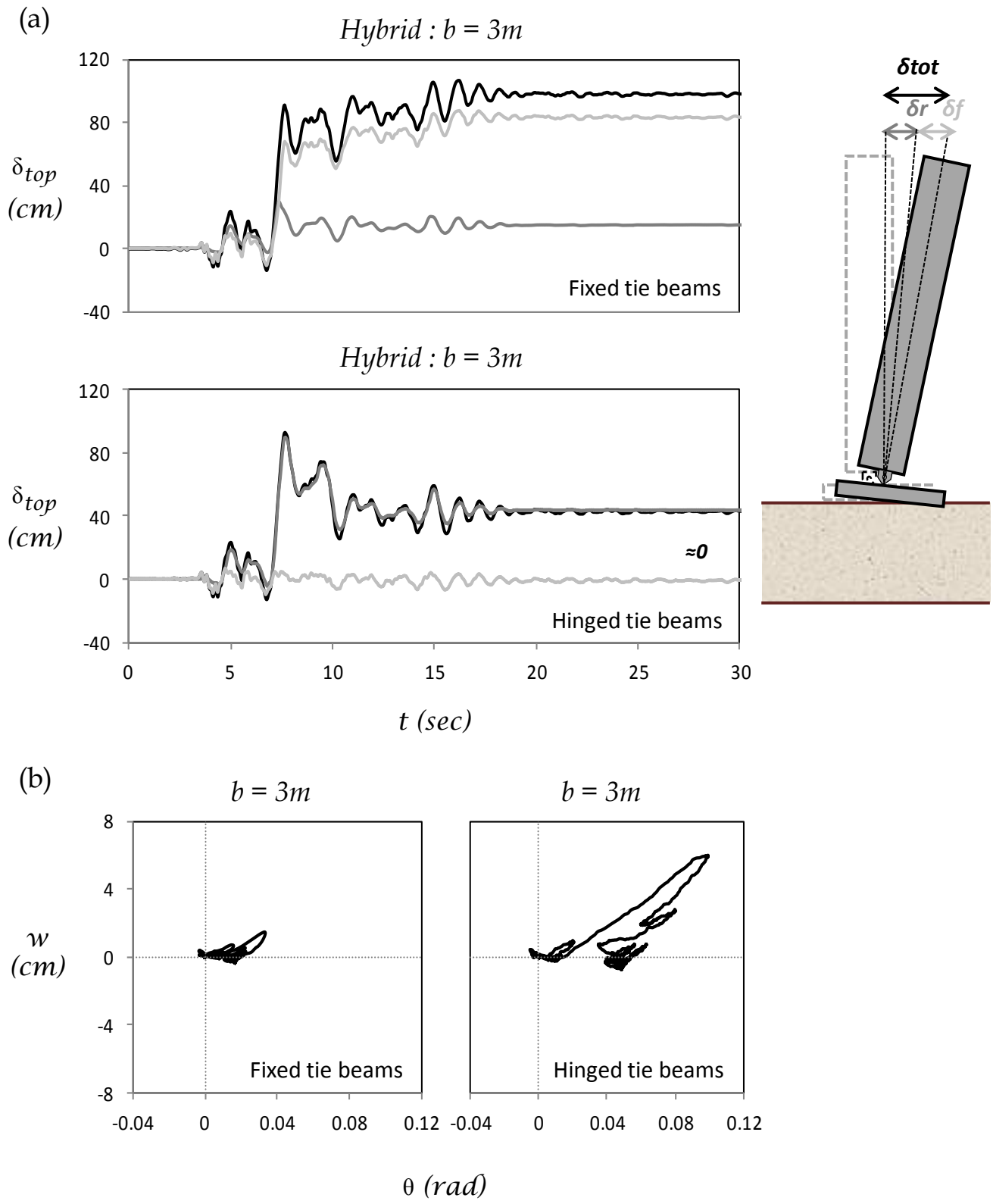

Figure 5.12 (a) Time history of displacement at the top of the shear wall and **(b)** settlement with regard to rotation angle of shear wall foundation, for retrofitted building with hybrid foundation (b = 3m , t = 0.05m) and hinged tie beams while submitted to the record of Takatori.

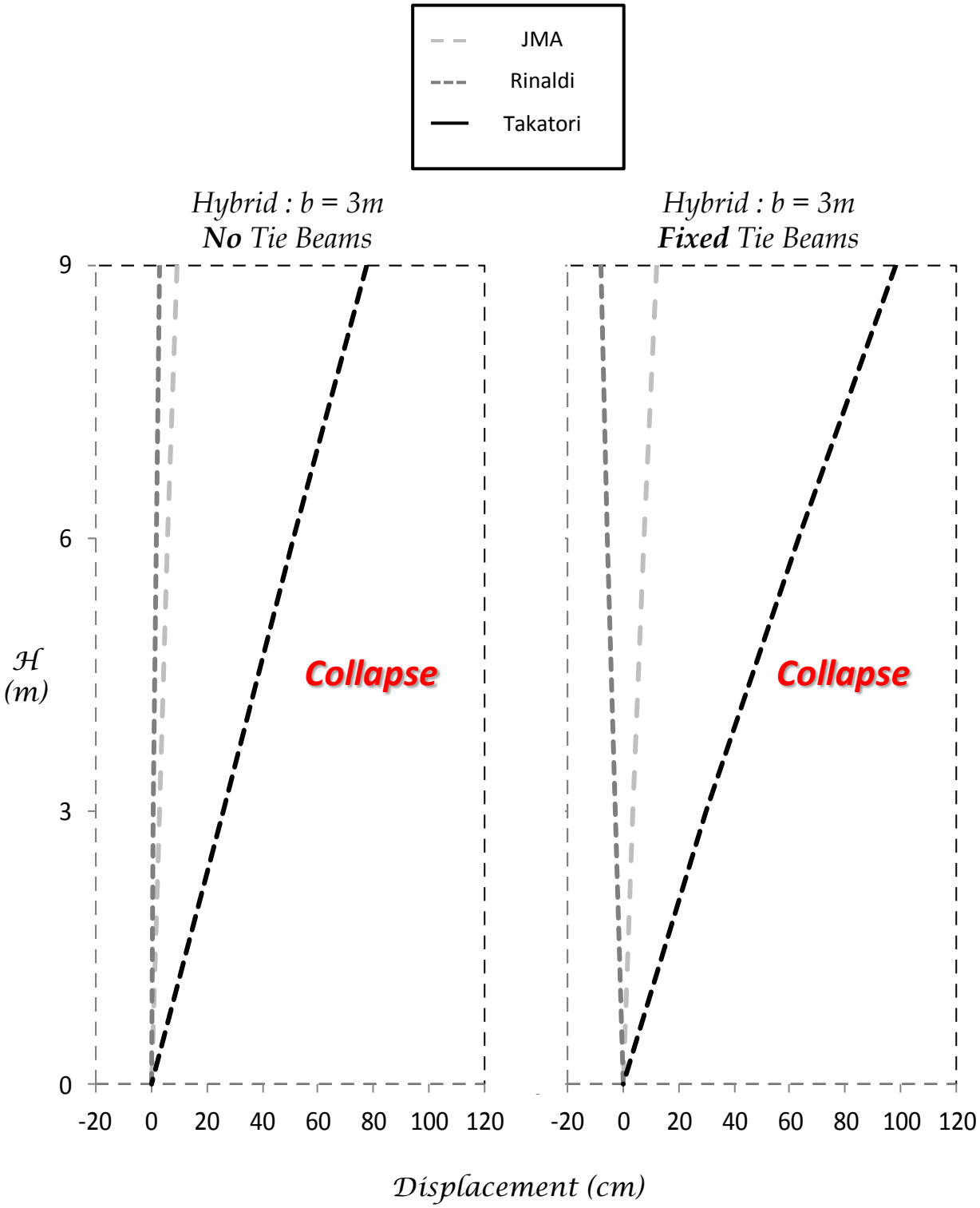

Figure 5.13 Comparison of displacement distribution with height between retrofitted building with rocking isolation (b = 3m) and with fixed tie beams after being submitted to seismic records of high intensity.

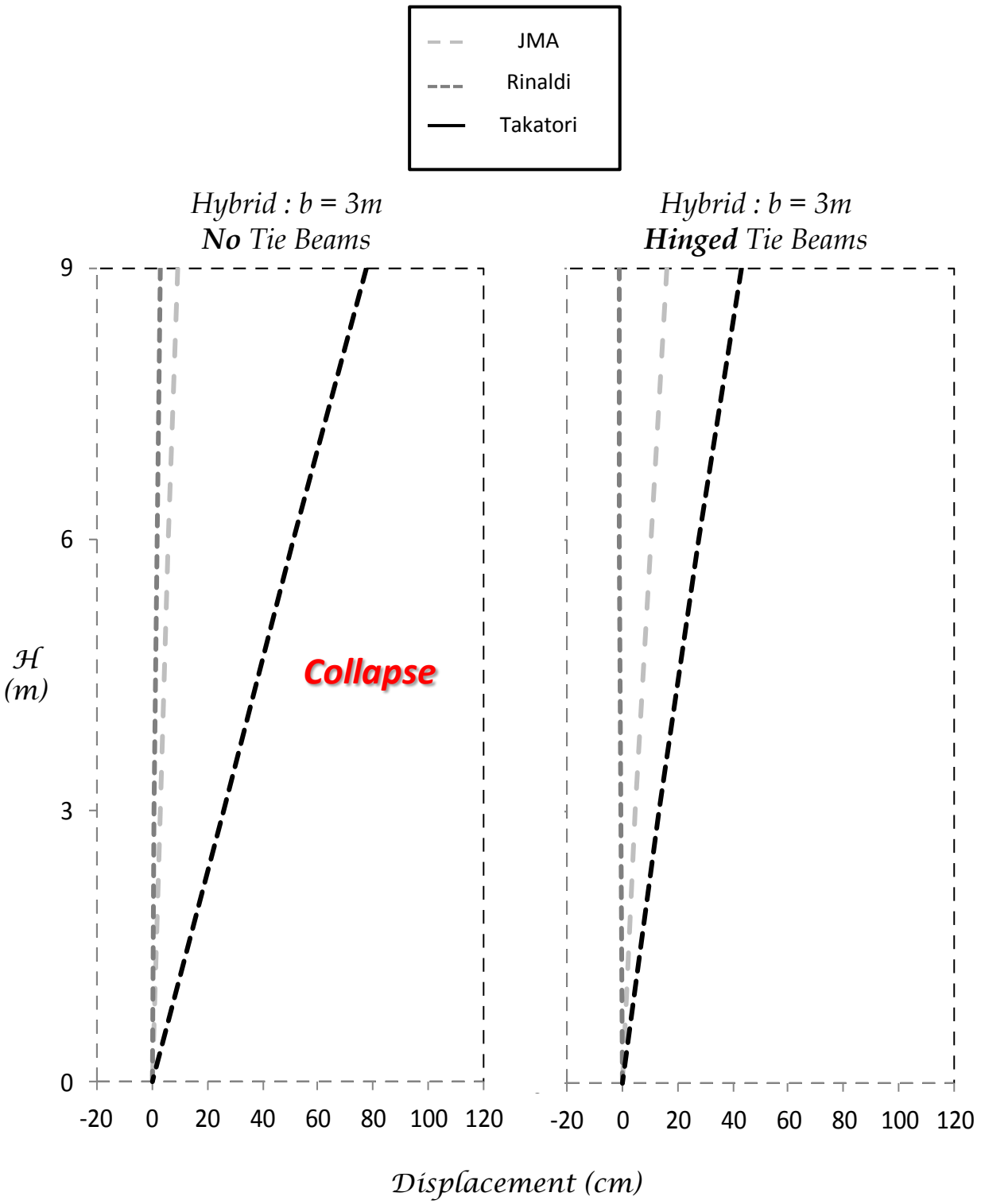

Figure 5.14 Comparison of displacement distribution with height between retrofitted building with hybrid foundation (b = 3m , t = 0.05m) and with hinged tie beams after being submitted to seismic records of high intensity.

6

Conclusions

6. CONCLUSIONS – COMPARISON OF RESULTS

This thesis mainly aimed to shed light to the behavior of rocking isolation as a means of retrofitting an existing structure. As an experimental study, the research faced practical problems and modeling imperfections.

One problem that may have affected the results of this study was the inability of the column – to – beam connections to rotate limitlessly. A technical defect caused the artificial plastic hinges to prevent the rotation of the members over a specific, large value. This affected the results for strong seismic shaking, where significant deformation of the structure gradually accumulated. In order to avoid mobilizing unrealistic strength and taking into account faulty measurements, tests were conducted for both the full sequence of seismic records and the small sequence of strong seismic records separately. Figures that depict results for strong seismic shaking refer to the second type of tests.

In addition, the deformation of the experimental setup during strong seismic shaking can sometimes cause the instruments to acquire distorted measurements. The conduction of tests as mentioned in the previous paragraph alleviates this problem as well.

Figures 6.1 – 6.3 qualitatively depict the deformed shape at failure for each type of system examined throughout this study. In general:

- Designed in the 70's, in accordance with obsolete seismic codes, the original 3-storey building cannot withstand seismic motions even of moderate intensity. It is found capable of surviving the Kalamata and Aegion seismic motions, but collapses when subjected to the Lefkada 2003 record. Besides from having inadequate strength and ductility, the lack of capacity design (*weak columns–strong beams*) leads to the development of a soft-storey mechanism and collapse.

- Addition of a RC wall with conventionally *over-designed B* = 6 m foundation proves to be a successful way of retrofitting the structure, leading to a substantial increase of strength and ductility, but also to homogenization of deformation and evenly

distributed inter-storey drifts on all floors. The structure collapses during very strong seismic shaking, when a plastic hinge is formed at the base of the shear wall.

- Further improvement proves to be possible through applying rocking isolation to the shear wall. Its advantageous performance is revealed when subjected to very strong seismic motions substantially exceeding the design limits. In stark contrast to the conventionally retrofitted structure, it is found capable of surviving with minimal to severe damage. Evidently, due to its inherent self-centering characteristics, rocking isolation allows the superstructure to return to its initial position even after such strong seismic excitations. Sliding and/or settlement and rotation of the wall – foundation system are the price to pay for limiting the inertia transmitted to the superstructure. Conventional design of the existing footings can prove problematic, as the differential sliding or settlement may lead to collapse in case of a very strong earthquake that exceeds the design.

- The combination of fixed tie beams between footings and rocking isolation is not successful since the tie beams cancel the efficiency of rocking. The structure behaves similarly with the conventional alternative.

- On the other hand, hinged tie beams allow rocking while simultaneously preventing differential sliding by utilizing their axial stiffness and strength. The combination of rocking isolation with hinged tie beams proves to be an efficient solution.

In the figures that follow (6.4 – 6.9) the results for all retrofitted systems and excitations are presented in the form of residual drift ratio (%) per storey with regard to storey height. More specifically, the first set of figures (6.4 – 6.6) depicts the performance of the retrofitted structure for all alternative types of wall foundation under moderate intensity seismic shaking, whereas the second set (6.7 – 6.9) similarly depicts the results for strong to very strong seismic shaking. The first row of all figures shows the results for the conventional (B = 6 m) and the rocking isolated (B = 3.5 m) alternatives. The first figure of each set also includes the diagrams for hybrid footings of t = 0.05 m and reducing width in its second and third row (Figures 6.4 and 6.7), the second figure of each set includes the respective

diagrams for hybrid footings of same width and varying thickness t (Figures 6.5 and 6.8) and, finally, the third the alternative that was tested with and without tie beams (b = 3 m) (Figures 6.6 and 6.9).

It is evident that all retrofitted systems perform satisfyingly under seismic shaking within their design limits, since they display values of residual drift ratio lower than 1 %. Nevertheless, the alternatives included in Figure 6.5 are the most satisfactory, with residual drift ratio no more than 0.4 %. Apparently, further reduction of the footing is not beneficial for the performance of the structure during these motions.

With regard to performance under strong seismic shaking, it can be concluded that most retrofitted alternatives are able to sustain the records of JMA and Rinaldi with significant damage (residual drift ratio < 3 %). However, the rocking isolated systems with wall foundation width equal to 3.5 m, 3 m (t = 0.05 m) and 2.5 m (t = 0.05 m) are proven to be more efficient, as they display residual drift ratio of impressively small value for such strong seismic shaking (≈ 1 %). Under extremely strong shaking (Takatori record) the performance of the alternative solutions worsens as the footing's width reduces below 3.5 m. Yet, the hybrid alternative of 2.5 m appears to respond more satisfyingly than the 3 m alternative. Due to its reduced width the latter has settled significantly after being subjected to the previous seismic records, thus having mobilized the upper component of the hybrid (B = 3.5 m). Finally, the only systems that can sustain the shaking induced by the record of Takatori are the rocking isolated alternative with B = 3.5 m and the hybrid alternative with b = 3 m, t = 0.05 m and hinged tie beams, which prove to be practically equivalent.

Figures of Chapter 6

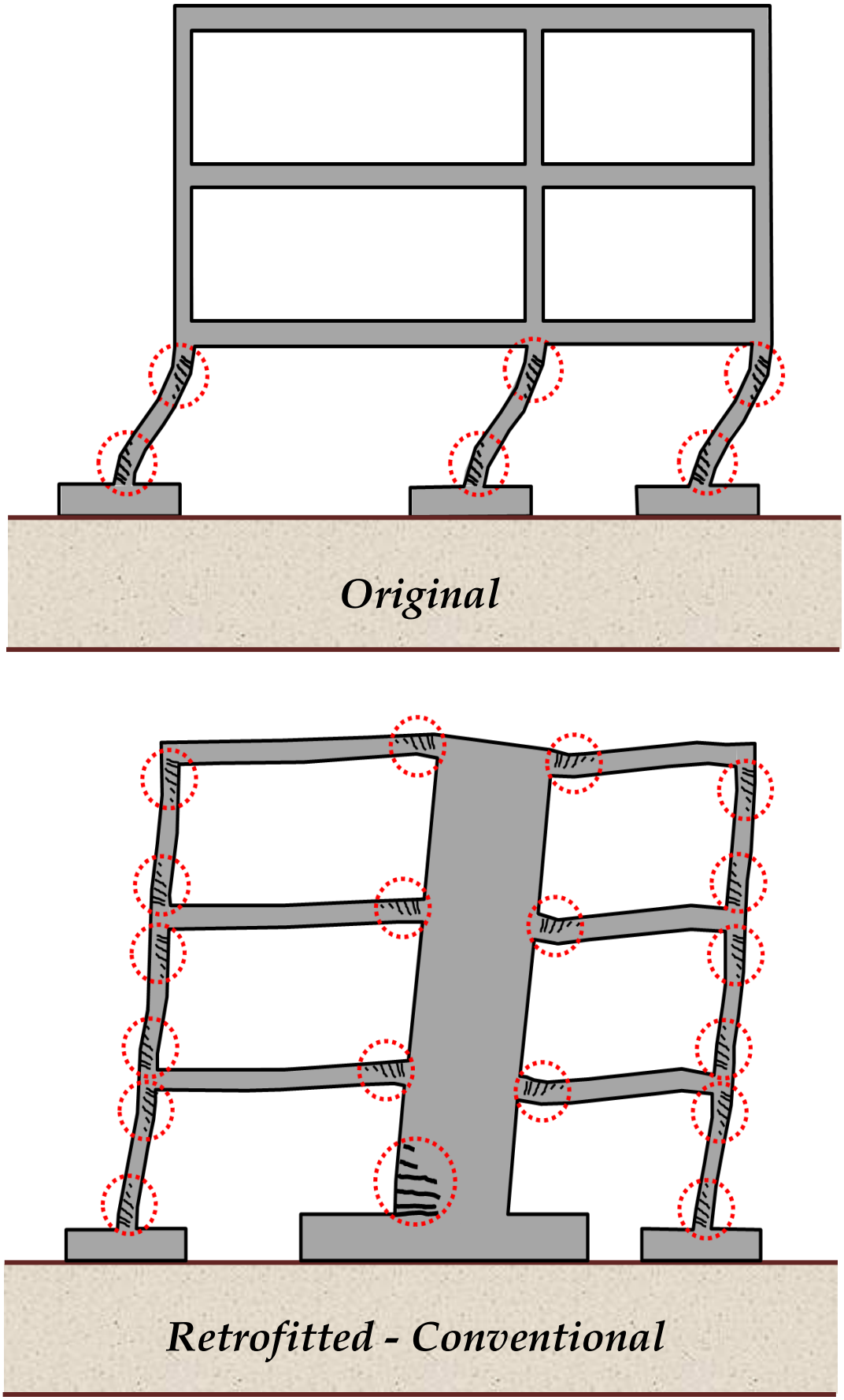

Figure 6.1 Schematic illustration of type of failure for original and retrofitted building respectively.

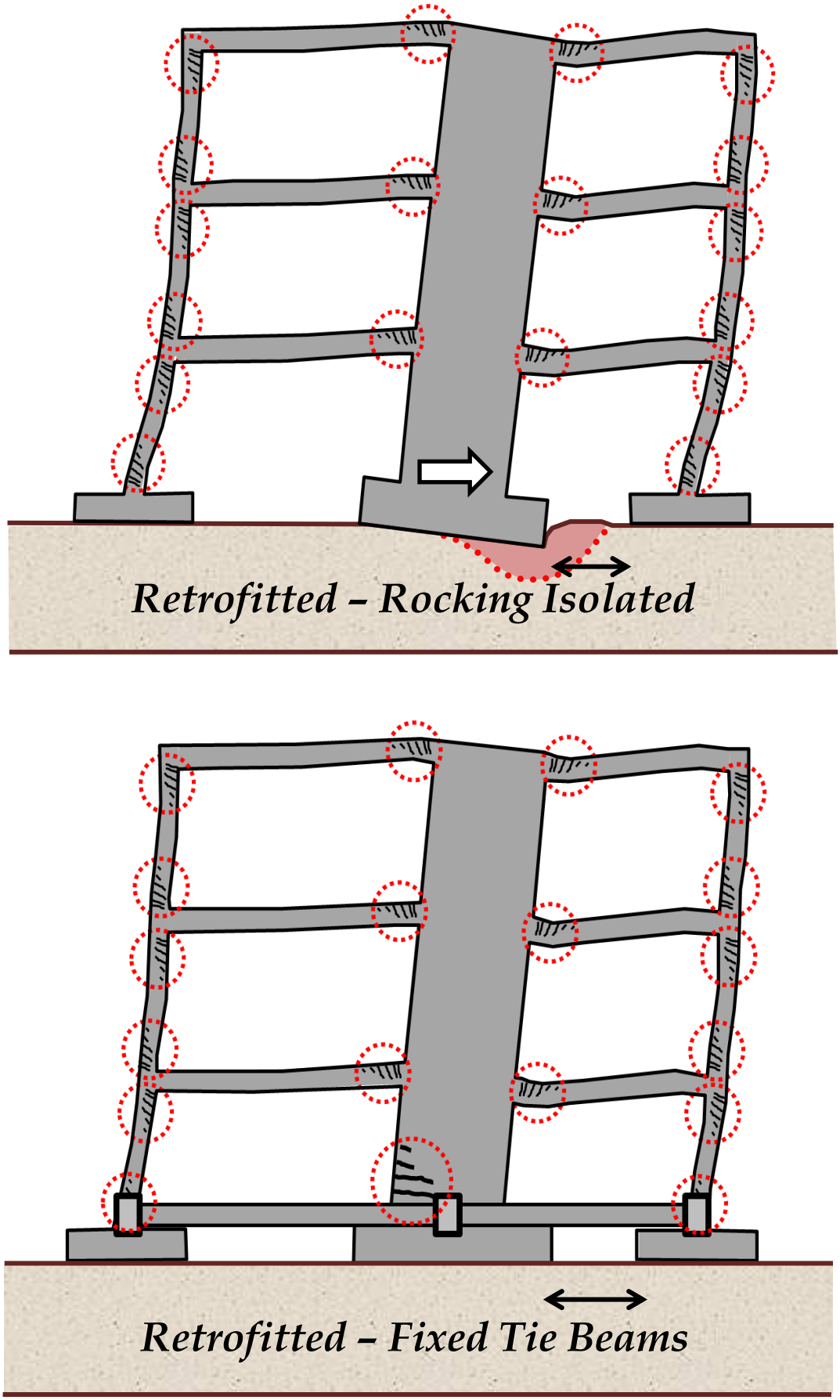

Figure 6.2 Schematic illustration of type of failure for retrofitted building with rocking isolation and with the addition of fixed tie beams respectively.

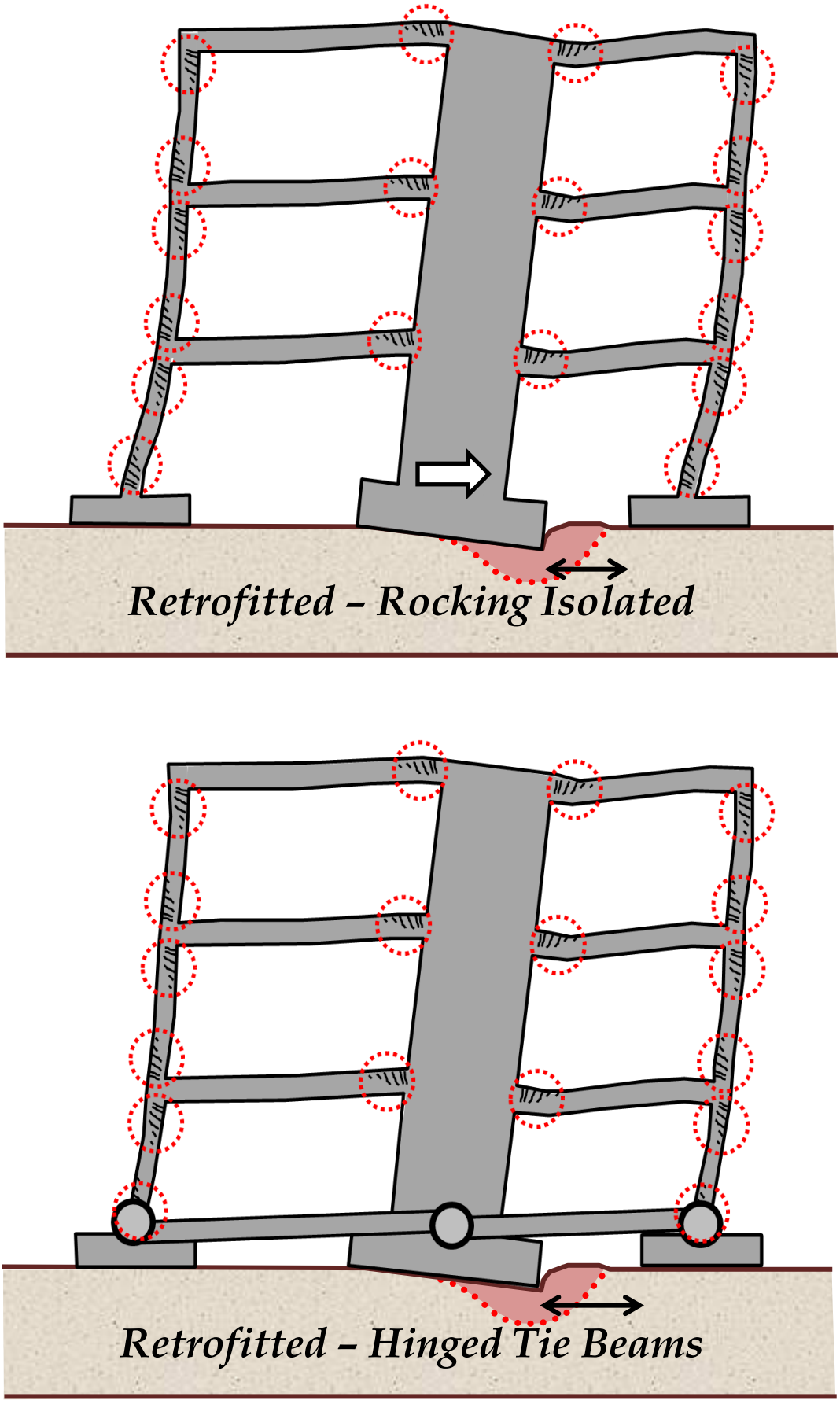

Figure 6.3 Schematic illustration of type of failure for retrofitted building with rocking isolation and with the addition of hinged tie beams respectively.

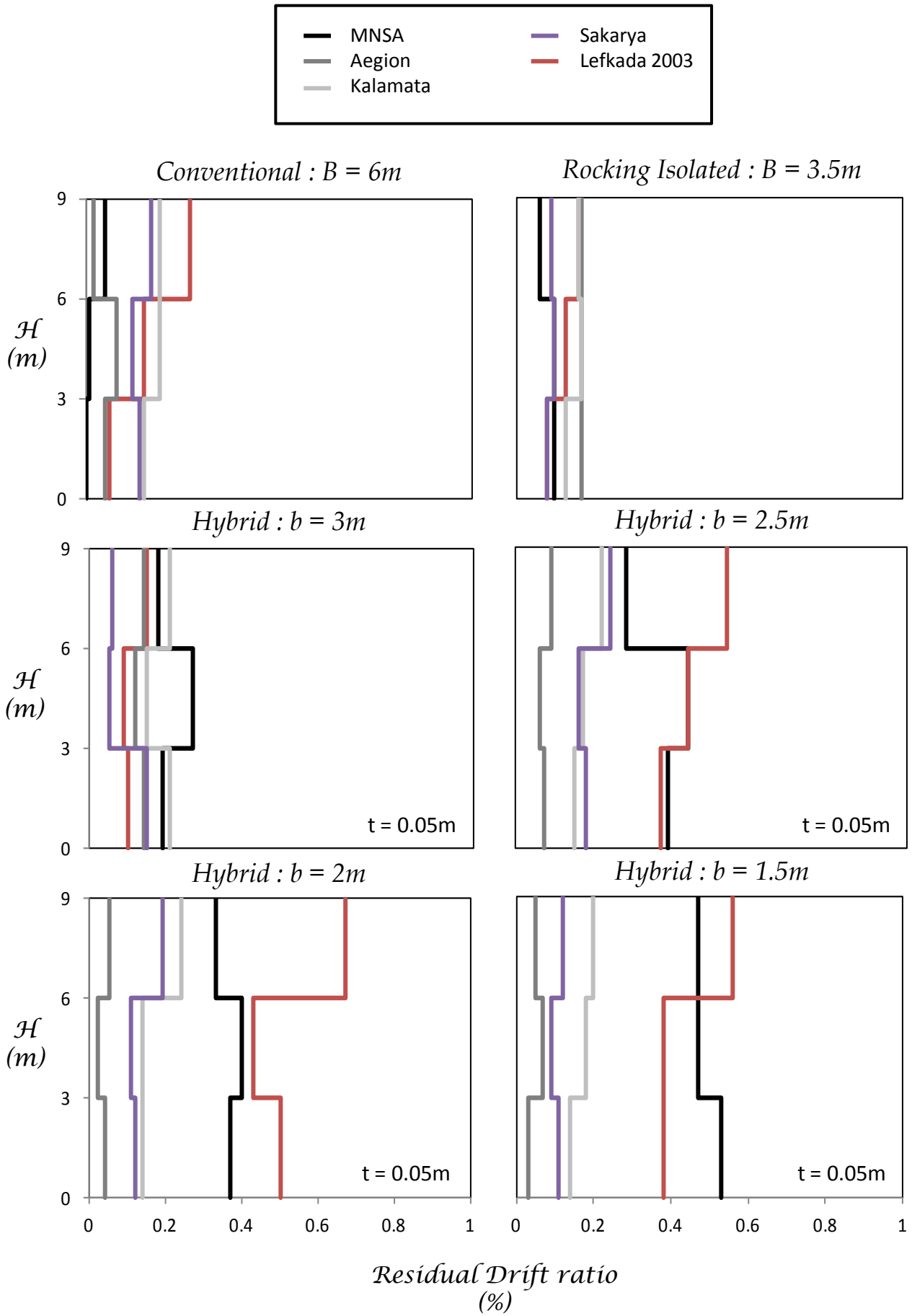

Figure 6.4 Residual drift ratio (%) per storey for the retrofitted building after being submitted to moderate intensity seismic records : comparison of systems with reducing width of shear wall foundation.

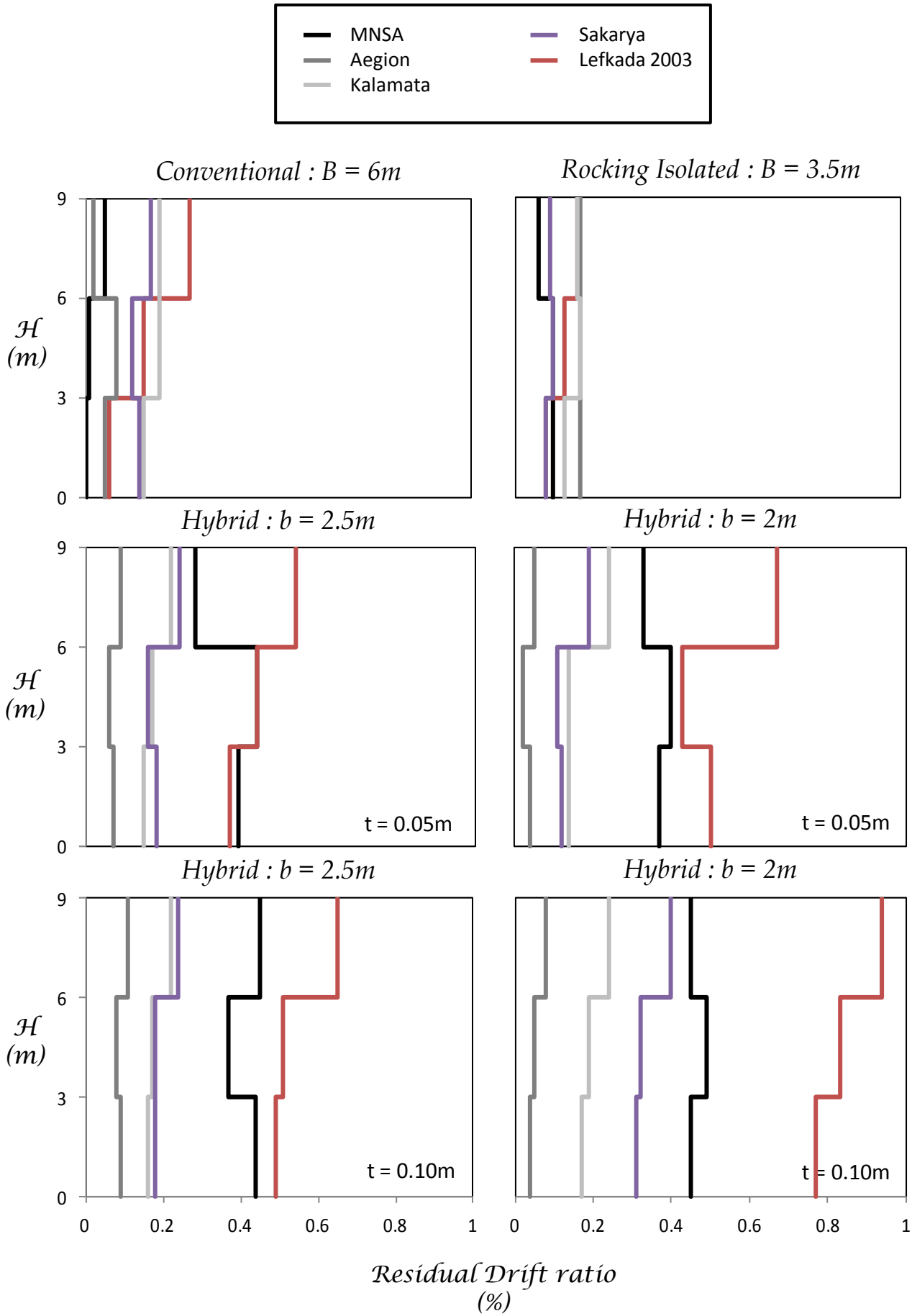

Figure 6.5 Residual drift ratio (%) per storey for the retrofitted building after being submitted to moderate intensity seismic records : comparison of systems with increasing height of hybrid shear wall foundation.

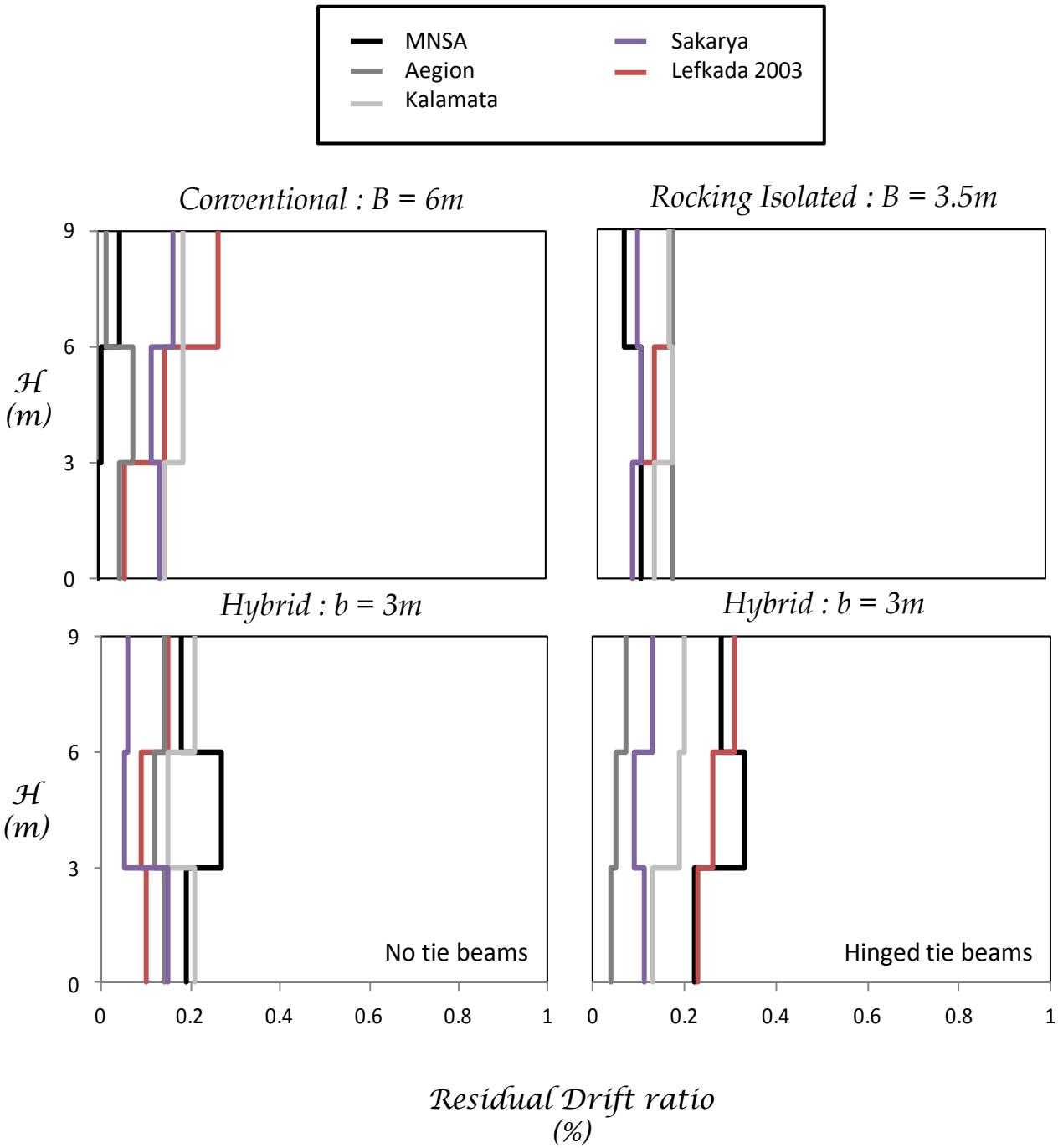

Figure 6.6 Residual drift ratio (%) per storey for the retrofitted building after being submitted to moderate intensity seismic records : comparison of systems with and without hinged tie beams.

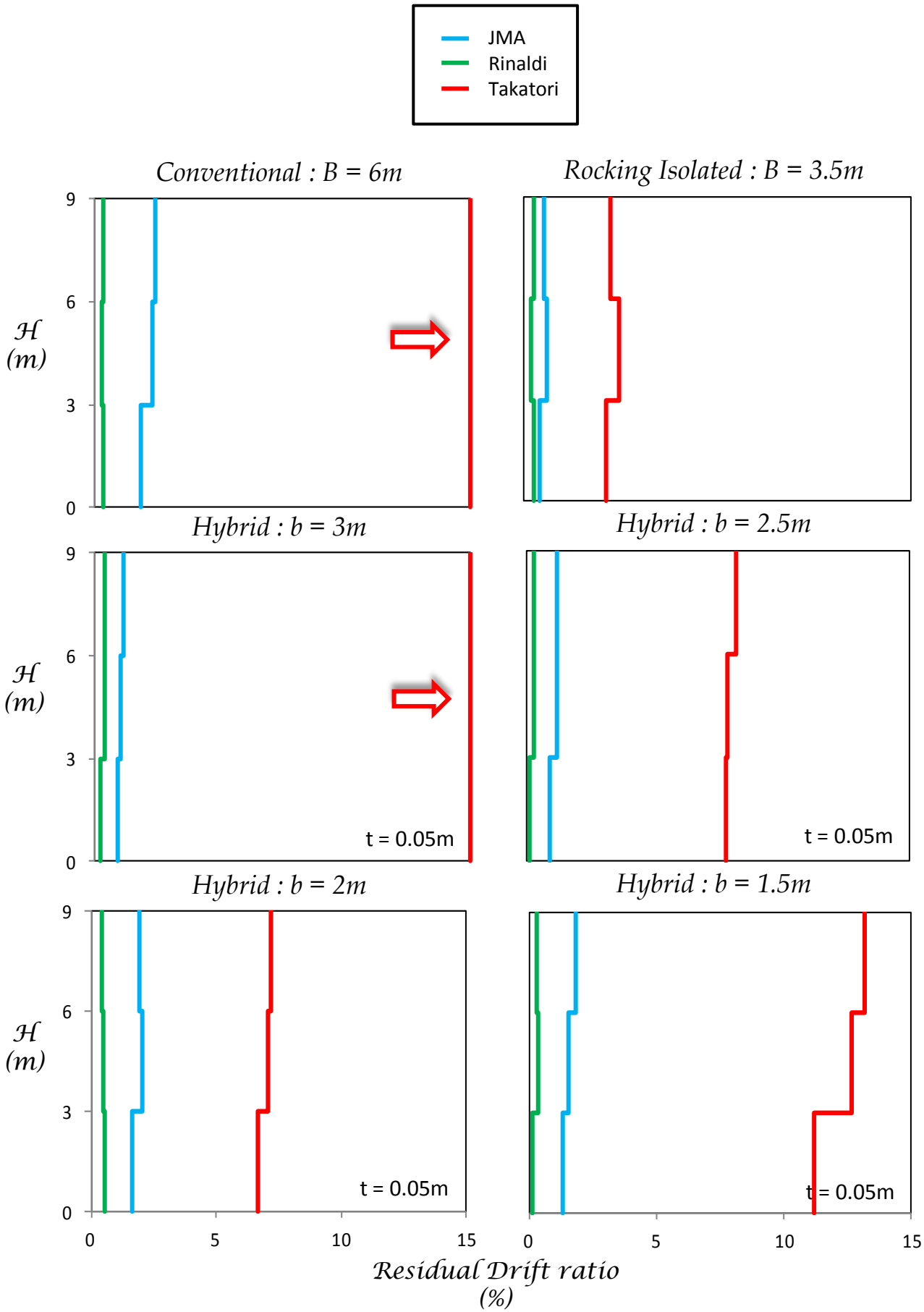

Figure 6.7 Residual drift ratio (%) per storey for the retrofitted building after being submitted to strong seismic records : comparison of systems with reducing width of shear wall foundation..

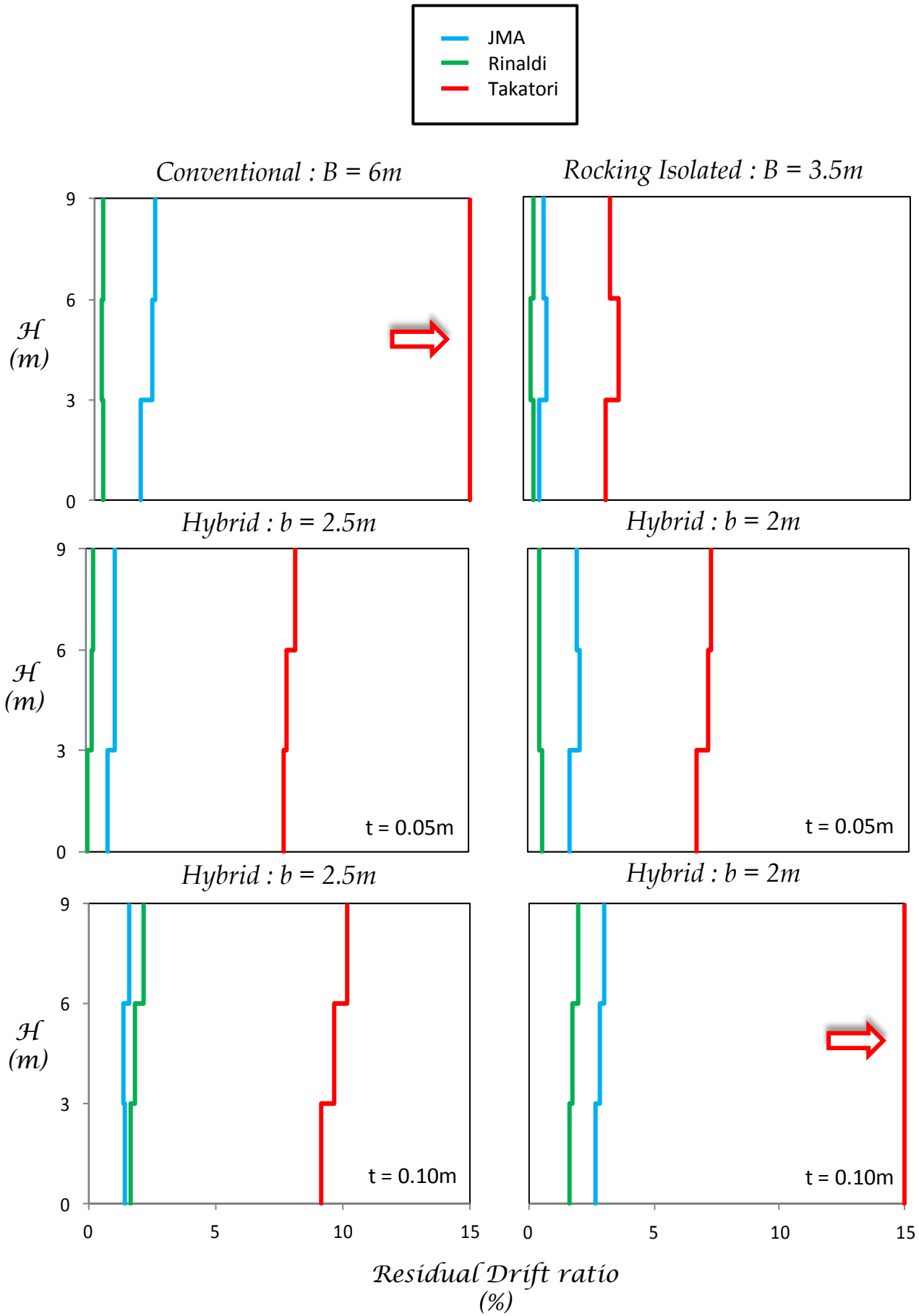

Figure 6.8 Residual drift ratio (%) per storey for the retrofitted building after being submitted to strong seismic records : comparison of systems with increasing height of hybrid shear wall foundation.

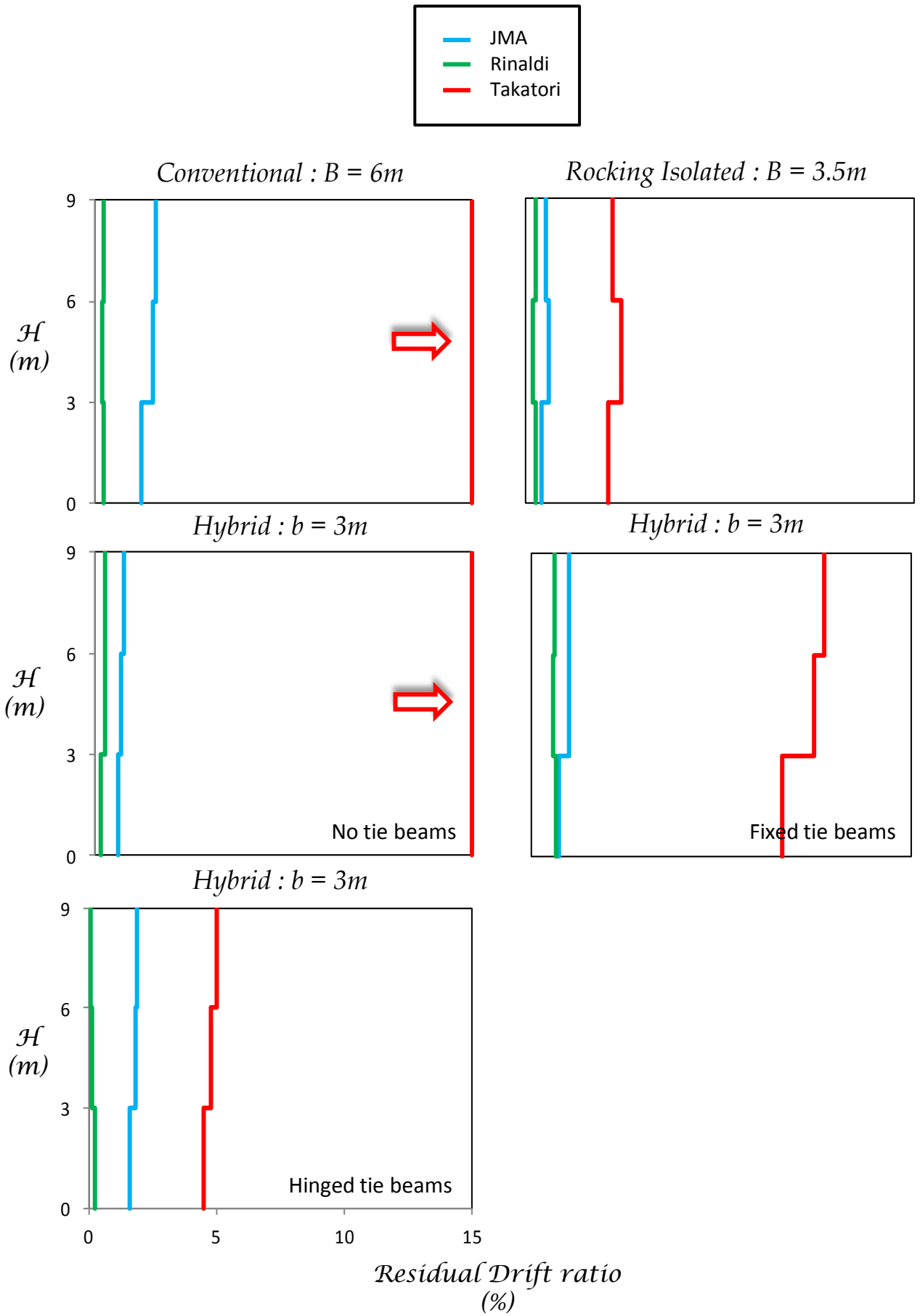

Figure 6.9 Residual drift ratio (%) per storey for the retrofitted building after being submitted to strong seismic records : comparison of systems with and without tie beams.

List of References

REFERENCES

Anastasopoulos I., Gazetas G., Loli M., Apostolou M, Gerolymos N. (2010a). Soil Failure can be used for Earthquake Protection of Structures. *Bulletin of Earthquake Engineering* **8:2**, 309-326.

Anastasopoulos I., Georgarakos T., Georgiannou V., Drosos V., Kourkoulis R. (2010b). Seismic Performance of Bar-Mat Reinforced-Soil Retaining Wall: Shaking Table Testing versus Numerical Analysis with Modified Kinematic Hardening Constitutive Model. *Soil Dynamics & Earthquake Engineering* **30:10**, 1089-1105.

Anastasopoulos I., Gelagoti F., Kourkoulis R., Gazetas G. (2011), Simplified Constitutive model for Simulation of Cyclic Response of Shallow Foundations: Validation against Laboratory Tests, *Journal of Geotechnical and Geoenvironmental Engineering,* ASCE, Vol. 137, No. 12, pp. 1154–1168.

Anastasopoulos I., Kokkali P., Tsatsis A. (2011). 1-dof System Lying on Square Foundation : Monotonic and Cyclic Loading.

Anastasopoulos I., Kokkali P., Tsatsis A. (2011). Experimental Investigation of Vertical Load Capacity of Surface Footings.

Anastasopoulos I., Kourkoulis R., Gelagoti F., Papadopoulos E. (2012), Rocking response of SDOF systems on shallow improved sand: An experimental study, *Soil Dynamics and Earthquake Engineering*, **40**, pp. 15–33.

Apostolou M., Gazetas G., Garini E. (2007). Seismic response of slender rigid structures with foundation uplifting, *Soil Dynamics and Earthquake Engineering*, **27:7**, pp. 642–654

Bertero V. (1996). State of the art report on: design criteria. *Proceedings of 11th World Conference on Earthquake Engineering*. Acapulco, Mexico. Oxford: Pergamon.

Calvi G.M. (1999). A displacement-based approach for vulnerability evaluation of classes of buildings. *Journal of Earthquake Engineering*, **3:3**, 411-438.

Di Ludovico M. (2007), *Comparative Assessment of Seismic Rehabilitation Technique on the Full Scale SPEAR Structure,* Doctoral Thesis. Università degli Studi di Napoli Federico II.

Drosos V., Georgarakos T., Loli M., Anastasopoulos I.**,** Zarzouras O., and Gazetas G. (2012), Soil–Foundation–Structure Interaction with Mobilization of Bearing Capacity : An Experimental Study on Sand, *Journal of Geotechnical and Geoenvironmental Engineering,* ASCE (*in press*).

Fardis M.N. (2002). *Design of an irregular building for the SPEAR project—description of the 3-storey structure*. Research report University of Patras, Greece.

Fardis M.N., Negro P. (2006). SPEAR—seismic performance assessment and rehabilitation of existing buildings. *Proceedings of the international workshop on the SPEAR project*, 4-5 April, Ispra, Italy.

Gajan S., Kutter B.L., Phalen J.D., Hutchinson T.C., and Martin G.R. (2005). Centrifuge modeling of load-deformation behavior of rocking shallow foundations. *Soil Dynamics and Earthquake*

Engineering, **25**, 773–783.

Gajan S., Kutter B.L. (2008). Capacity, settlement, and energy dissipation of shallow footings subjected to rocking. *Journal of Geotechnical and Geoenvironmental Engineering*, ASCE, **134:8**, 1129-1141.

Gajan S., Kutter B.L. (2009). Effects of Moment-to-Shear Ratio on Combined Cyclic Load-Displacement Behavior of Shallow Foundations from Centrifuge Experiments. *Journal of Geotechnical and Geoenvironmental Engineering,* ASCE, **135:8**, 1044-1055.

Gelagoti F., Kourkoulis R., Anastasopoulos I., Gazetas G. (2012). Rocking-isolated frame structures: Margins of safety against toppling collapse and simplified design approach. *Soil Dynamics and Earthquake Engineering* **32:1**, 87-102.

Gibson A.D. (1997). *Physical scale modeling of geotechnical structures at One-G*. Report no. SML 97-01. Pasadena, CA: California Institute of Technology, pp. 413.

KAN.EPE. (2009). *Regulation for Strengthening and Rehabilitation*. OASP, Athens-Greece.

Kourkoulis R., Gelagoti F., Anastasopoulos I. (2012), Rocking Isolation of Frames on Isolated Footings: Design Insights and Limitations. *Journal of Earthquake Engineering* **16:3**, 374-400.

Mergos P.E., Kawashima K. (2005). Rocking isolation of a typical bridge pier on spread foundation. *Journal of Earthquake Engineering*, **9:S2**, 395-414.

Paolucci R. (1997). Simplified Evaluation of Earthquake Induced permanent Displacement of Shallow Foundations. *Journal of Earthquake Engineering,* **1:3**, 563-579.

Paolucci R., Shirato M. and Yilmaz M.T. (2008). Seismic behaviour of shallow foundations: Shaking table experiments vs numerical modeling, *Earthquake Engineering and Structural Dynamics*, **37**, 577–595.

Panagiotidou A.I., Gazetas G., Gerolymos N. (2011). Pushover and Seismic Response of Foundations on Stiff Clay: Analysis with P-Δ Effects, *Earthquake Spectra* (in print).

Papadopoulos G. A., Drakatos G., Papanastassiou D., Kalogeras I., and Stavrakakis G. (2000). Preliminary Results about the Catastrophic Earthquake of 7 September 1999 in Athens, Greece. *Seismological Research Letters* **71**, 318-329.

Park R., and Paulay T. (1976). *Reinforced Concrete Structures*. John Wiley & Sons, New York.

Pecker A. (1998). Capacity Design Principles for Shallow Foundations in Seismic Areas, *Procedings, 11th European Conference on Earthquake Engineering*, A.A. Balkema Publishing.

Pecker A. (2003). A seismic foundation design process, lessons learned from two major projects: the Vasco de Gama and the Rion Antirion bridges", ACI International Conference on Seismic Bridge Design and Retrofit, University of California at San Diego, La Jolla, USA.

Pender M. (2007). Seismic design and performance of surface foundations, *4th International Conference on Earthquake Geotechnical Engineering*, Thessaloniki, Greece (CD-ROM).

Priestley M.J.N. (2000). Performance based seismic design, *Proc. 12th World Conference on*

Earthquake Engineering (12WCEE). Auckland, New Zealand, Paper No. 2831.

Raychowdhury P., Hutchinson T.C. (2011), Performance of seismically loaded shearwalls on nonlinear shallow foundations, *International Journal for Numerical and Analytical Methods in Geomechanics*; **35**:846–858.

Rontogianni A. (2011). Seismic Rehabilitation of an Existing 3 – storey Building : Conventional Design and Rocking Isolation System. Diploma Thesis, NTUA.

Shirato M., Kouno T., Asai R., Nakani N., Fukui J., and Paolucci R. (2008). Large-scale experiments on Nonlinear Behaviour of Shallow Foundations Subjected to Strong Earthquakes. *Soils & Foundations*, **48:5**, 673–692.

Vassiliou M.F., and Makris N. (2011), Analysis of the rocking response of rigid blocks standing free on a seismically isolated base. *Earthquake Engineering and Structural Dynamics*, **41:2**, 177–196.